Improving Performance of an Energy Efficient Hydraulic Circuit

A Thesis Submitted to the
College of Graduate Studies and Research
in Partial Fulfillment of the Requirements
for the Degree of Master of Science
in the
Department of Mechanical Engineering
University of Saskatchewan
Saskatoon, Saskatchewan

By
Tonglin Shang
April 2004

Permission to Use

In presenting this thesis in partial fulfillment of the requirements for a Postgraduate degree from the University of Saskatchewan, I agree that the Libraries of this University may make it freely available for inspection. I further agree that permission for copying this thesis in any manner, in whole or in part, for scholarly purposes, may be granted by the professors who supervised my thesis work or, in their absence, by the Head of the Department or Dean of the College in which my thesis work was done. It is understood that any copying, publication or use of this thesis or parts thereof for financial gain shall not be allowed without my written permission. It is also understood that due recognition shall be given to me and to the University of Saskatchewan in any scholarly use which may be made of any material in my thesis.

Requests for permission to copy or to make other use of material in this thesis, in whole or in part, should be addressed to:

Head of the Department of Mechanical Engineering
University of Saskatchewan
Engineering Building
57 Campus Drive
Saskatoon, Saskatchewan, S7N 5A9
Canada

Abstract

Hydraulic circuits with fast dynamic response are often characterized by low power efficiency; on the other hand, energy-efficient circuits under certain circumstances, can demonstrate slow transient responses. Continuously rising energy costs combined with the demand on high performance has necessitated that hydraulic circuits become more efficient yet still demonstrate superior dynamic response. This thesis introduces a new hydraulic circuit configuration which demonstrates high dynamic performance and high efficiency.

A pump-controlled hydraulic motor system was used as the basis of the study because of its high circuit efficiency. This is primarily because there is no power loss between the pump and motor. To improve the dynamic response of the pump, a DC motor was designed to control the pump swashplate (and hence flow rate) directly. The pump and DC motor were mathematically modeled and their parameters were experimentally identified. Based on the model and experimental results, a nonlinear PID controller was designed for the DC motor. By means of the DC motor's quick dynamic response (in the order of 10 ms), the DC motor controlled pump demonstrated a fast dynamic response with a rise time of 15 to 35 ms depending on the pump pressure.

As the dynamic response speed of the pump flow rate was increased, overshoot of the hydraulic motor output also increased. To reduce this overshoot, a bypass flow control circuit was designed to bypass part of the flow during the transient. Due to the unique operating requirements of the bypass flow control system, a PID controller with a resetable integral gain was designed for the valve to reduce the rise time of the bypass control valve. The feasibility ("proof of concept") of the bypass flow control concept was first established using simulation techniques. The simulation results showed that the bypass flow control system could significantly reduced the overshoot of the hydraulic

motor rotational speed.

The bypass controller was applied to the experimental test circuit. The transient results for the pump-controlled motor system with the bypass flow control are presented under a constant resistive and an inertial load. The test results showed that the bypass flow control could reduce the overshoot of the hydraulic motor rotational speed by about 50%. The relative efficiency of the circuit with the bypass flow control system was 1% to 5% lower for the particular pump-controlled system that was used in this study. For a pump/motor that does not demonstrate significant flow ripple of the magnitude experienced in this study, the relative efficiency would be the same as the pump/motor system without bypass. It was concluded that the proposed bypass control system, combined with the DC motor-swashplate driven pump, could be used to create an energy efficient circuit with excellent dynamic transient responses.

Acknowledgements

The author would like to express his gratitude to his supervisors, Dr. R. T. Burton and Dr. G. J. Schoenau, for their invaluable guidance, advice and encouragement throughout the course of this research and the writing of this thesis. Also, the author would like to express his sincere appreciation to Mr. D. V. Bitner for his consistent help throughout the project. Finally, the author wishes to thank his wife, Weijia Qi, and all other family members for their understanding, support and sacrifice during the study.

The author acknowledges the financial assistance provided in the form of a scholarship from the University of Saskatchewan.

Table of Contents

List of Figures

List of Tables

Nomenclature

A_p	Piston area (m^2)
B_d	Viscous damping coefficient of the DC motor ($Nm \cdot rad^{-1}s$)
B_m	Total viscous damping coefficient ($Nm \cdot rad^{-1}s$)
B_p	Damping coefficient of the swashplate yoke assembly ($Nm \cdot rad^{-1}s$)
C_{em}	External leakage coefficient of the hydraulic motor ($m^3s^{-1}Pa^{-1}$)
C_{tp}	Total pump leakage flow coefficient ($m^3s^{-1}Pa^{-1}$)
C_{im}	Internal leakage coefficient of the hydraulic motor ($m^3s^{-1}Pa^{-1}$)
C_t	Total leakage coefficient of the pump and motor ($m^3s^{-1}Pa^{-1}$)
C_{tm}	Total leakage coefficient of the hydraulic motor ($m^3s^{-1}Pa^{-1}$)
D_m	Volumetric displacement of the hydraulic motor (m^3rad^{-1})
D_p	Pump displacement ($m^3 \cdot rad^{-1}$)
i	Armature current of the DC motor (A)
i_c	Current through the coil of the servo valve torque motor (A)
J_d	Moment of inertia of the DC motor rotator ($Nm \cdot rad^{-1} \cdot s^2$)
J_m	Total inertia of the hydraulic motor and load ($Nm \cdot rad^{-1} \cdot s^2$)
J_p	Average moment of inertia of swashplate yoke assembly ($Nm \cdot rad^{-1} \cdot s^2$)
K_a	Gain of the servo valve amplifier (VA^{-1})
K_b	Back EMF constant of the DC motor ($V \cdot rad^{-1} \cdot s$)
K_d	Derivative gain of the PID controller
K_i	Integral gain of the PID controller
K_p	Proportional gain of the PID controller
K_{p1}	Pressure torque constant ($N \cdot m \cdot Pa^{-1}$)
K_{p2}	Pressure torque constant ($Nm \cdot Pa^{-1} \cdot rad^{-1}$)

K_{pf} Pump flow rate coefficient

K_q Linear flow gain of the servo valve ($m^3s^{-1}A^{-1}$)

K_t Torque sensitivity of the DC motor (NmA^{-1})

L Terminal inductance of the DC motor windings (Henry)

L_c Coil inductance of the servo valve torque motor (Henry)

N Number of pistons

P_m Outlet pressure of the hydraulic motor (Pa)

P_p Pump pressure (Pa)

Q_{ep} External leakage flow of the pump (m^3s^{-1})

Q_{ip} Internal leakage flow of the pump (m^3s^{-1})

Q_m Input flow rate of the hydraulic motor (m^3s^{-1})

Q_p Output flow of the pump (m^3s^{-1})

Q_v Flow rate of the servo valve (m^3s^{-1})

R Terminal resistance of the DC motor windings (Ohm)

R_c Coil resistance of the servo valve torque motor (Ohm)

R_p Radius of the piston pitch (m)

S_1 Simplified pump model constant (Nm)

S_2 Simplified pump model constant ($Nm \cdot rad^{-1}$)

T_d Torque applied to the yoke by the DC motor (Nm)

T_{dl} Load torque acting on the DC motor shaft (Nm)

T_{dc} Coulomb friction torque of the DC motor (Nm)

T_{ds} Static friction torque of the DC motor (Nm)

T_e Electrical time constant of the DC Motor (sec)

T_f Torque produced by swashplate friction forces (Nm)

T_{fc} Torque produced by the coulomb friction force of the pump (Nm)

T_{fm} Coulomb friction torque of the hydraulic motor (Nm)

T_l	Load applied on the hydraulic motor shaft (Nm)
T_m	Mechanical time constant of the DC Motor (sec)
T_p	Torque relating to the pump pressure effect (Nm)
T_r	Torque relating to the rotation of the pump barrel (Nm)
V	Input voltage of the DC motor (V)
V_b	Back EMF voltage of the servo valve torque motor armature (V)
V_c	Voltage across the coil of the servo valve torque motor (V)
V_{emf}	Back EMF voltage of the DC motor (V)
V_m	Forward chamber volume of the hydraulic motor (m^3)
V_p	Volume of the pump forward chamber (m^3)
V_t	Total pressurized fluid volume of the pump, pipe and motor (m^3)
γ	DC motor Damping factor
θ_m	Angular position of the hydraulic motor shaft (rad)
θ_p	Angular position of the DC motor shaft and pump swashplate (rad)
ω_n	Hydro-mechanical natural frequency of the servo valve ($rad \cdot s^{-1}$)
ω_p	Rotational speed of the pump prime driver ($rad.s^{-1}$)
ξ	Fundamental damping ratio of the servo valve

Chapter 1

Introduction

1.1 Background

Hydraulic systems are used to transfer energy by converting mechanical energy to fluid energy, and then back to mechanical energy. The principle reason for converting to fluid energy is the convenience of transferring energy to a new location. Hydraulic drives have many advantages over other technologies. The ratio of weight, volume and inertia to available power is significantly lower than in electromechanical drives, especially for linear motion. The dynamic performance is superior when compared to electrical or electrical-mechanical drive systems in large power drive systems [Li et al., 1998]. For those systems that require an output power larger than 10 kW and a fast response speed, hydraulic drive systems are often the appropriate choice. Hydraulic systems are especially suitable for those operations characterized by abrupt loading, frequent stops and starts, reversing and speed variations that cause sharp peak, cyclic and fluctuating power demands. These advantages make them very popular in applications such as aircraft, mobile equipment, lifting machines and forest machines.

Compared with other systems (e.g., mechanical electrical system), hydraulic systems can be energy inefficient. The typical efficiency for a single mechanical gearbox is about 98%~99% and for a triple reduction gearbox is above 95%. However, the typical efficiency for a hydraulic pump or motor is only 85%. The overall efficiency for a very simple pump-controlled hydraulic system under ideal operating conditions is about 70% [Cundiff, 2002]. The total efficiency of a pump/motor combination is much less when the system operates in a low rotational speed range. If hydraulic control valves are included to control the actuators in hydraulic drive systems, the overall efficiency can be substantially

reduced under certain loading conditions.

Poor efficiency can translate into other problems in hydraulic systems. Not only is power consumption increased, but also exhaust emissions (in the case of internal combustion engines) and operating costs increase which lead to the necessity of installing larger pumps and more elaborate cooling equipment to dissipate the heat.

In the past, power efficiency has not been a high priority for hydraulic circuit and component design. Much attention has been oriented towards the pursuit of high system performance and to the fulfillment of the demanded functions. In recent decades, high performance still remains a priority, but systems which are energy efficient have been the focus of much study; this is primarily due to fuel economy and environmental considerations. The demand for highly efficient hydraulic drives (especially when compared with their electrical and mechanical counterparts) has also increased. If the efficiency of hydraulic drive systems cannot be improved, many traditional applications in which they are found will be converted to other power drive systems.

In summary, continuously rising fuel costs and increasing environmental pollution concerns combined with the challenge from other competing technologies has meant hydraulic drives must become more efficient yet still demonstrate competitive cost and superior dynamic response.

1.2 Achievements in Improving Power Efficiency

The power efficiency of hydraulic systems is affected by both the component and system design. Because of the interest in improving hydraulic system efficiency, individual components (pump, motor, actuator, valve etc) have been studied extensively by component manufactures and researchers; much progress over the past decade has been made on the improvement of the component efficiency. However, what is more important for system efficiency is how these components are combined to meet the load demands.

There are many combinations of components which can be used to accomplish a single task. For example, a variable displacement pump/fixed displacement motor, a fixed displacement pump and motor with a variable speed motor drive or a fixed displacement pump and motor with a flow modulation valve can all be used to vary the rotational speed of a load. However, the efficiency of each system can be vastly different depending on the loading conditions even though the efficiency of pumps and motors can be very similar. Thus circuit design is the most important factor for power efficiency consideration.

Any kind of power transmission technology must be controllable yet efficient. The control of a hydraulic system is achieved by modulating the flow rate of the fluid. Four main methods are used to control flow: (1) controlling the power supply unit (engine or electric motor), (2) controlling the displacement of the hydraulic pump, (3) modulating flow through hydraulic valves, and (4) controlling the displacement of the hydraulic actuator (rotary). Each method will now be considered in relationship to their operation and relative efficiency.

1.2.1 Valve Control and Load Sensing System

Valve control is widely used in hydraulic systems because of its high controllability and good performance. A “conventional” valve-controlled system consists of a fixed displacement pump (non-pressure compensated), a relief valve, a flow modulating valve and an actuator (cylinder or motor). The output flow from the pump is constant. If loading conditions are such that the load flow demand is less than the output flow from the pump, then the excess flow must be diverted to tank through a relief valve (R.V). The pump pressure is now at a value dictated by the relief valve setting. This results in flow passing through the R.V to tank at a substantial pressure drop (all wasted power) and a pressure drop across the flow modulating valve (also wasted power). These losses are demonstrated schematically in Figure 1.1(a). In this case, P_S is the pump pressure, P_L is

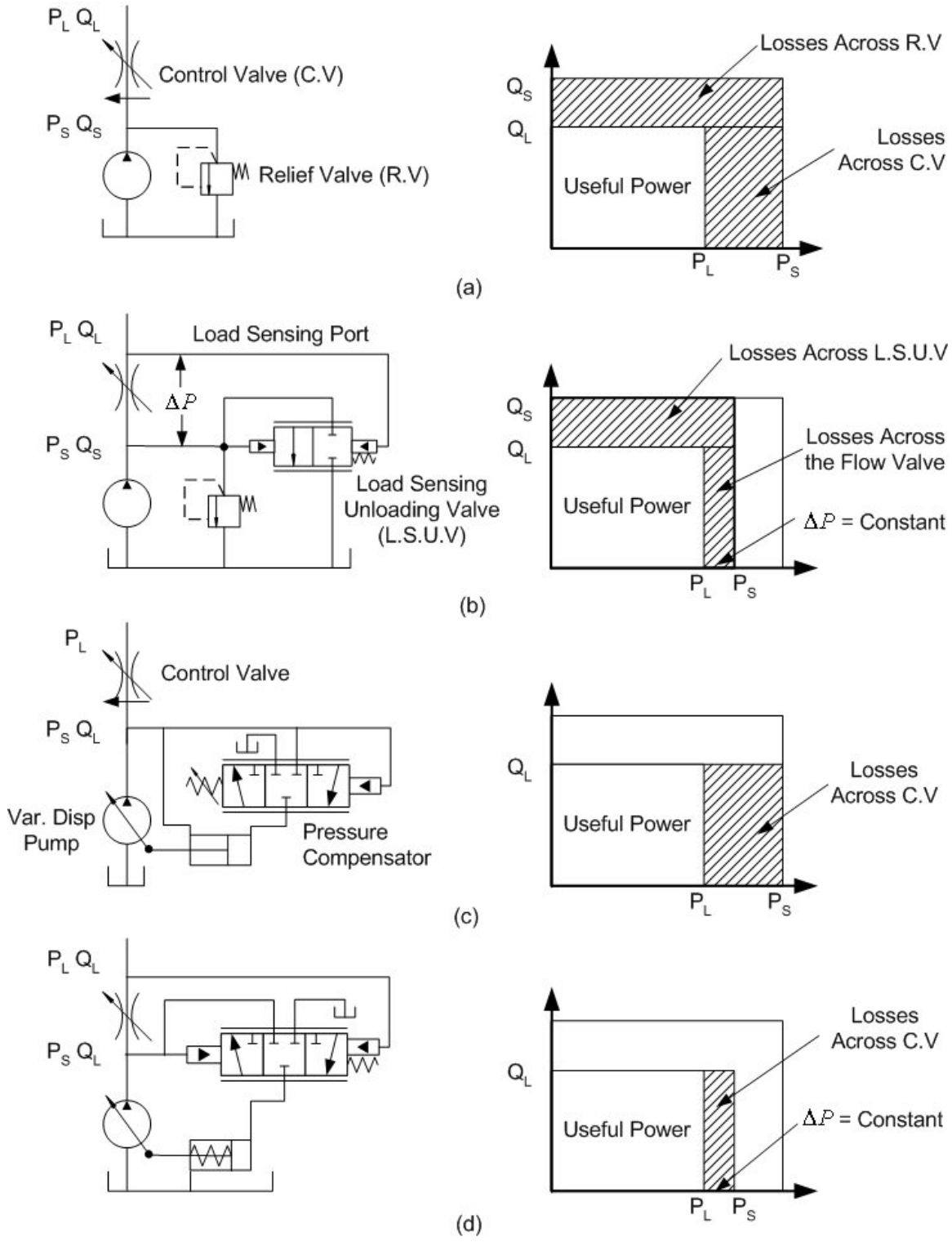

Figure 1.1 Power losses of valve-controlled systems

the load pressure, Q_S is the flow from the pump and Q_L is the demanded flow to the load (Q_S-Q_L is the flow which passes through the R.V). The shaded areas indicate the power that is lost across the R.V. and control valve (C.V). As the load pressure and load flow demands decrease, the efficiency of the circuit drops. These losses are compounded if a symmetric valve is used to control an asymmetric cylinder due to the discontinuity of the pressure in the two sides of cylinder when the direction of cylinder movement is changed [Liang, 1999]. In general, the pump/valve/actuator system is simple, reliable and inexpensive, and has good controllability. However, it can be very inefficient as illustrated in this figure.

Because the pressure losses of conventional systems are often unacceptable, hydraulic systems, which use variable pressure and/or variable flow, are often employed. One such system is shown schematically in Figure 1.1(b). Variable pressure control uses a "load sensing unloading valve" to sense the load pressure. The directional valve includes a load sensing port which is connected to the unloading valve. Flow from the pump not required by the load is diverted to tank at a pressure, 70-140 kPa higher than the load pressure via the load sensing unloading valve. This system is the same as the conventional system except that the "effective" relief valve setting (via the unloading valve) is always 70-140 kPa above the load pressure. The losses are shown by the shaded regions in Figure 1.1(b).

A third system shown in Figure 1.1(c) uses a "pressure compensated" pump. This system is called a demand flow system because the pump supplies only the flow which is required. However because the pressure of the pump is fixed by the compensator, metering losses across the control valve still exist (see shaded area). For pressure compensated systems, a variable displacement pump is always required.

Although variable pressure or pressure compensated systems can be used to improve efficiency, loss across the flow valve or control valve still exists. This has led to the

development of a different “load sensing system”, which is commonly found in mobile hydraulics as a “driving concept” with high running efficiency [Backe, 1991]. Load sensing systems use a load-sensing valve (Figure 1.1(d)) to sense the load pressure which is then fed back to a pump compensator. By means of a compensator control valve, the displacement of the pump is adjusted to deliver the required flow and maintain a pressure 70-140 kPa higher than the load pressure. This desired constant pressure difference across the flow metering valve is set by the compensator. Thus the pump pressure follows changes in the load pressure, while the pump provides only the flow demanded by the metering valve. As illustrated in Figure 1.1(d), the power losses of a load sensing system are substantially smaller than other systems.

Load sensing systems are very efficient in single load applications. However, they are often used in multiple load applications (single pump/multiple load). The pressure at each load is sensed: only the pressure which has the highest value is fed back to the compensator. This means the pump pressure will follow the load with the highest pressure demand. This results in an efficient circuit for that particular load. If load pressures of all other loads are less than the one with the highest load, then the pressure drop across each valve can be substantial and some power losses are introduced into the other circuit.

One problem with load sensing systems for multi load applications is stability which can arise from load interactions through the feedback line. To minimize these interactions, pressure compensated (PC) control valves are often used. Although they are not more efficient than the traditional load sensing systems, they can be used to minimize interactions [Lantto et al., 1991].

Another problem with load sensing systems is the risk of instability which can occur through the pressure feedback line (or load sensing line). To make the load sensing system more stable, different kinds of hydraulic “signal filters” (such as the combinations of orifices, check valves and accumulators) may be used in the load sensing line. However, in

many cases, this kind of filtering slows down the system dynamic response. Many studies have attempted to improve the dynamics of load sensing systems, such as using electric hydraulic load sensing systems [Backe, 1991, 1993; Luomaranta, 1999]. In their studies, the load pressure was measured using a pressure transducer on the load sensing valve; in addition the pump was equipped with an electro-hydraulic directional valve to control the displacement of the pump. The load sensing line was replaced by an electric signal line including a pressure transducer, electrical controller/filter and an electrically controlled load sensing pump. With this electric load sensing line, different control strategies would be implemented. With the help of an electronic filter and controller, any oscillation in the load sensing signal would be attenuated; thus, it was possible to design a load sensing system that was stable but still demonstrated fast response.

Matching the pump flow to a varying demand load flow can improve the power efficiency due to the elimination of the loss across the relief valve. Normally, a variable displacement pump is used. A study by Mansouri et al. [2001] gives another approach. A latching valve, which switches the on/off position extremely rapidly (750μs), but remains latched in the closed or open position using residual magnetism, was used to control the flow output in order to achieve a variable flow supply (schematically shown in Figure 1.2). When the latching valve is in the closed position, pump flow is directed to the “hydraulic rail” and compressed to high pressure fluid. In the open position, flow is “shorted” back to the inlet of the pump (at low pressure). By applying switched-mode control to change the state of the control valve, the flow could be modulated with minimal losses; further a variable pump with excellent transient response characteristics can be emulated. Energy can be saved with this approach compared to conventional variable displacement pumps, particularly at partial pump load conditions.

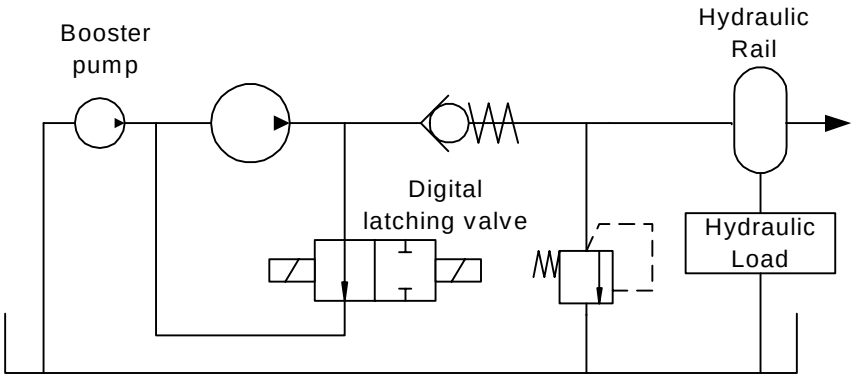

Figure 1.2 Variable flow supply using latching valve [Mansouri, 2001]

In recent years, the trend is to replace mechanical valves with electrically controlled valves, to which sophisticated electronic control algorithms can be applied in order to improve power efficiency. A typical hydraulic system using a conventional four-way proportional valve is shown in Figure 1.3(a). The proportional valve can be considered as two variable orifices (upstream and downstream to the actuator) which are linked together. Such a circuit can meet the loading requirement with high performance, but is not particularly energy efficient. The reason for this is as follows: the meter-in (upstream flow) and meter-out (downstream flow) orifices are mechanically linked together. The pressure losses across the meter-in and meter-out orifices are the same because they are of the same structure. This design can increase pressure losses, when compared with a system in which only meter-in or meter-out orifice is used.

A different circuit (shown in Figure 1.3(b)) can be used to realize the same system function [Liang et al., 1999]. This configuration allows meter-in or meter-out control and gives the control design more flexibility to improve the system power efficiency. For example, if the cylinder is extended with a resistive load, the flow and pressure in the meter-in side of the cylinder are designed to satisfy the velocity and force requirements of the load, whereas the pressure in the meter-out side of the cylinder is designed only to deliver the flow back to tank. The pump pressure can be automatically changed by a

proportional relief valve according to the model of the system. Thus, the pressure drop in the meter-in orifice can be minimized by the control strategy and the pressure loss in the meter-out orifice can be neglected. The drawback of this system is the strong dependence on the knowledge of the system models. Further, some form of velocity or flow feedback is required for flow control.

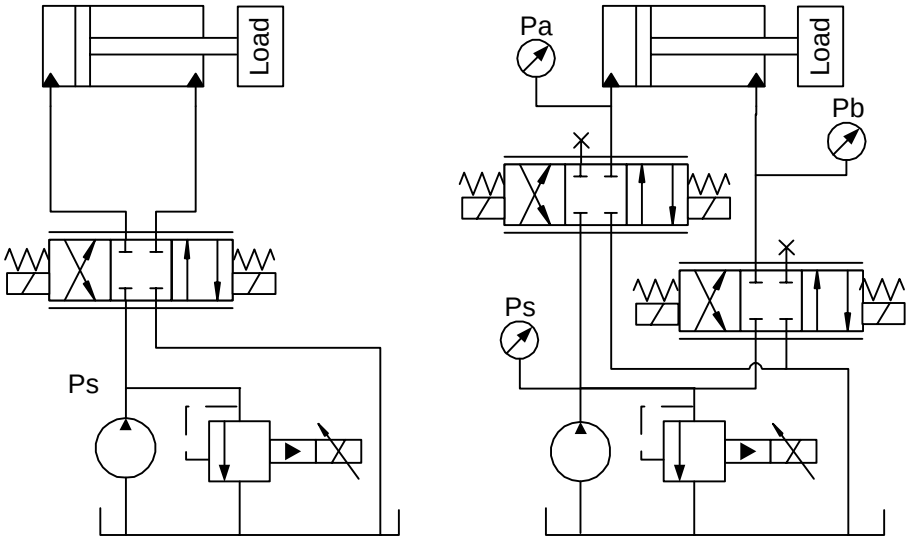

(a) (b) [Liang et al., 1999]

Figure 1.3 Systems with meter-in and meter-out control

A great deal of research has been focused on theoretical and practical benefits from the applications of energy efficient strategies in valve-controlled hydraulic systems; however, reported overall power efficiencies are still very low. In a study by Liang and Virvalo [2001 (1)], four types of valve control systems (which were previously shown in Figure 1.1 (a) ~ (d)) used to control a hydraulic crane were discussed. The overall average efficiencies during a typical load cycle are shown in Table 1.1.

Although these results are from only one particular example, the power efficiency of the valve–controlled hydraulic system is still very poor.

Table 1.1 Overall average efficiency of valve-controlled hydraulic crane [Liang, 2001]

Driving Strategies	Conventional System (a)	Variable Pressure System (b)	Variable Flow System (c)	Load sensing System (d)
Efficiency	10.6%	27.4%	14.4%	35.6%

1.2.2 Pump Control

Pump-controlled systems are preferred hydraulic power drive systems for applications in which large horsepower is required. The actuator (motor or cylinder) in a pump-controlled system is controlled by adjusting the displacement of the pump which is driven by a constant rotational speed power source. The advantage of these kinds of systems is high efficiency because there are no “system dependant” losses (pressure and flow losses) in the system. However, a limitation of pump-controlled systems is that one pump can only control one load although a pump can supply flow to many actuators.

Pump-controlled systems can appear in two forms, one is an open circuit shown in Figure 1.4(a), and the other is a closed circuit shown in Figure 1.4(b) (commonly defined as a hydrostatic system in which the return fluid is ported directly back to the inlet of the pump rather than through a reservoir.). The advantages of open circuit pump control systems are simple configuration and the capacity of heat dissipating; on the other hand a closed circuit pump control system is characterized by the reduced system size and oil volume. Hydrostatic systems contain a fixed displacement motor and a replenish circuit which is used to keep a minimum pressure in each line and supply supplemental fluid to each line due to the leakage.

When compared with valve-controlled systems, pump-controlled systems have higher system efficiency; however their dynamic performance is often poor. This is the result of two factors: (1) the natural frequency is reduced by a factor of $\sqrt{2}$ because only one line between the pump and actuator is controlled; thus the trapped oil spring rate is one half of that of the valve-controlled system [Merritt, 1967]; (2) if the length of the line

between a valve and actuator is same to the length for a pump, the compressed fluid volume is larger with a pump than that of a valve.

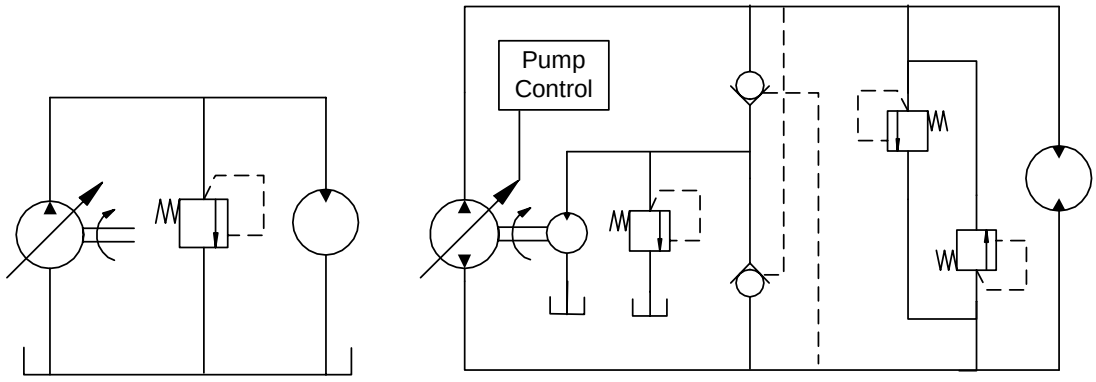

(a) Open circuit pump control (b) Closed circuit pump control

Figure 1.4 Typical pump controlled hydraulic system

The actuator in a closed pump control system can be a motor or a symmetric cylinder. Rahmfeld [Rahmfeld, 2000; Rahmfeld and Ivantysynova, 2001] has used a differential cylinder in a closed hydraulic circuit (Figure 1.5). The differential volume is balanced on the low pressure side through a charge pump together with an accumulator. The main advantage of this approach is that low pressure lines of multi-actuator systems can be coupled. Another advantage is that when the cylinder reverses motion due to the load force, the pump works in a “motoring” mode and the accumulator is filled from the low pressure side. A simulation result in Rahmfeld’s study for a demolition excavator for pump control and load sensing control showed that the power efficiency of this system was better than that of the load sensing system.

1.2.3 Secondary Control

One of the most effective strategies to improve the circuit efficiency is secondary control. The pressure within a secondary control system is kept at a "quasi-constant" level by means of a pressure compensated pump (such as the pump shown in Figure 1.1(c)). The main feature of a pressure compensated pump is that it can deliver the demanded flow to

the system by changing the pump pressure within a small region set by a pressure compensator. Increasing the pump pressure slightly can decrease the pump flow rate dramatically until the pump is fully destroked. On the other hand, decreasing the pump pressure slightly can increase the pump flow rate until the pump is fully stroked. An accumulator on the high pressure side is used to recover the energy when lowering or decelerating a load. The flow is transferred from the primary side to the load without throttling loss. The rotational speed of a hydraulic motor in a secondary control system can be controlled by adjusting the motor displacement.

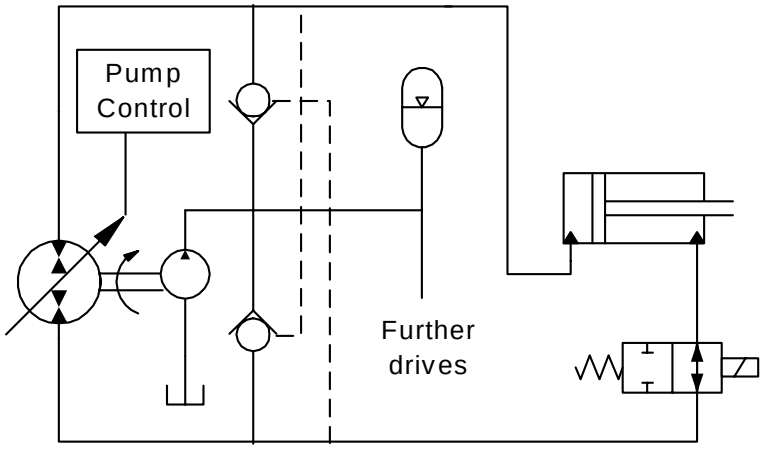

Figure 1.5 Pump controlled cylinder [Rahmfeld, 2001]

A secondary control system with two secondary units is shown in Figure 1.6. Advantages of the secondary control are that multiple motors can be connected to a constant pressure "net" or rail, providing a means of hydraulic energy recovery. The motor can work as a pump (by changing the position of the swashplate) and supply recovered energy to the pressure net during lowering a weight or braking a vehicle. A study by Backe and Kogl [1993] showed that the dynamic behavior of secondary-controlled motors is not affected by the hydraulic time constant of the system because the system pressure is approximately constant; however interactions between motors can still exist.

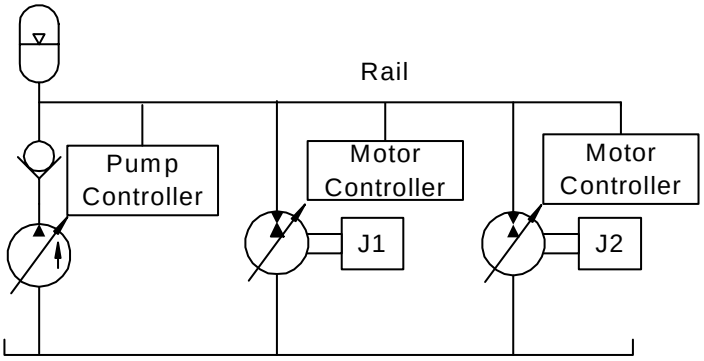

Figure 1.6 A secondary control system with two secondary units

Secondary control technology cannot be directly applied to linear cylinders because their displacement (piston area) cannot be changed. In order to apply secondary control to cylinders without introducing extra throttling pressure losses to the system, a hydraulic "transformer" is required. A conventional transformer developed by Rexroth [Vael ea al., 2000] is schematically shown in Figure 1.7. It consists of a variable axial piston pump/motor (A in Figure 1.7) and a fixed axial piston pump/motor, B. Two pump/motors are coupled mechanically.

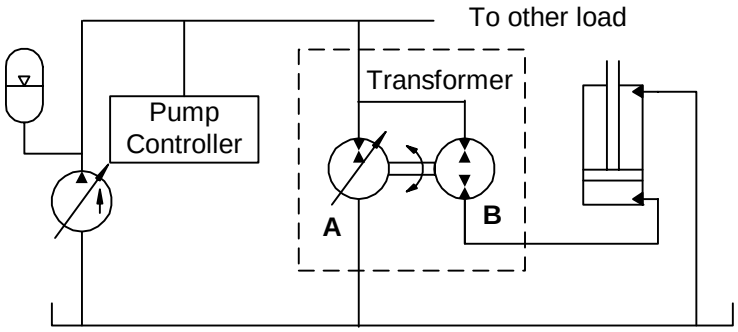

Figure 1.7 Application of a conventional transformer

The principal of operation is as follows: Flow passes through the fixed displacement pump/motor B to the bottom of the actuator. Additional flow can be added to or removed from the system by changing the displacement of pump/motor, A, in the transformer. Thus the flow supplied to the actuator can be changed. For instance, if pump/motor, A, works in

“pump” mode and pump/motor, B, works in “motor” mode, an increase in the flow rate of pump, A, will increase the pressure at the inlet to Motor, B because of the increased torque on motor, B. This will result in a decrease of flow from the pump due to its pressure compensator characteristic, which decreases flow as pressure increases. Thus, an increase in the displacement of pump, A, decreases the flow to the actuator, whereas a decrease in the pump displacement increases the flow to the actuator.

The use of a transformer eliminates the throttling losses since no valves are required to control the actuator. However the benefit of using such a transformer is limited by itself. One reason is that the total efficiency of a transformer is less than the efficiency of a single pump/motor with same specifications since the transformer includes two piston units. The other reason is that the efficiency of the transformer also depends on loading conditions. A piston pump/motor usually has the highest efficiency only when it works under the rating loading condition (rating flow rate and pressure). The total efficiency of a piston pump/motor decreases when it works under partial loading conditions (small flow rate and/or low pressure) since the inner friction and/or leakage become significant. For a transformer, at most of operating points, at least one of the two units operates under partial loading condition. This operating condition makes the pump/motor unit work in a low efficiency region and the whole efficiency of the transformer is decreased.

In order to increase the component efficiency, a new type transformer has been developed by Innas (hereafter referred to as IHT) [Vael et al., 2000]. The main difference between the conventional and IHT transformers is that the two axial piston units in the conventional transformer are replaced by one axial piston unit which has three ports (shown in Figure 1.8), one is the supply port connected to the pressure net, the second one is the load port connected to the load and the third one is the tank port. The transmission ratio (P_{system}/P_{load}) as well as the output flow of the transformer can be varied by changing the control angle (between a reference point on the port plate and the “top dead center”

position of the plungers in the cylinder barrel). The details about the IHT can be found in [Vael et al., 2000; Malsen et al., 2002]. The efficiency of the IHT is higher than that of a conventional transformer because no real partial load conditions occur.

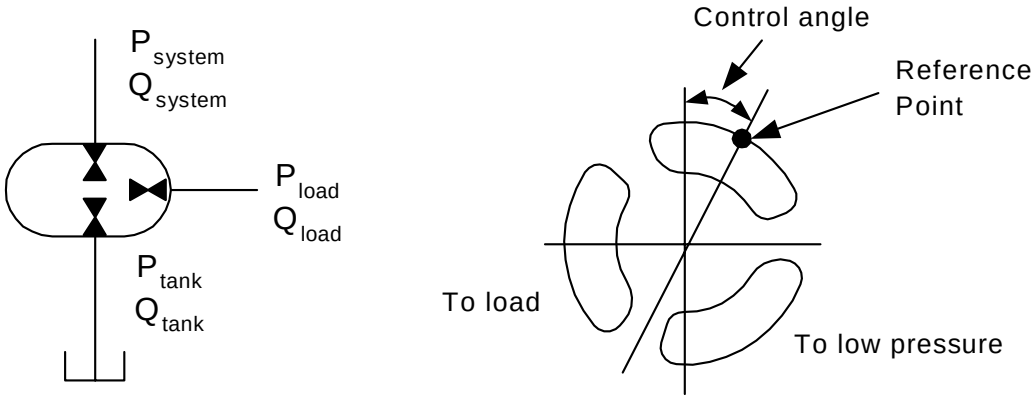

Figure 1.8 Schematic and port plate of an IHT transformer

1.2.4 Power Supply Control

Instead of changing the displacement of the pump, the power supply control method changes the delivery flow rate of a fixed displacement pump by changing rotational speed. An energy saving power source proposed by Nakano and Tanaka [Nakano and Tanaka, 1988; Tanaka et al., 1989] is shown in Figure 1.9, in which a fixed displacement pump is driven by an induction motor that uses a frequency converter to control the rotational speed. In this system, the flow rate is nearly proportional to the converter frequency. Because the inertia of the induction motor is so large that it cannot respond rapidly to the demanded input, the pump could not supply the demanded flow rate to the load during the transient. To solve this problem, an accumulator was used to provide supplemental flow to the system in the transient condition. The principle of this system is similar to a pressure compensated pump. The rotational speed of the pump is controlled to supply the necessary amount of oil to the system, and to maintain the system pressure at a certain constant level without the use of a relief valve. In order to maintain the system pressure at a constant value, the system pressure is sensed and fed back to a frequency converter controller by

which the rotational speed of the induction motor is controlled. When compared with the conventional constant flow hydraulic power source (such as shown in Figure 1.1(a)), the use of the frequency converter drive demonstrated a 36% saving of the total power.

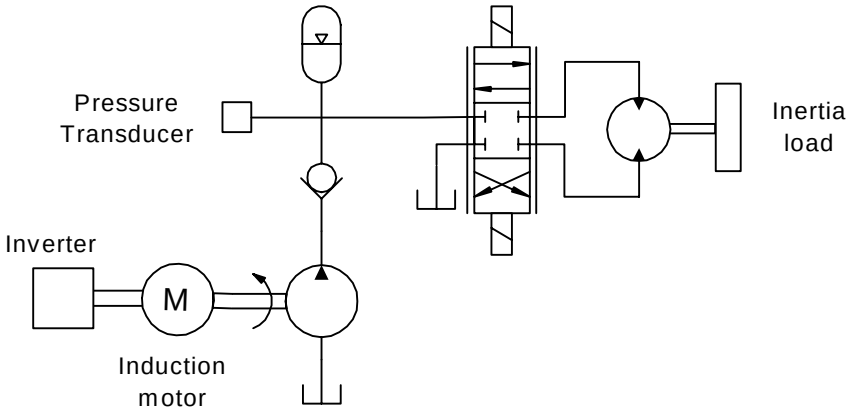

Figure 1.9 Energy-saving power source with inverter-motor drive

[Nakano and Tanaka, 1988]

The pumps of most mobile hydraulic systems are directly driven by diesel engines. An innovative approach to high efficient drive is to use a “hydraulic free piston engine” in a mobile hydraulic system [Vael and Achten, 1998]. A hydraulic free piston engine combines a diesel engine and a hydraulic pump into one compact component. The piston assembly contains a combustion chamber on one side and a hydraulic piston pump chamber on the other side. The combustion piston assembly moves linearly back and forth between the left and right extreme as a result of diesel combustion. Simultaneously the hydraulic piston cycles and directly produces hydraulic energy. An application of a hydraulic free piston engine can be found in a forklift truck in [Vael and Achten, 1998]. The hydraulic power for wheel drive, lift and tilt systems are provided by a hydraulic free piston engine. Because of the small number of parts, high power to weight ratio and better efficiency, it was suggested that this unit was a good alternative to the conventional diesel hydraulic power unit. However, a study by Tikkanen et al. [2001] showed that the lack of crank mechanism may affect its use. When compared with the conventional engine-pump

combination, control systems were more complicated and the controllability of the output was poor because of its constant pump displacement.

Usually there is only one power supply unit and one pump in a hydraulic system. The best system efficiency can be achieved when only one function is carried out at one time or when two or more simultaneous functions have the same pressure requirements. However, if a hydraulic power source consists of multi pumps, this configuration can improve the efficiency since more combinations can be used to meet the flow demand. For multi-pump systems in which pressure levels of simultaneous functions vary, actuators with approximately equal average pressure level can be placed in a same pump system. However, a question arises as to how many pumps should be used in a system. A study for a forest machine by Kappi [2000] showed that the change of power efficiency from one pump to two pumps was considerable; however, the improvement of efficiency from two pumps to three pumps was only marginal and considering financial aspects, hardly worthwhile.

1.2.5 Accumulator and Energy Reutilization

The energy saving methods and strategies discussed above are only designed to decrease power losses in a hydraulic system. Another effective way to improve overall system efficiency is energy reutilization. The simplest way to reutilize the energy is the usage of an accumulator in which the energy is stored and discharged. An accumulator is an essential component in many power efficiency systems. Burgt and Post [Burgt, 1993; Post and Druten, 2001] applied a new energy saving concept to a situation in which a cyclic load occurs. They used a pump and accumulator combination to achieve what was defined as a “Learning Hydraulic System” (shown in Figure 1.10). This system consists of a switchable constant delivery pump and a switchable accumulator. The pump and accumulator are optimally switched to meet the requirement of loading conditions which are detected by a load characterization program. This system can meet the load flow

requirement by operating on/off valves and proportional relief valve.

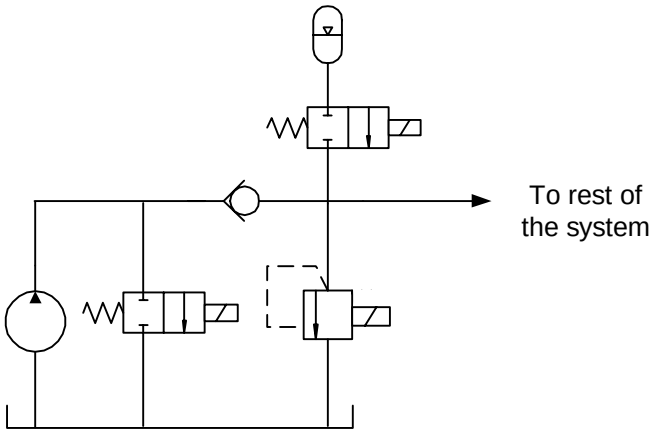

Figure 1.10 Learning hydraulic system [Post, 2001]

In some applications such as lifting hydraulic systems, accumulators are used in an independent circuit without other power sources. In an application studied by Liang and Virvalo [2001 (2)], a system consisting of an accumulator and a balance cylinder, schematically shown in Figure 1.11, is used to drive the joint of a crane together with a load-sensing system. In this application, the accumulator is connected to a balance cylinder, B, that gives a lifting force proportional to the pressure in the accumulator. During a duty cycle, for the downward movement, the load force, including the gravitational force of the load and crane arm, is overrunning; the accumulator is charged and produces a resistive force to the movement of the load. For the upward movement, the load force is resistive; the accumulator is discharged and produces a positive force to lift the load together with cylinder A, driven by a load-sensing system. The power produced by the accumulator during the upward movement is recovered energy. The pressure of the relief valve must be set less than the pressure generated by the weight of the load and crane arm during a duty cycle, in order that it can be possible to lower the crane arm by the weight without applying an extra hydraulic power to force it down. Results show that this drive concept can improve energy utilization and, as a result, reduce the power consumption.

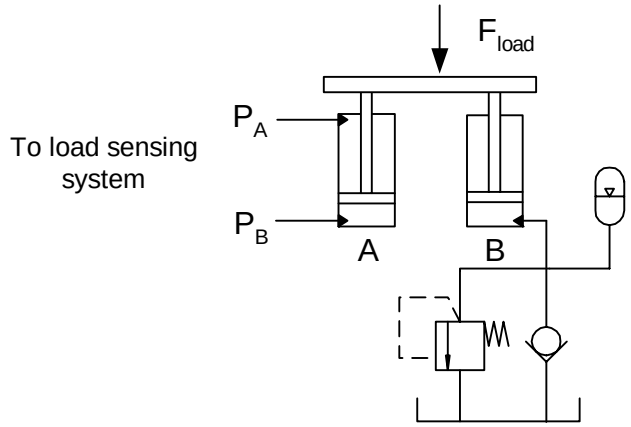

Figure 1.11 Schematic of an energy reutilization system

[Liang and Virvalo, 2001 (2)]

Another way to reutilize energy is to drive other loads in the same circuit with recovered energy. In many hydraulic systems using multiple pumps, pumps are driven by the engine through a common driven shaft or a multiple output gearbox. When the energy is recovered from lowering the load or braking the vehicle, the pump works in a "motoring" mode, and converts the energy to the torque that acts on the driven shaft. The recovered torque can be used to drive other loads.

In a study on a Caterpillar 330B hydraulic excavator, Wendel [2000, 2002] used an energy storage system consisting of an accumulator and a pump/motor to store the recovered energy and to convert it to a torque acting on the driven shaft (schematically shown in Figure 1.12). The pump/motor is connected to a multiple output gearbox together with other pumps. Results show that the regenerative system, which eliminates the metering valve losses in actuating loads and recovers energy rather than dissipating it when lowering or decelerating a mass [Wendel, 2002], can reduce power consumption up to 46% for this system studying. This design can improve overall efficiency, as well as reduce the size of the engine.

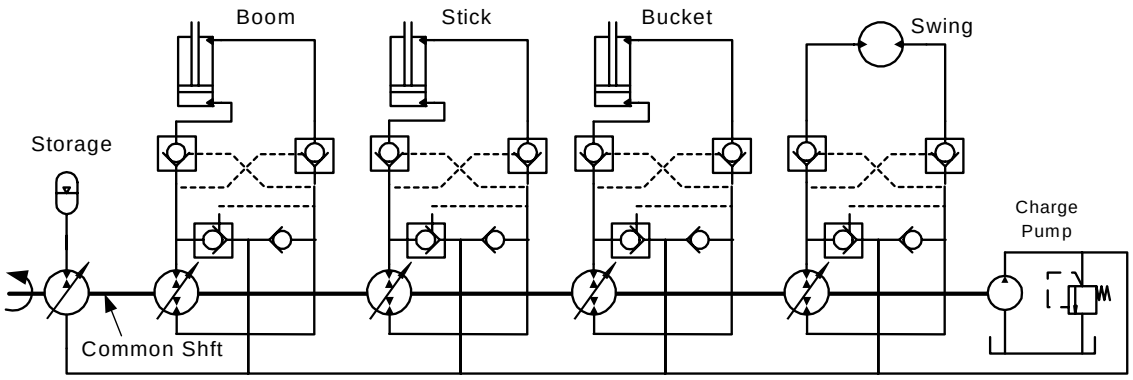

Figure 1.12 Regenerative circuit for the HE330E [Wendel, 2002]

1.3 Dynamic Performance of Hydraulic Systems

Circuit efficiency is very important for all hydraulic systems. However, for many systems (such as position and speed control systems), the dynamic performance is also a very important performance parameter.

The dynamic performance of a hydraulic system can be affected by many factors, such as the circuit configuration and component selection. A large fluid volume between the actuator and hydraulic control component, (long hoses, or accumulators), can result in a slow transient period of the output actuator from start to steady state conditions. Different types of hydraulic components display different dynamic performance. For example, a servo valve exhibits a faster dynamic response (smaller transient period) compared with that of a solenoid valve. Hence, the selection of the hydraulic component definitely has an effect on the performance of a hydraulic system. A further factor enters here in that the dynamic performance of a hydraulic control component (such as proportional valves and servo valves) is also affected by the design of the controller driving these components. The loading conditions and actuator performance also have an effect on the dynamic response of the complete system.

To facilitate a discussion on the compromises that often must be made between efficiency and dynamic performance, the control of the rotational speed of a hydraulic

motor under a resistive load is considered. There are many hydraulic circuit configurations which can be used to control the rotational speed of the motor. For example, both pump controlled and valve controlled motor configurations introduced in the last sections can be used to realize the load requirement.

As mentioned, the most efficient hydraulic system is a pump controlled system since there is no power loss between the pump and motor; however, because of the very fast transient response of servo valves, the valve controlled system can display the best overall dynamic performance when both the transient period and overshoot are considered. The following sections will consider the dynamic response of valve-controlled versus pump-controlled systems.

1.3.1 Dynamic Performance of Valve Controlled Systems (Constant Flow Supply)

Figure 1.13 shows a valve controlled motor system. In this system, a servo valve is used to vary the rotational speed of the hydraulic motor. The pump supplies a constant flow rate to the system which matches the maximum load flow requirement. For this discussion, the flow to the load is assumed to be less than the maximum flow capacity of the pump. The excess flow from the pump is bypassed to tank through a relief valve when the load flow is less than the pump flow. The system pressure is determined by the relief valve setting since it is always in open state to bypass the excess flow. This configuration often displays a fast dynamic response because of the use of the servo valve as the component to modulate the flow; servo valves are well known for their superior transient performance.

The response of this kind of system is essentially dependent on the response of several of the circuit components. Typically, the rise time of the relief valve flow rate is in the order of 10 ms [Yao, 1997], and that of the servo valve (Model: Moog 760) is between 6 and 16 ms depending on the rated flow rate [760 Series Servo valve, Moog Inc.]. Thus, a typical response time for the pump, relief valve and servo valve combination is also of this

order and in many cases is much less than the dynamic characteristics of the load itself.

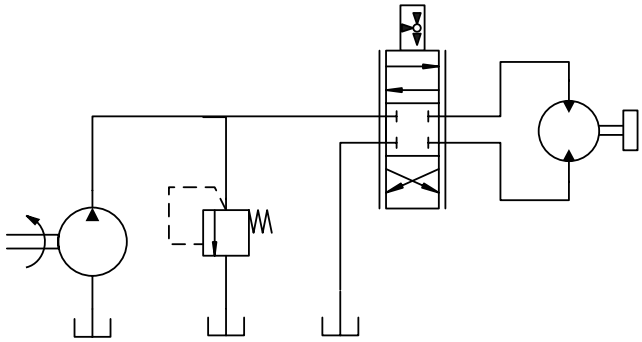

Figure 1.13 Valve controlled motor system with a constant flow supply

The difficulty with this configuration is that in order to achieve the best dynamic performance of the servo valve, the pressure drop across the valve must be higher than 6.9 MPa [Merritt, 1967]. This value is very component sensitive but 6.9 MPa is typical. Because the upstream pressure from the relief valve is constant, the pressure drop across the valve can be much larger under low loading conditions. Despite the excellent transient response characteristics, a very large disadvantage of this system is the low efficiency due to the dramatic pressure losses that can occur across both the flow modulating valve and the relief valve.

1.3.2 Dynamic Performance of Valve Controlled Systems (Demand Flow Supply)

A slight variation of the circuit (Figure 1.13) is one in which the pump and relief valve are replaced by a pressure compensated pump (Figure 1.14). This circuit is more efficient than that shown in Figure 1.13 because the pump only supplies the flow demanded by the valve; thus the losses across the relief valve are avoided. The pump compensator is a pressure sensing system, which destrokes the pump (reduces flow) when the pressure exceeds a preset value. It is called a “demand flow” system.

A typical pressure compensated pump (model: Vickers PVB5) was studied by You [1989]. You found that the rise time of the pump swashplate (and hence output flow) was in the order of 30 to 50 ms, and the settling time, about 60 ms. Thus both the pump-relief

valve and pressure compensated pump configurations have response times that are comparable with each other for common loading conditions. However, as mentioned above, the demand flow system is more efficient.

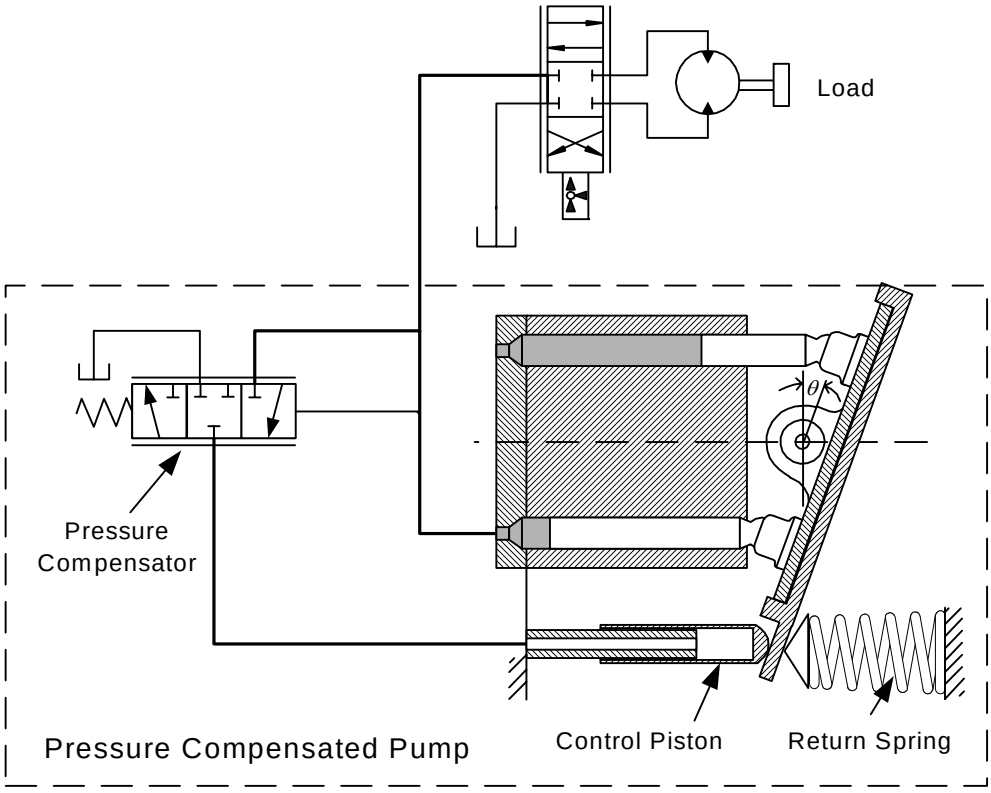

Figure 1.14 Valve controlled motor system with demand flow supply

1.3.3 Dynamic Performance of the Pump Controlled System

The dynamic performance of the valve controlled system with a demand flow supply (pressure compensated pump) not only depends on the performance of the flow modulation valve, but also on the performance of the pump. If the dynamic response of the valve is much faster than that associated with the pump swashplate (which it usually is), the system dynamic performance will be primarily dictated by the pump performance. Thus, to improve the pump response and hence the overall system response, other means to actuate the swashplate other than from an internal pressure compensator, could be considered. Mack [1985], for example, used a step DC motor attached directly to the

swash plate to do exactly this.

If the flow modulation valve is now removed from the circuit and an external driver used to directly control the pump swashplate, the valve controlled motor system shown in Figure 1.14 is converted to a pump controlled motor system. In addition, if a pressure transducer is used to feedback an appropriate signal to a controller to limit the system pressure, the pump controlled system can realize most functions of the valve controlled system with the same dynamic performance if the loading conditions are the same and if the dynamic performance of the external swashplate controller is the same as that of the flow modulation valve.

The advantage of the pump controlled motor system is the high efficiency due to the elimination of the pressure loss across the flow modulation valve. The disadvantage of this kind of system is that an additional power supply is required to actuate the external swashplate controller. This, however, is compensated by the removal of the power source for the control valve.

For the pressure compensated pump (shown in Figure 1.14) or other similar pumps, the dynamic response of the pump swashplate angle (or pump flow rate) mainly depends on torques acting on the swashplate. Large driving torques on the swashplate are required to accelerate the swashplate to its desired position. In existing pressure compensated pumps, the torque is controlled by the system pressure and effective area of the compensator control piston. Due to limitations of most pump structures and other design considerations (such as the pump stability), the total torque applied on the swashplate by the pump controller is limited. This, in essence, defines the upper limit on the dynamic response of most pressure swashplate actuated pumps.

There exists, then, the opportunity to improve the dynamic response of the pump controlled system by using an approach other than electro-hydraulic control of the swashplate, such as using an electrical motor to directly control the pump swashplate. It is

anticipated that the dynamic response of the pump swashplate should be increased by using some other swashplate control approach. This, then, is one of the motivations for this research.

Another issue that needs to be noted is the response of inertial loaded systems to flow rate changes in both the valve and pump controlled systems. The inertia of a load will usually result in an overshoot in the desired steady state value, especially if damping is limited. A valve controlled system can compensate for this because the valve introduces a controlled resistance downstream of the actuator. Unless the pump controlled system is a closed system (hydrostatic system), this overshoot cannot be compensated for by the pump itself. Thus, a pump controlled system with rapid transient response properties may show significant stability issues. This situation must therefore be considered when performance versus efficiency is examined.

1.4 Research Objective

In the past few years, considerable effort has been made to improve the power efficiency of hydraulic systems; many energy saving strategies have been successfully developed and used. However, most of them can only be useful in specific applications. For instance, displacement control and secondary control only focus on those systems in which the efficiency concerns are more important. Although these systems have very high efficiency, they are not designed for applications in which the flow rate is varied during the duty cycle. Compared with pump controlled systems and other energy efficient systems, the valve controlled system demonstrates good dynamic performance and controllability especially for inertia dominated loads but at the expense of power efficiency. For hydraulic circuits which employ load-sensing systems for example, the design objective has been made to combine the advantages of high dynamic performance with better energy utilization. However, this high efficiency can only be obtained under particular operating conditions, such as single-load or multi-loads with similar load

pressure requirements. No one approach is available for general system design where both good dynamic performance and high-power efficiency are important.

The general objective of this study was to develop a specific hydraulic circuit configuration and the appropriate controllers for a pump - motor hydraulic system that will yield: 1. similar dynamic performance than that of a valve-controlled system, and 2. circuit power efficiency comparable to that of a pump-controlled system but superior to that of a valve-controlled system. The specific objectives of this study were: 1. to establish the "proof of concept" of the proposed hydraulic circuit and control system through simulation, and 2. to experimentally assess the dynamic performance and efficiency of the proposed hydraulic circuit. This can be realized by improving the performance of an existing pump-controlled system without sacrificing its overall high efficiency. The total power efficiency of the new developed circuit may be slightly less than the conventional pump-controlled system, but more than a valve-controlled system; however, the performance should be at a level equivalent to a valve-controlled system.

The overall efficiency of a hydraulic circuit is affected by the component selection and circuit configuration. To simplify the analysis and calculation, this study only focuses on the relative circuit efficiency in which the efficiencies of components are not considered. The term "relative efficiency" is used hereafter to describe the power efficiency of the hydraulic circuit without considering the efficiencies of hydraulic components. For a pump-controlled motor system, the relative efficiency represents the power efficiency of the circuit between the pump outlet and hydraulic motor inlet.

1.5 Thesis Outline

The thesis is organized as follows. A pump-controlled hydraulic system with electric interface is described in Chapter 2. In chapter 3, the mathematical models of the DC motor and pump is tested and modified based on the experimental results. Based on this model, a controller is designed for the DC motor which controls the swashplate of the pump. In

Chapter 4, a bypass flow control system is added to the pump-controlled system to improve the dynamic response. A controller is designed for the bypass flow control valve. A series of experimental tests under different loading conditions are presented in Chapter 5 to verify the new energy saving approach proposed in the previous chapter. Some conclusions and recommendations for further work are provided in Chapter 6.

Chapter 2

Proposed Circuit Configuration and Experimental Set

The first specific objective of this study was to develop a hydraulic circuit with both high dynamic performance and high relative efficiency. The basis of this circuit is a pump-controlled system which has high efficiency. The purpose of this chapter is to give an overall description on the operation and configuration of this novel circuit configuration.

2.1 Circuit Overview

The proposed hydraulic circuit was a rotational speed control system as shown in Figure 2.1. It mainly consisted of a variable displacement axial piston pump, a fixed displacement motor, a flow modulation valve and two relief valves.

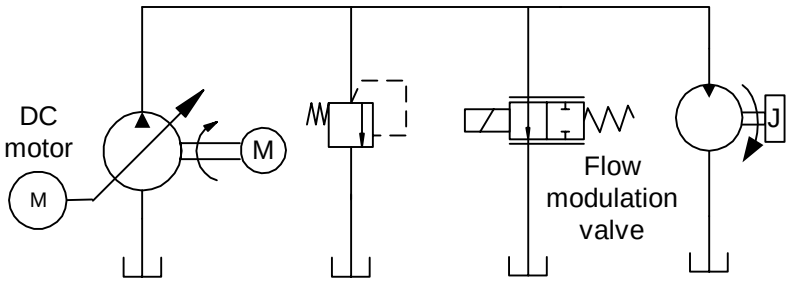

Figure 2.1 Pump-controlled system with the bypass flow control

Unlike traditional variable displacement, axial piston pumps, the angle of the swashplate was controlled by a DC motor whose output shaft was directly attached to the swashplate through a pintle. It was anticipated that using the direct DC motor drive should increase the response of the pump swashplate. The flow modulation valve, which functioned as a bypass flow modulation valve, was used to remove or minimize the

overshoot of the hydraulic motor rotational speed after the transient. The bypass modulation valve was opened only during the overshoot and was closed under the steady state conditions. The total relative efficiency of the system would be comparable to a pump controlled motor system since there was no power loss between the pump and motor. The following sections will discuss in details the rationale for this particular approach.

2.2 Pump Displacement Control

Hydraulic pumps are used to convert the mechanical energy transmitted by a prime mover to hydraulic energy. The type of pump mostly used in hydraulic circuits is a positive displacement pump. Although there are many types of pumps which are used in hydraulic applications, this research only concentrates on axial piston pumps because of their high efficiency and high operating pressure capabilities.

2.2.1 Variable Displacement Pump

The most common way to vary the flow rate of a pump is to vary its “displacement” or “piston stroke” when it is operated under a constant rotational speed. A variable displacement pump is designed such that the displacement can be varied from zero to some maximum value while the pump is operating. One such pump is the variable displacement axial piston pump.

A variable displacement axial piston pump basically consists of a cylinder barrel, valve plate, pistons with shoes, shoe plate, an adjustable swashplate and swashplate control mechanism (Figure 2.2). A series of cylinders are mounted parallel to the axis rotation. The swashplate remains stationary while the barrel rotates with the drive shaft. When the swashplate is at an angle to the shaft, the pistons move back and forth in the cylinders as the barrel rotates. The cylinder port is connected to the suction port of the valve plate as the volume of the cylinder chamber is increased. When the volume of the cylinder chamber is decreased, the cylinder port is connected to the discharge port of the

valve plate. The suction port is connected to the pump inlet and the discharge port is connected to the pump outlet. During one revolution, a cylinder charges fluid through the suction port then discharges it through the discharge port.

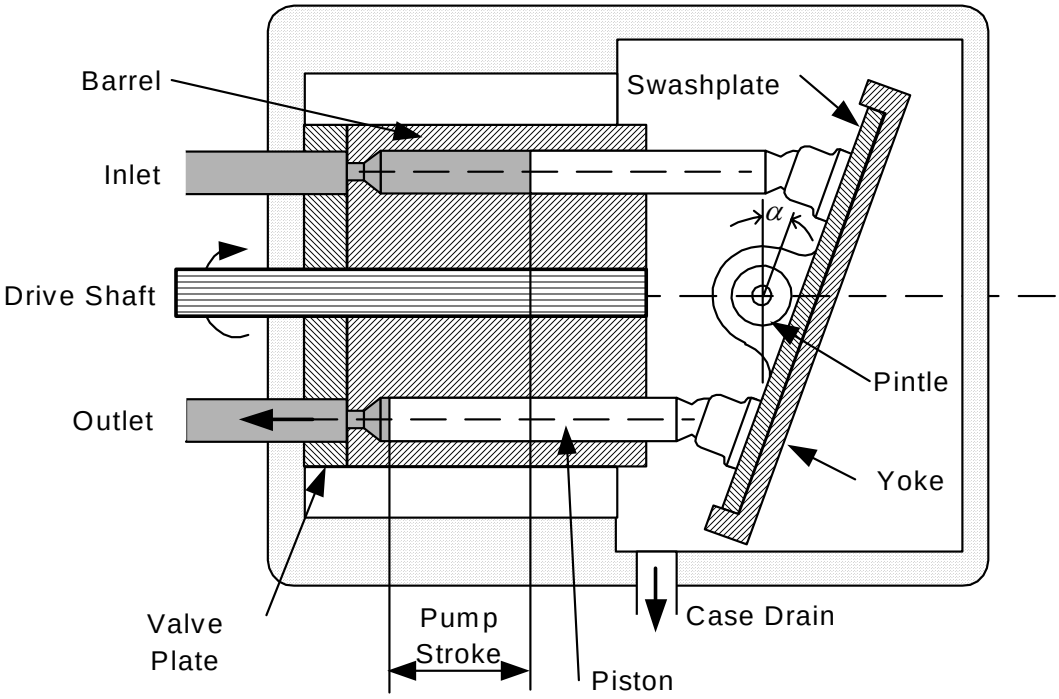

Figure 2.2 Schematic of variable displacement piston pump

The swashplate of a variable displacement piston pump is fixed on a yoke that rotates about the yoke pivot on two short shafts (called a pintle). Changing the angle of the swashplate can change the piston stroke. Since the displacement of the pump is proportional to the piston stroke, the displacement can be changed by varying the angle of the swashplate or yoke.

2.2.2 Pump Displacement Control

The most common way to change the displacement of the pump is to use a hydraulic valve (or compensator) to control the hydraulic force acting on the swashplate (as previously shown in Figure 1.14). The position of the swashplate is normally controlled by

a control piston. The “pressure” force applied to the swashplate by the control piston is balanced by a return spring. Changing the control pressure of the piston can change the angle of the swashplate. In the absence of control pressure, the swashplate will be located at its maximum angle (initial position) by the spring force. This is designed to build the pressure quickly during pump start-up.

This research used another approach to vary the angle of the pump swashplate. A DC motor was directly coupled to the pintle of the swashplate as shown in Figure 2.3. It was anticipated that a DC motor should provide a more rapid dynamic response to the pump swashplate. The reason for this anticipation was that the maximum torque provided by the DC motor was about 60 Nm [HT-High Torque, Direct Drive Series], which was much higher than the torque generated by its hydraulic counterpart (13 Nm to fully destroke the pump). Then, the dynamic response of the pump flow rate should be increased. Further, it was much easier to integrate a DC motor to an electronic feedback circuit. This design strategy provided a means to apply sophisticated electronic control algorithms to the DC motor controller.

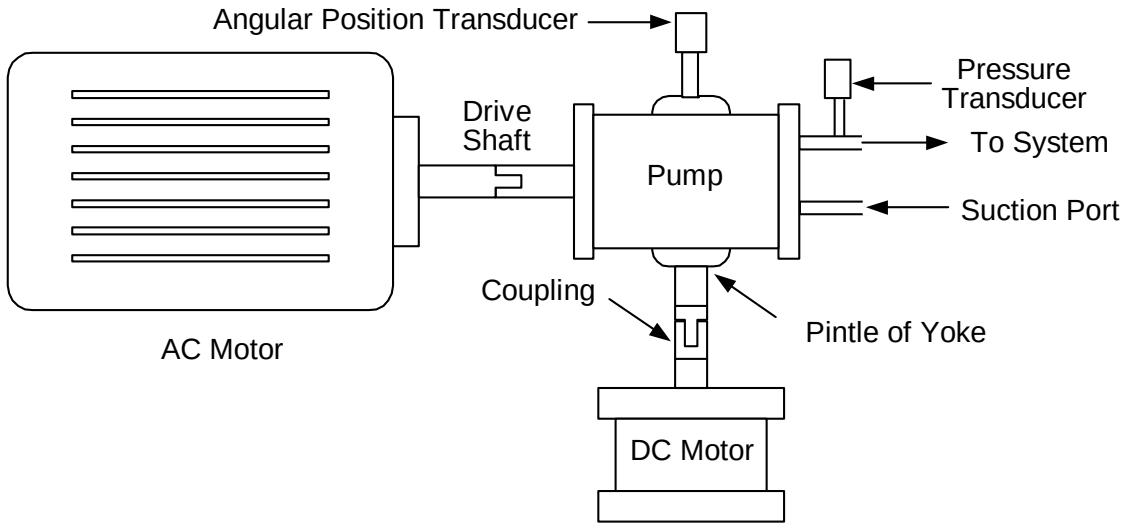

Figure 2.3 Direct swashplate control with a DC motor

Since all pumps are not designed to connect a DC motor, a general variable displacement piston pump was modified for this purpose. As illustrated in Figure 1.14, the control piston in a regular piston pump can only act on the swashplate in one direction (decreasing the swashplate angle); therefore, a return spring must be used to balance the hydraulic force applied to the swashplate by the control piston. The return spring is also used to rapidly build up the system pressure by locating the swashplate at the maximum angle during pump start-up, otherwise the control piston cannot work properly due to the lack of pressure. Since a DC motor can generate the torque in two rotational directions, the control piston and return spring were no longer necessary for a DC motor controlled pump and were removed. The pintle of the yoke was directly connected to the shaft of the DC motor; hence the angle of the swashplate was directly controlled by the DC motor instead of the control piston. Because there was no return spring in the pump, the torque generated by the DC motor was mainly used to overcome the friction torque and the “back” torque [Kavanaugh, 1987] produced by the pump pressure.

An advantage of using a DC motor is that the swashplate can be initially located at any angular position, even at zero position. It is much easier to control the initial flow rate of the pump and to build the system pressure using this design.

2.3 Hydraulic Circuit Design

2.3.1 New Concept Hydraulic Circuit

Valve-controlled hydraulic systems usually imply that the flow rate of the actuator is directly controlled by the valve orifice located before or after the actuator. A meter-in flow modulation (orifice 1) and a meter-out flow modulation (orifice 2) shown in Figure 2.4(a), can be used individually or together. The most common situation is that the meter-in and meter-out controls are used together to get a higher damped natural frequency and higher stiffness [Merritt, 1967]. The main factor which affects the damped frequency of a hydraulic circuit is the volume of the hydraulic lines and the actuator.

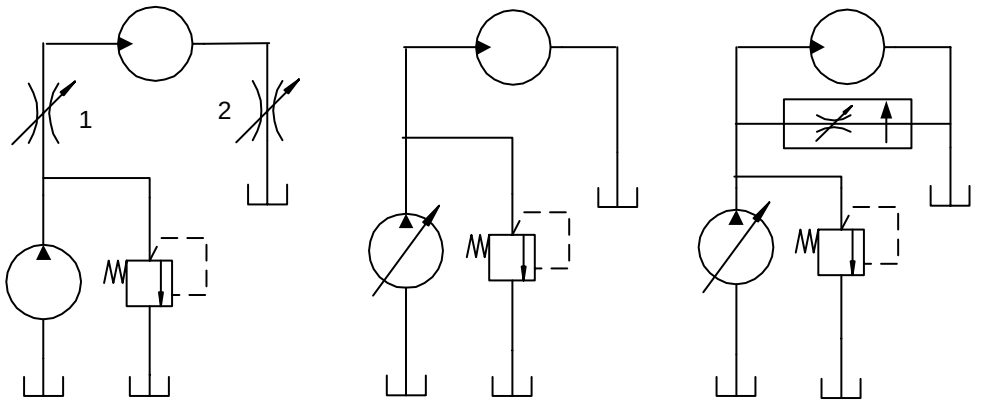

(a) Meter in/out flow control (b) Pump control (c) Bypass flow control

Figure 2.4 Schematic of valve and pump controlled systems

Removing the flow modulation valve from the hydraulic lines and replacing the fixed displacement pump with a variable displacement pump, the valve-controlled system changes to a pump-controlled system (Figure 2.4(b)), in which the actuator is directly connected and controlled by a variable displacement pump. The pump-controlled system is energy efficient since there are no system dependant losses associated with throttling flow between the pump and actuator.

The DC motor driven pump allows the pump to stroke rapidly which allows pressure to build up rapidly, which in turn accelerates the load. Once the system has accelerated, the hydraulic motor can overshoot its position due to the inertia of the fluid, overshoot of the swash plate (if not at the maximum or minimum flow) and the inertia of the load. The overshoot of the motor rotational speed can be very large depending on the overshoot of the pump swashplate, pressurized fluid volume and load conditions. To solve this problem, a bypass flow modulation system (see Figure 2.4(c)) is introduced to remove the overshoot of the motor rotational speed. When the bypass flow modulation system detects an overshoot of the rotational speed, the bypass valve is opened to bypass the excess flow.

The reasons why the bypass flow control system can reduce the load overshoot are as follows:

- The bypass valve can bypass the excess flow from the pump when the pump swashplate demonstrates an overshoot during the transient. The pump flow overshoot partially results in a load overshoot.
- The pressure at the motor inlet is reduced due to the opening of the bypass valve.
- From the viewpoint of the hydraulic motor, the bypassed fluid can be considered as an increased motor leakage which increases the damping ratio of the motor.

This new concept hydraulic circuit is efficient since the motor rotational speed is mainly controlled by a variable displacement pump; the power loss across the bypass valve is very small since the bypass control valve only opens during the transient. Further the effective dynamic response and effective stability of the circuit is improved because the bypass flow control valve can remove or minimize the overshoot and allow the system to reach the steady state faster when the system undergoes a transient response.

2.3.2 Principle of the Hydraulic Circuit

The main objective of this study is to establish “proof of concept” for this proposed circuit through mathematical modeling, simulation and experimental tests. A brief explanation of the system operation which will achieve this objective is explained in this section.

The stroke of the variable displacement pump is controlled by a DC motor. This control strategy is anticipated to increase the dynamic response of the pump flow rate. However, under certain loading conditions, a fast response can result in undesirable stability problems, such as oscillatory response or limit cycle oscillations. For example, a large gain on the DC motor controller can be used to reduce the rise time of the motor response for a large load (large system load pressures). But if the load decreases (lower pressure conditions) and the gain stays the same, the system can become unstable or

exhibit limit cycle oscillations. Thus the gain must be lowered until an acceptable rise time is accomplished. In essence, the gains of the pump controller can be strongly dependent on the pump pressure. Hence a nonlinear controller would be desirable. The principle of the nonlinear pump controller design would be based on the premise that the gains of the controller would automatically adapt to the changes of the system pressure so that the pump would work at different pressure levels and give acceptable output performance.

Although a large gain for a large load can improve the rise time, it also would result in a large overshoot in the pump flow (via the pump swash plate dynamics) and load rotational speed. The overshoot of the rotational speed is a consequence of the dynamic response difference between the pump flow and actuator response. If the actuator responds slower than the pump swashplate, the pressure will quickly rise and the system deadheads or flow goes over a relief valve. The pressure on the motor accelerates the load until the pump flow equals the flow into the motor. Ideally, at this point, the acceleration of the load should decrease to zero and the pressure should decrease to steady state values (dictated by friction etc.). However, due to the compressibility of the fluid, the pressure decline is not instantaneous but is at some slower decreasing function. Consequently, the load overshoots its steady state rotational angular velocity value. The pressure now suddenly decreases because the effective flow into the motor exceeds the actual flow in from the pump; friction or back pressure on the motor slows the system rotational speed until pump flow and motor flow are reestablished (steady state conditions). The overshoot can also be compounded by any overshoot that occurs in the swashplate system.

Instead of passing all fluid to the load, it is proposed that the surplus fluid from the pump or expanding fluid in the lines, to the load be directed to tank. Hence the philosophy of this design is: use a nonlinear controller to minimize the rise time according to the load conditions, and to bypass the fluid to tank when overshoot occurs. Unfortunately, for most systems, if a large overshoot occurs, then it is very likely that an undershoot will also be

present. The undershoot means that too little flow is reaching the load from the pump, and that the pressure has not recovered enough to re-accelerate the load to its steady state point. One solution is to have a “make up” circuit add fluid during this part of response to maintain system pressure. Although this approach was appealing to reduce the undershoot, preliminary design considerations indicated that the circuitry to accomplish this task was very complex and hence was not attempted in this study. However, preliminary test studies also revealed that if the overshoot was reduced, the undershoot followed accordingly.

The bypass of the fluid was to be realized using a bypass valve which in itself had a fast dynamic response (compared to the speed of response of the motor system). When the bypass valve controller detected an overshoot of the load response during the transient, the valve was opened to bypass the surplus flow (due to the expansion of the compressed fluid or overshoot of the pump swashplate) to tank and reduce the motor overshoot. During the steady-state operation, the valve was closed to save power. By using both nonlinear swashplate control and bypass flow control, it was anticipated that the dynamic response of the pump would be improved, a stable response of the motor rotational speed would result and the total efficiency of the system would approach that of the pump controlled system because the valve would be open only during the transient response.

2.3.3 Hydraulic Circuit Design

The hydraulic circuit designed for this research was a speed control system (Figure 2.5). It consisted of a variable displacement axial piston pump, a fixed displacement motor, two relief valves and a flow modulation valve. The prime mover of the pump was a constant speed AC motor. The swashplate angle was controlled using the direct drive DC motor described previously in section 2.2.2. For the purpose of safety, a relief valve (valve 1) was used to limit the system pressure. Another relief valve (valve 2) was used to simulate a resistive load. A flywheel was connected to the shaft of the hydraulic motor to provide an inertial load. A servo valve was used as the flow bypass valve due to its fast response.

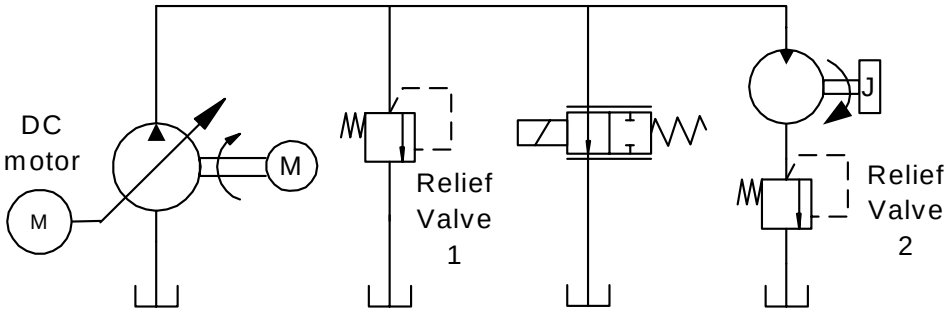

Figure 2.5 Pump-controlled system with bypass flow control

The components used in this hydraulic circuit are listed in Table 2.1.

Table 2.1 Hydraulic components of the circuit

Name	Type	Company	Model
Pump	Variable displacement	Vickers	PVB5
DC Motor	Permanent magnet servo motor	Emoteg	HT05005
Relive valve	Two stage relief valve	Vickers	Ct 06 F 50
Bypass valve	3 position 4 way servo valve	Moog	760-233A
Hydraulic motor	Fixed displacement piston motor	Sundstrand	15-3021 MF

The flow rate range of the experimental tests was between 0 and 3.15×10^{-4} m^3s^{-1} [5GPM], which was the maximum flow rate of the pump. The pressure range was between 0 MPa and 13.8 MPa.

2.4 Electrical Interface and Measurement System

A closed loop control system was required to enable the DC motor to accurately control the swashplate angle. The feedback signal was the angular position of the shaft. By means of the controller, the flow rate of the pump was approximately proportional to the input signal to the DC motor. The block diagram of the DC motor control is shown in Figure 2.6.

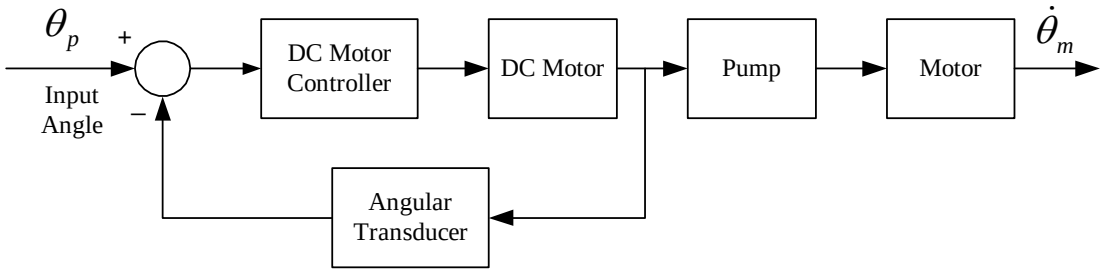

Figure 2.6 Block diagram of DC motor control

The electrical interface and measurement system design are shown in Figure 2.7. The data acquisition system (DAQ) collected the appropriate signals through different transducers installed in the system. These included pressure, angular position, flow rate and angular speed transducers. The calibration of the DAQ and transducers can be found in Appendix A. All the data collected by the DAQ were processed by a computer program which also functionally worked as a controller. The computer also output the control signals to amplifiers which controlled the DC motor and servo valve through the output channels of the DAQ.

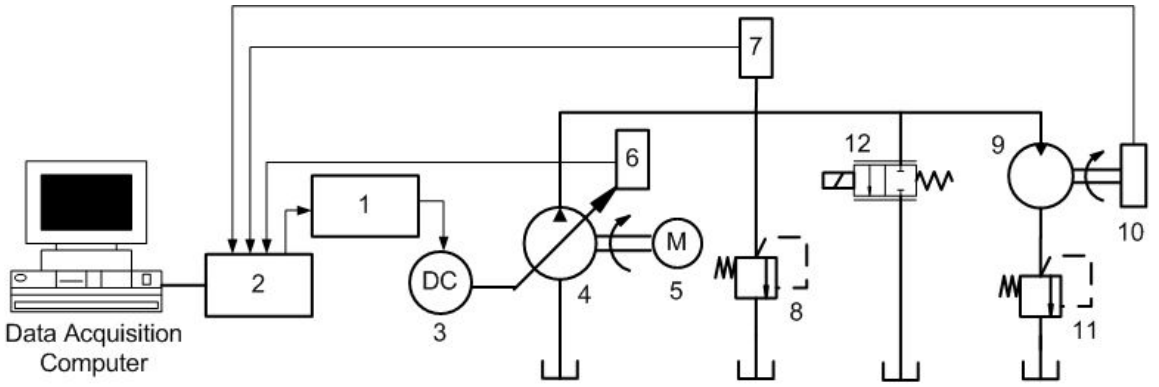

Figure 2.7 Electrical interface and measurement system design

In summary, a pump controlled hydraulic motor system was to be designed to achieve high system relative efficiency. It was anticipated that the dynamic performance of this system would be improved in two ways. The first was to increase the dynamic

response of the pump flow rate by controlling the pump swashplate using a DC motor. The second was to reduce the overshoot by using a bypass flow control system. The bypass control valve would only be opened during the transient and be closed during the steady state. The details of the DC motor controlled pump and bypass flow control are discussed in the following chapters.

2.5 Definition of Dynamic Response Specifications

To evaluate the performance of the hydraulic system proposed in Section 2.3, several performance indicators are defined in this section which will be adopted in the rest of this thesis. Figure 2.8 shows a typical dynamic response of the hydraulic motor (in terms of its rotational speed) under a step input signal.

The specifications for evaluating the performance of the dynamic response are illustrated in the figure. The definitions of some of the specification terms in the figure are given as follows.

Steady State Value

In this study, most of measured system output signals (such as the rotational speed, system pressure and swashplate angle) reached steady state but with a non-uniform but periodic ripple superimposed on it. Hence, the steady state value is calculated using an average value in this study. It is defined as follows:

$$X_{SS} = \frac{1}{n}\sum_{i=1}^{n} x(i) \tag{2.1}$$

where x is a series of measured data after the transients die down.

Rise Time

In this study, the rise time, as illustrated in Figure 2.8, is defined as the time required for the dynamic response to cross over the final (steady state) value the first time after a step signal input. The value of the rise time reflects the rate of the dynamic response.

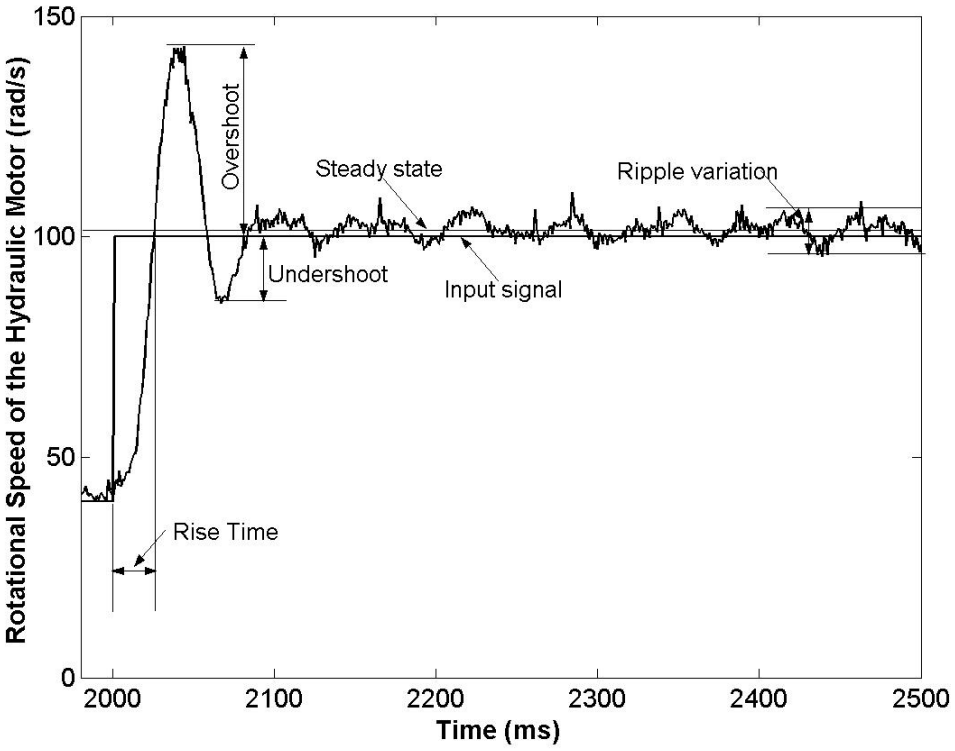

Figure 2.8 A typical response of the hydraulic motor rotational speed

Overshoot and Percent Overshoot

The overshoot equals the peak value subtracted by the steady state value. The percent overshoot is defined as the ratio of the overshoot to the increment of the measured signal from the initial value to the final value.

Magnitude of the ripples during the Steady State

Due to nonlinearities of the hydraulic system, the system signal reached the steady state with ripples. The root mean square (RMS) value of the ripple amplitude is used as an indicator for the magnitude of the ripple. It is defined as:

$$\sigma = \sqrt{\frac{1}{n}\sum_{i=1}^{n}\left[x(i) - X_{SS}\right]^2} \tag{2.2}$$

where x is a series of measured data during the steady state, n is the number of the data being considered and X_{SS} is the steady state value.

Relative efficiency of the Bypass Flow Control

Assuming that the pressures at the pump outlet and motor inlet are the same, the relative efficiency (the efficiencies of the pump and motor are not considered) of the pump controlled motor system shown in Figure 2.5 is defined as follows:

$$\eta = \frac{\overline{Q_m}}{\overline{Q_p}} \tag{2.3}$$

where $\overline{Q_m}$ = Average flow rate of the hydraulic motor (m^3s^{-1})

$\overline{Q_p}$ = Average flow rate of the pump (m^3s^{-1})

The ideal relative efficiency of the system without using the bypass flow control is 100% since all the flow supplied by the pump passes through the hydraulic motor. However, when the bypass flow control is used, the relative efficiency of the circuit is less than 100% because the bypass valve diverts a small portion of the pump flow back to tank.

Compared with the measurement of the motor rotational speed, it is not easy to accurately measure the flow rate of the hydraulic motor and bypass valve especially for small flow rates. Since the rotational speed of the hydraulic motor is approximately proportional to the input flow rate for a fixed displacement motor, an alternative way to measure the flow rate is to measure the rotational speed. Hence, the average motor rotational speed during a fixed time period is used to replace the average flow rate in Equation 2.3. The rotational speeds of the hydraulic motor are measured under the same test conditions for the system with and without the bypass flow control. Thus, Equation 2.3 is rewritten as follows:

$$\eta_\omega = \frac{\overline{\omega_{by}}}{\overline{\omega_{no}}} \tag{2.4}$$

where η_ω = Relative efficiency of the bypass control system

$\overline{\omega_{by}}$ = Average motor rotational speed with the bypass control (rad/s)

$\overline{\omega_{no}}$ = Average motor rotational speed without the bypass control (rad/s)

For multiple tests under the same test conditions, the average relative efficiency is:

$$\bar{\eta} = \frac{(\eta_1 + \eta_2 + ... + \eta_n)}{n} \tag{2.5}$$

It must be noted that calculating the flow rate using this approximation can be in error if leakage exists in the motor. The leakage coefficient of the hydraulic motor is 2×10^{-13} m^3/s which will result in a leakage of 2.76×10^{-6} m^3/s at the pressure of 13.8 MPa. This leakage is only 0.88% of the maximum pump and hydraulic motor flow rate. Hence, the leakage in the motor used was minimal and this approximation was reasonable.

Stability and Stable Response

The output of a stable linear control system will remain bounded for any bounded input and for any bounded initial condition. Since hydraulic systems are highly nonlinear, the stability of hydraulic systems is different from that of linear systems. Some hydraulic systems may be stable for certain inputs and may become unstable if different inputs are applied. In this study, a stable system response is defined as follows: a system is stable if it exhibits overshoots during the transient but approaches and reaches the steady state without any limit cycle oscillation.

PID Controller Design and Critical Gain

There are many types of controllers that can be used to control the DC motor and servo valve. One of the most common controllers is the PID (proportional plus integral plus derivative) controller. This type of controller is frequently used in industrial applications. A typical PID controller has following transfer function form

$$G_c(s) = K_p + \frac{K_i}{s} + K_d s \tag{2.6}$$

where K_p = Proportional gain,

K_i = Integral gain and

K_d = Derivative gain.

The process of selecting controller parameters to meet given performance specifications is known as “controller tuning”. Two effective methods for PID controllers have been suggested by Ziegler and Nichols [1942]. These methods are based on the value of K_p which results in a marginal stability when only the proportional control action is used. The first method is limited to a plant where neither integrator nor dominant complex-conjugate poles are involved. The second method is applied to a plant that can exhibit sustained oscillations when K_p is increased from 0 to a critical gain (see Figure 2.9).

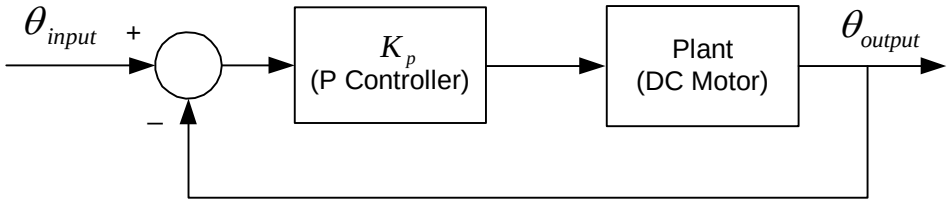

Figure 2.9 Closed loop system with a proportional controller

In the second method, the integral gain and derivative gain are set to zero. Increase K_p from 0 to a critical value K_{cr} where the output first exhibits a sustained oscillation. Thus, the critical gain, K_{cr}, and the corresponding oscillation period time, P_{cr}, are experimentally determined. The gains of the controller, K_p, K_i and K_d, are represented by following equations.

$$K_p = 0.6K_{cr} \tag{2.7}$$

$$K_i = 1.2K_{cr} / P_{cr} \tag{2.8}$$

$$K_d = 0.075K_{cr}P_{cr} \tag{2.9}$$

Chapter 3

Controller Design of the DC Motor Controlled Pump

As described in Chapter 2, the pump was controlled by a DC motor. The objective of this chapter is to present the design of a practical DC motor controller so that the pump could perform in a prescribed fashion. By means of this controller, the DC motor controlled pump should be able to function as a direct controlled variable displacement pump (as opposed to a hydraulic actuated variable displacement pump). The performance of the DC motor controlled pump was mainly evaluated for its dynamic performance. The main indicators of the dynamic performance for the DC motor controlled pump in this study were the response speed and operating stability. The speed of the dynamic response was demonstrated by the rise time as defined in Section 2.5. It is a very important specification in assessing the dynamic performance of the pump. A smaller rise time means a faster response. To achieve the research objective proposed in Section 1.4, the dynamic response of the pump was required to be as fast as possible; however, this response was limited by the operating stability considerations of the complete system. The pump had to work in a stable manner, which means without limit cycles, under various loading conditions.

To achieve the best performance of the pump, the DC motor controller was required to meet the following requirements:

- Fast dynamic response (small rise time) at any operating point and
- Stable operation (elimination of any limit cycle oscillations) under various loading conditions.

Before designing the controller, it was important to determine the dynamic performance of the DC motor and pump swashplate assembly. As a result, a model of the

DC motor and pump was attempted. Based on this model, a nonlinear motor controller was designed based on Ziegler-Nichols turning PID rules. This controller was then applied to the experimental system, and after some minor refinements, was able to accurately control the angle of the swashplate at any pressure level and to respond to the input signal as fast as possible. Finally, the steady state and dynamic performance of the DC motor controlled pump were experimentally evaluated and are presented at the conclusion of the chapter.

3.1 Modification and Verification of the Model

3.1.1 Setup of the Model Verification

The mathematical model of the DC motor and pump is developed in Appendix B and all model parameters listed in Appendix C. Before using the model for the controller design of the DC motor, the model output was compared to its experimental counterpart and the results are presented in this section. The verification was implemented by comparing model predictions with experimental measurements. Since there was no specific controller designed for the DC motor, a simple proportional controller (P controller) was used for purposes of verification for both the model and actual pump. The gain of the P controller was the same for both the model and actual DC motor controlled pump system. The model and actual pump were examined at a specific load condition for the same input signal. Some modifications (i.e. fine tuning) to the model were made so that the model could represent the physical system sufficiently for subsequent controller design. A block diagram of the model, actual pump system and controller used in simulation studies is illustrated in Figure 3.1.

The purpose of modeling the pump and DC motor was to be able to develop a basic model from which a practical motor controller could be designed off line and then applied to the actual DC motor-pump system. The model can be compared to its experimental

counterpart by examining the steady state and dynamic performance (via swash plate angle and system pressure) of both for similar loading conditions. For the controller design of the DC motor, the main requirement was that rise time of the motor-swashplate combination be as small as possible but without going into limit cycle oscillations.

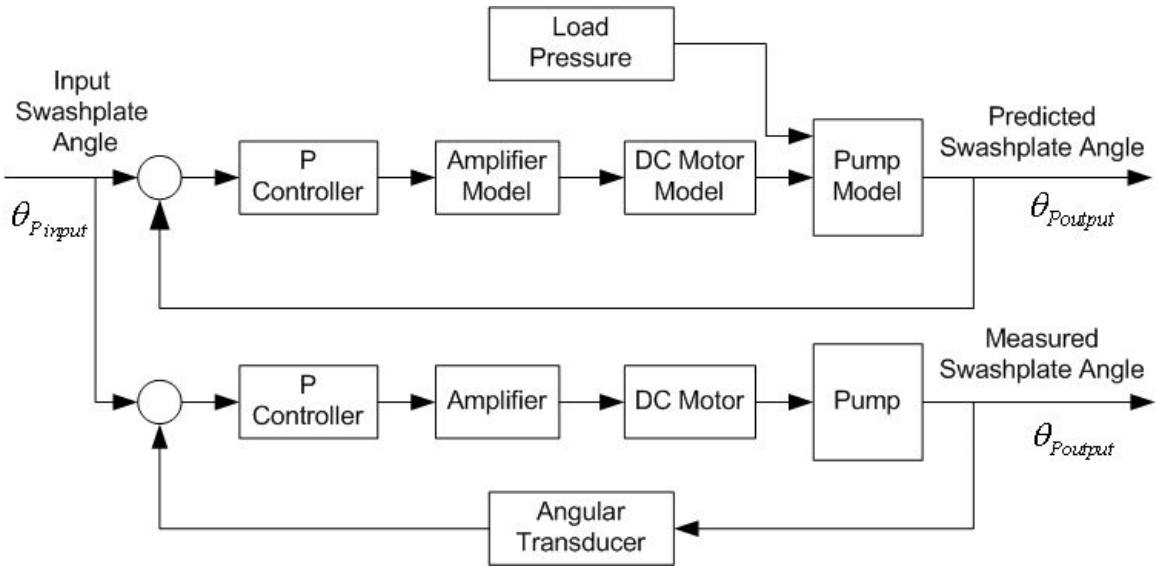

Figure 3.1 Block diagram of pump performance test

Preliminary studies showed that it was easy to achieve a fast dynamic response by increasing the gain of the P controller; however, this was at the expense of system stability for a highly nonlinear system, such as the DC motor controlled pump system. Hence, verification of the model of the DC motor and pump was primarily based on stability considerations; that is, the model and actual pump system should demonstrate the same trends (approaching the same steady state values, or exhibiting a limit cycle oscillation) under the same gain and load condition.

The procedure used to refine and verify the model was as follows:

1) The experimental pump system was tested at different load conditions (by changing the pressure). The gain of the P controller was increased until the swashplate angle exhibited sustained limit cycle oscillations. Critical gains and oscillation frequencies of the system were recorded.

2) The model was subjected to the same input signal and same critical gains at the same loading conditions. Some of the model parameters were then adjusted to yield the same limit cycle oscillation as the experimental output.
3) Steps 1) and 2) were repeated until the model could predict the limit cycle oscillation as the experimental test did at any loading conditions.

3.1.2 Pump Test (Experimental)

This test was designed to measure the critical gain and oscillation frequency of the actual DC motor controlled pump when the pump was marginally stable. The block diagram of the experimental setup was shown in Figure 3.1. To perform the test, a relief valve was used to simulate the load by keeping the pressure approximately constant throughout the test. The pressure was increased from zero to 13.8 MPa in increments of 1.725 MPa. At each pressure level, the proportional gain of the DC motor P controller was increased from 0 until the pump exhibited a sustained oscillation; then the critical gain and frequency of the sustained oscillation were recorded. The temperature was kept constant at 25±1.5°C for all tests. Typical experimental results are listed in Table 3.1.

Table 3.1 Critical gain and oscillation frequency of the DC motor controlled pump at different pressures (experimental)

Pressure (MPa)	Critical Gain	Oscillation Frequency (Hz)
0	0.14	15.7
1.73	0.17	18.3
3.45	0.21	21.3
5.18	0.27	25.3
6.9	0.33	29.5
8.63	0.42	30
10.35	0.58	33
12.08	0.76	35
13.8	1.05	38

It was observed that the critical gain and oscillation frequency were not the same under different loading conditions as the gains increased with increasing pressure. It was interesting to note that at the same pressure level, the pump operation tended to be stabilized by decreasing gain and destabilized by increasing gain. On the other hand, at the same gain, the pump tended to be stable with increasing pressure and unstable with decreasing pressure. Thus, the pump demonstrated a highly nonlinear characteristic which was strongly dependent on the operating pressure and controller gains.

3.1.3 Model Analysis and Modification

To verify the model, the same proportional gains and same pressures were applied to the model for the same input; the model output, however, did not exhibit any oscillations under any conditions listed in Table 3.1. This result indicated that the model did not accurately represent the real plant and that some important factor had not been properly modeled or the parameters measured were inaccurate. Because the parameters were based on experiential data, this was not considered to be the main cause.

The original model included the dynamics of the DC motor and pump. The model of a hydraulic pump which was similar to that used in this study had been verified by Kavanagh [1987]. The parameters of the pump model were experimentally measured over a wide range of the pressure. Hence, it was believed that the model of the pump was correct and that the error in model predictions was possibly due to the model of the DC motor rather than the pump. Further, it was believed that the major problem was the prediction of the electrical time constant which was mainly related to the inductance of a DC motor.

Upon reexamination of the DC motor, a model assumed for a brushless DC motor was found to be much more complex than that of a DC motor with brushes. The model developed in Section B.1 assumed a DC motor with brushes. It was also determined that the control mode of the amplifier used in this research was in fact “current control”,

instead of the more common “voltage control”. The inductance of the DC motor for current control is known to change with the current during the transient response.

Based on the above knowledge of current control, the electrical time constant (T_e) of the DC motor (see Equation B.5) was now assumed to be variable and dependent on the load. The procedure to identify this assumed variable electrical constant was as follows:

1) The same proportional critical gain (P controller) and pressure was applied to the model as was for the experimental system.
2) The electrical time constant of the DC motor model was adjusted until the pump model exhibited a sustained oscillation.
3) The test was repeated until all pressure levels were tested.

The modified electrical time constants for various pressures are listed in Table 3.2.

Table 3.2 Modified electrical time constant at different pressure (experimental)

Pressure (MPa)	Critical Gain	Electrical Time Constant (s)
0	0.14	0.026
1.73	0.17	0.014
3.45	0.21	0.0085
5.18	0.27	0.0055
6.9	0.33	0.0039
8.63	0.42	0.0028
10.35	0.58	0.00187
12.08	0.76	0.00136
13.8	1.05	0.00094

The critical gains and modified electrical time constants are also shown in Figure 3.2 as a function of the pump pressure.

A fifth order polynomial expressing the time constant as a function of pressure (MPa) was obtained from an Excel® spread sheet and was found to be:

$$T_e = -2.52\times10^{-7}P^5 + 1.15\times10^{-5}P^4 - 2.07\times10^{-4}P^3 + 1.89\times10^{-3}P^2 - 9.61\times10^{-3}P + 0.026 \quad (3.1)$$

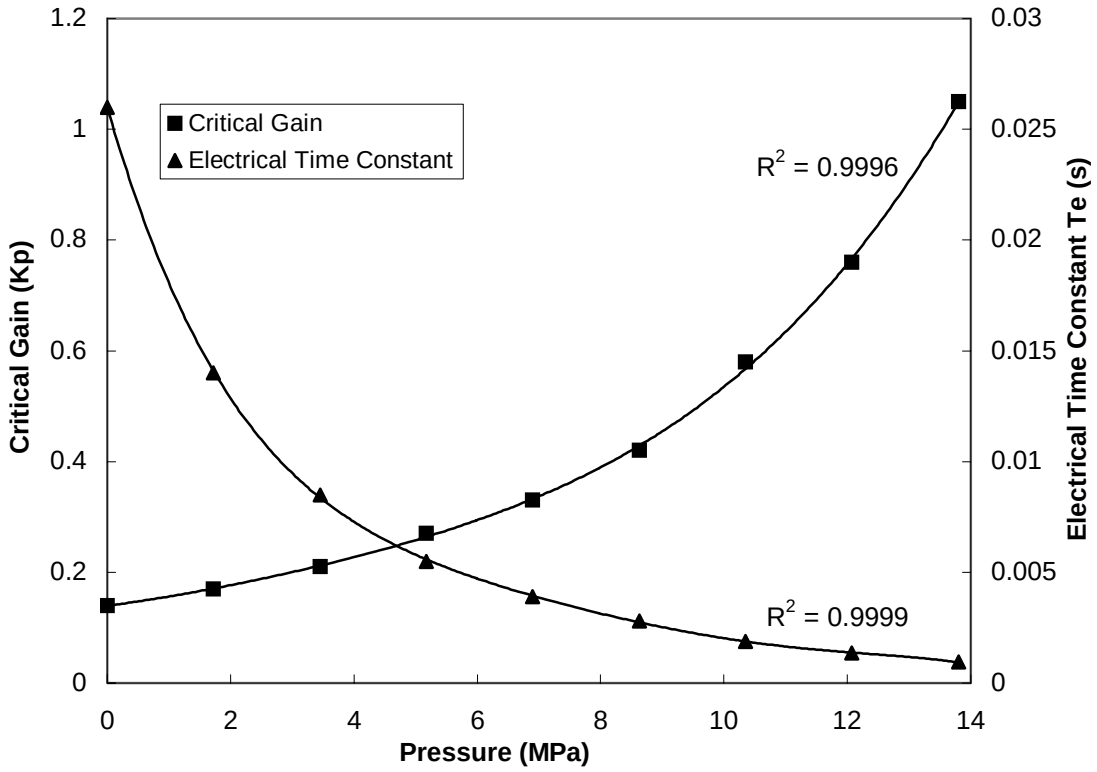

Figure 3.2 Critical gain and modified electrical time constant

3.1.4 Model Verification

The simulation results of the new model were compared with experimental results which were previously measured. The same proportional gains and pressures were applied to the new model under the same input conditions. Some typical results are shown in Figure 3.3.

Figure 3.3(a) shows the dynamic response of the pump at a low pressure (3.45 MPa). Both dynamic responses predicted by the simulation and measured approached the same steady state after a transient period. However, the transient period of the measured pump response ended in a relatively short time. This is compared with the measured response of the pump in which the transient response of the simulation settled down after a longer time period. When the proportional gain of the DC motor controller increased slightly from 0.19 to 0.21, both responses of the model simulation and experimental system exhibited

limit cycle oscillations (see Figure 3.3(c)). Figures 3.3(b) and (d) showed the dynamic responses of the pump at a high pressure level (10.35 MPa). The results were similar to those at the low pressure.

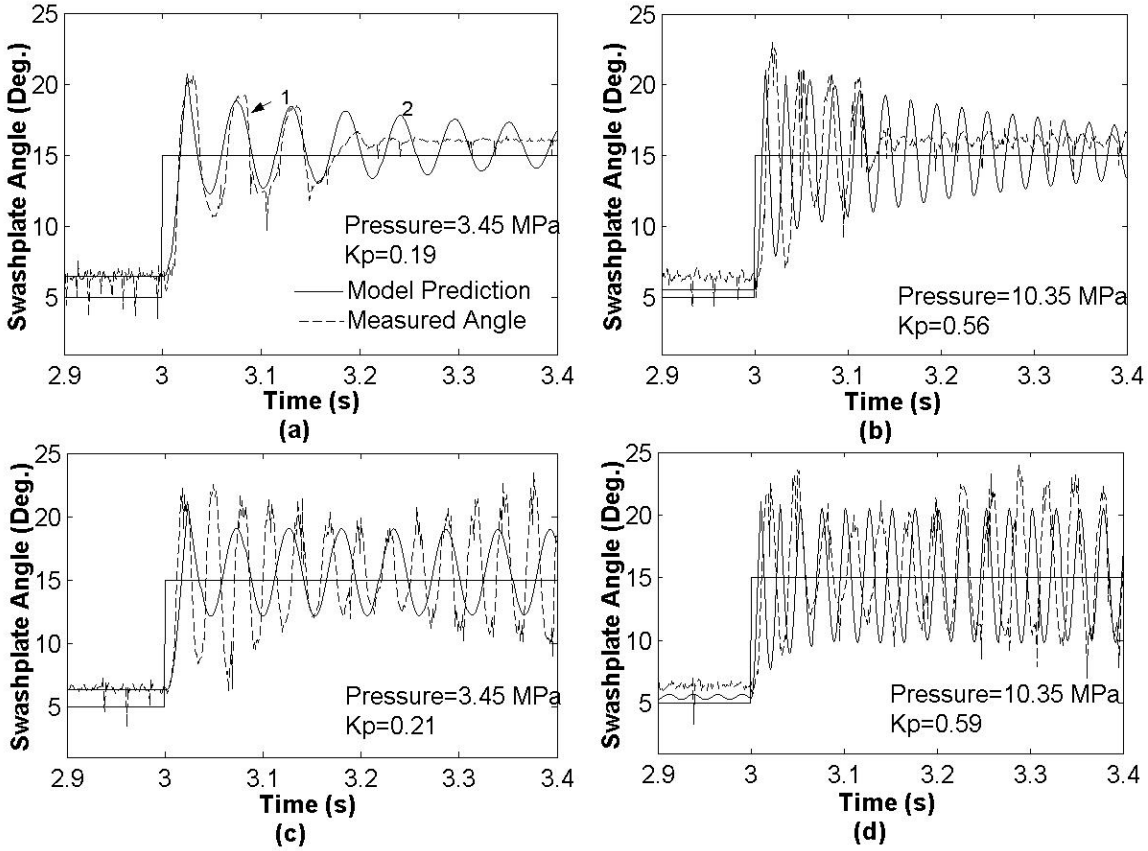

Figure 3.3 Comparison of measured swashplate angle and model prediction

It was observed that steady state values of the model simulation and experimental test did not approach the desired swashplate angle. This was because the controller was a P controller. The results shown in Figure 3.3 also indicated that dynamic response of the model simulation did not match with those obtained experimentally in some aspects of the performance. For example, when the pressure was low, the frequency of the limit cycle oscillation was lower than that of the measured response; however, the oscillation frequency was higher than the measured frequency when the pressure was high. A possible cause for this phenomenon was the highly nonlinear characteristics of the pump system.

This made it impossible to include all factors which could affect the pump performance into a simple model form.

Based on comparisons between model simulations and experimental tests, one conclusion could be made for the model of the DC motor and pump: the model dynamic response trends were “similar” to the physical system under the same loading conditions and same input signal. “Similar” means that both the model prediction and physical system output approached a common steady state value for smaller proportional gains and demonstrated a limit cycle oscillation of similar frequency when increasing the proportional gain to the critical gain (see Figure 3.3).

This characteristic of the model was important for the controller design of the DC motor. As discussed previously, the objective of modeling was not to derive an accurate model for the pump and DC motor. The model was mainly used to help the design of the DC motor controller such that the DC motor controlled pump could work at different loading conditions in a stable manner. As will be seen in the next section, the Ziegler-Nichols tuning PID rules are used to design the controller. Ziegler-Nichols tuning PID rules are only concerned with the critical gain and oscillation frequency for tuning the controller gains. At this point, although this model was not an accurate representation of the real system and the model prediction did not match the physical system very well, it was considered to be “sufficient” for use in the preliminary controller design of the DC.

3.2 Nonlinear DC Motor Controller Design Based on the Model

This section will discuss the controller design based on the model of the DC motor and pump. The requirement for the controller design at this stage was to design a DC motor controller which could drive the DC motor and pump swashplate at any pressure levels with a fast dynamic response but without exhibiting any limit cycle oscillations.

Many methods can be used to design the controller for a dynamic system; however, most of them are limited to linear systems. According to the preliminary experience using

Ziegler-Nichols tuning PID rules (see Appendix B.3.2), it was found that these rules were effective and convenient for the PID controller design, especially for the nonlinear DC motor controlled pump system. The controller designed using these rules provided satisfactory system performance. Hence, this method was also used as the basis of the controller design based on the model of the DC motor and pump.

In order to design the motor controller using Ziegler-Nichols rules, a Matlab program was written to calculate the critical gains and oscillation period time of the model at different pressure levels and assist the controller design. The procedure is as follows:

1) For the linearized model of Appendix B, the coefficients were evaluated at various operating points based on mathematical equations
2) The critical gain and oscillation period time were calculated at each operating point. The results indicated that the critical gain and oscillation period time were functions of the pressure.
3) PID controllers were designed at any pressure levels using the second Method of Ziegler-Nichols tuning PID rules.

Table 3.3 presents parameters of some typical PID controllers which were designed using this procedure at specific pressure levels.

It is to be noted that the controllers using the gains listed in Table 3.3 can only properly function near the specified operating points. For example, the controller designed for low pressure cannot work well at high pressure levels since the small gains do not produce a fast dynamic response. Controllers designed at high-pressure levels have a fast dynamic response at these levels, but they may exhibit sustained oscillations at low-pressure levels.

One solution to this problem was to design a nonlinear PID controller in which the gains of the controller were a function of pressure. This was done by using a Matlab program. Curves of the resulting PID gains as functions of the pressure are shown in Figure 3.4.

Table 3.3 Typical motor controllers designed at specific pressure levels

Controller	Pressure (MPa)	Period Time (s)	Critical Gain	K_p	K_i	K_d
PID 1	0	0.015	0.14	0.085	1.83	0.00098
PID 2	3.45	0.0085	0.21	0.13	4.70	0.00085
PID 3	6.9	0.0059	0.33	0.20	10.56	0.00092
PID 4	10.35	0.0042	0.57	0.34	26.25	0.0011
PID 5	13.8	0.003	1.01	0.61	63.74	0.0015

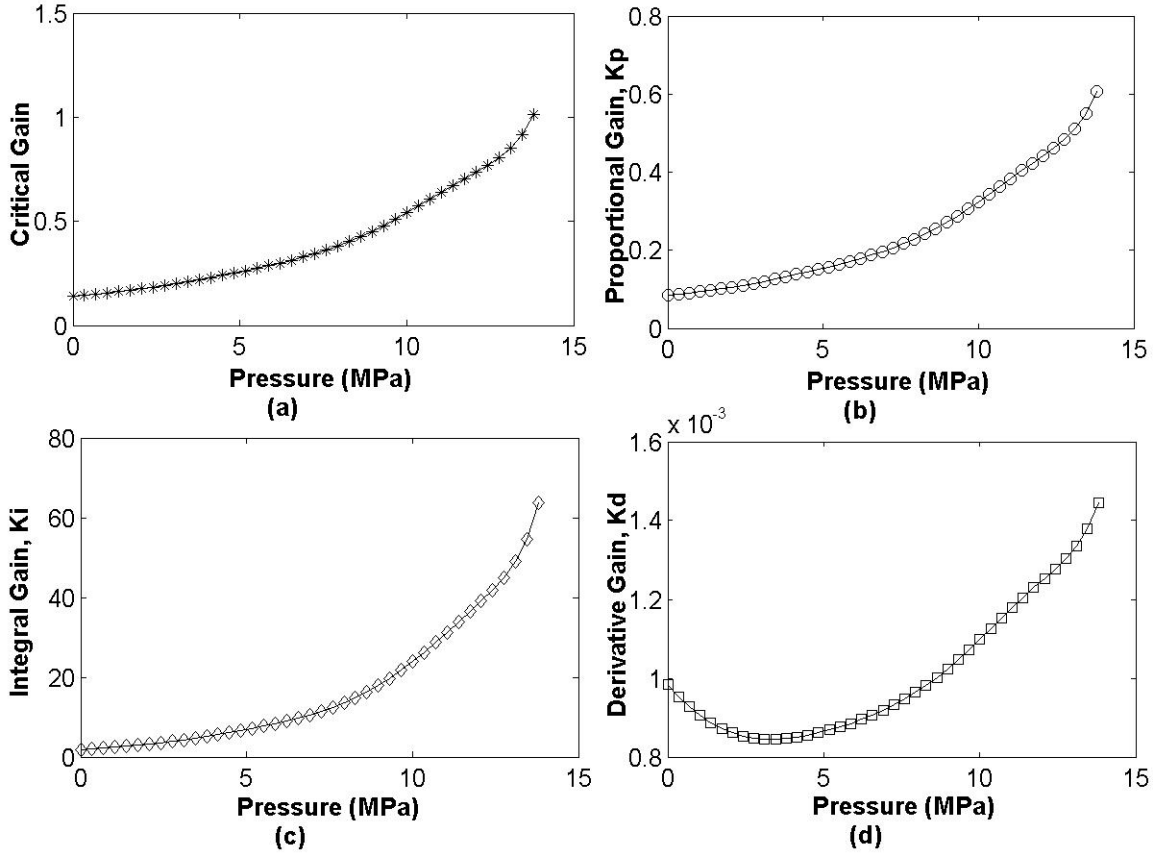

Figure 3.4 Nonlinear DC motor PID controller

The equations for the proportional, integral and derivative gains were represented as functions of the pressure (pressure unit: MPa):

$$K_P = 0.0777e^{0.142P} \tag{3.2}$$

$$K_I = 1.909e^{0.251P} \tag{3.3}$$

$$K_D = 5.75\times10^{-6}P^2 - 4.35\times10^{-5}P + 0.000943 \tag{3.4}$$

The controller designed was a variable PID controller which was pressure dependant. It must be emphasized that the number of significant figures does not represent accuracy of the experimental results but is a reflection of the program used to extract the function from the data.

3.3 Experimental test of pump performance

To summarize, a variable displacement pump was controlled directly by a DC motor attached to the swash plate of the pump. Through an iterative approach between experimental testing and modeling, the model of the DC motor and pump was developed and the controller of the DC motor designed off line using a variety of techniques. This controller was now applied to the actual DC motor and pump system.

To evaluate the performance of the DC motor controlled pump, an experimental system was designed to test the pump. As illustrated in Figure 3.5, it consisted of a modified hydraulic pump, a DC motor, a DC motor amplifier and a closed-loop angle control system. A pressure signal was fed back to the variable gain nonlinear controller. By means of the controller designed in the previous section, the stroke of the pump can be controlled in a stable fashion.

3.3.1 Pump Steady State Performance Test

The steady state performance of the pump was evaluated by comparing the desired swashplate angle to the measured swashplate angle at different pump pressures. In the beginning of the test, a constant signal was applied to the controller to achieve an angular displacement of 19.7˚ which was slightly less than the maximum swashplate angle (20˚). The pump swashplate was stabilized at this angle for one second. Then a negative ramp signal was applied to the DC motor to change the swashplate angle at a rate of 1º/sec until

no further motion of the swashplate occurred. The ramp signal was slow enough to minimize any system dynamics since this was to be a steady state performance test. The range of the input signal covered the full range of swashplate angle. The increment of the pressure level for each test was 0.69 MPa.

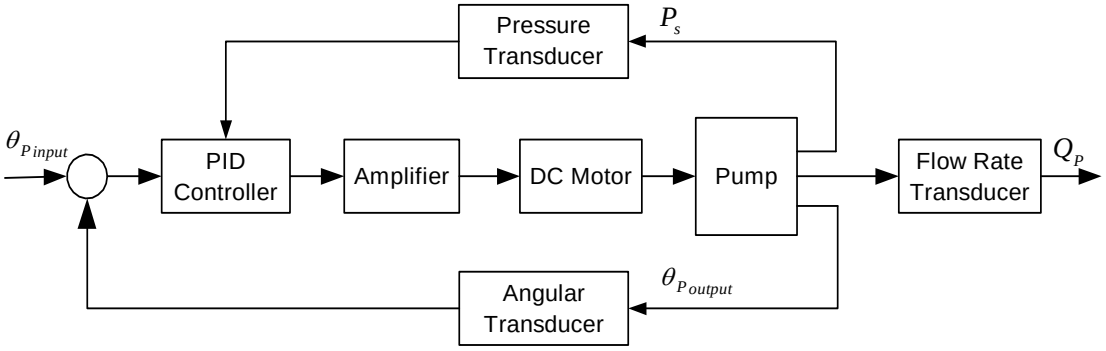

Figure 3.5 Block diagram of pump performance test

3.3.2 Pump Steady State Performance Test

The steady state performance of the pump was evaluated by comparing the desired swashplate angle to the measured swashplate angle at different pump pressures. In the beginning of the test, a constant signal was applied to the controller to achieve an angular displacement of 19.7˚ which was slightly less than the maximum swashplate angle (20˚). The pump swashplate was stabilized at this angle for one second. Then a negative ramp signal was applied to the DC motor to change the swashplate angle at a rate of 1º/sec until no further motion of the swashplate occurred. The ramp signal was slow enough to minimize any system dynamics since this was to be a steady state performance test. The range of the input signal covered the full range of swashplate angle. The increment of the pressure level for each test was 0.69 MPa.

Figure 3.6 shows a typical experimental swash plate angle, pressure and flow rate trace for a pressure of 3.45 MPa. The test result showed that the angle of the swashplate followed the input signal very well. There was no visual difference between the input signal and measured angle. The pressure decreased slightly with decreasing flow rate. As

the swashplate angle approached the zero position, the pressure and the flow rate quickly decreased to zero. It was also observed that the relationship between the swashplate angle and flow rate was not proportional. This phenomenon will be discussed in the next chapter. The tests were highly repeatable at different pressures.

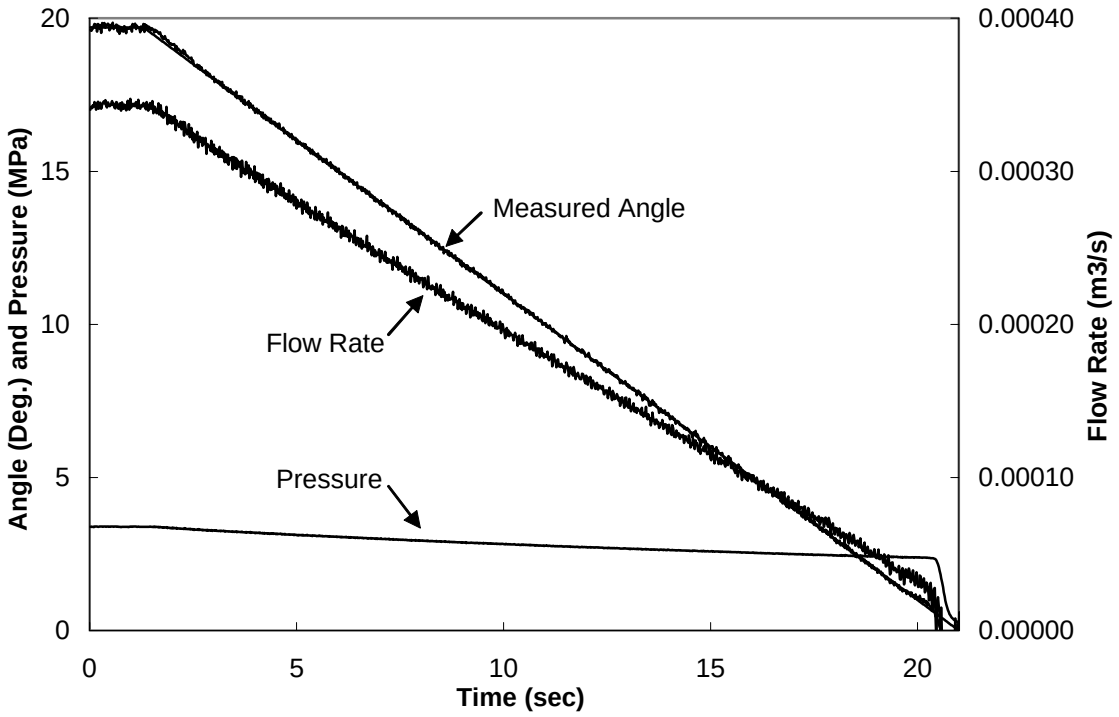

Figure 3.6 Measured steady state performance of the DC motor controlled pump (A typical experimental test result)

3.3.3 Pump Dynamic Response Performance Test

The dynamic performance of the pump can be established with a step input signal test. Two important dynamic parameters, rise time and overshoot, can be measured from this test. These terms are defined in Section 2.5. The test was realized by applying a step input signal to the controller (similar to the steady state test) and was carried out at different pressures.

The procedure for these tests was as follows:

1) The system pressure was adjusted by the main relief valve.

2) The swashplate was stabilized at 2 degrees by applying a constant input signal to the DC motor. The initial value of the input signal was used to prevent an interaction between the swashplate and its “hard stop”.
3) A step signal with a final value of 14 degrees (angular position) was applied to the controller. Initial transients at the initial settings were allowed to settle out: after three seconds, a step input was applied.
4) The fluid temperature was maintained at 25±1.5°C.
5) The test was repeated three times at the same pressure and temperature.
6) The test was repeated at different pressure levels.

Figure 3.7 shows one test result at a pressure of 6.9 MPa. The result showed that it only took about 17 ms to reach the desired angle. After a short time, the measured swashplate angle approached the desired angle with a large overshoot and a small undershoot.

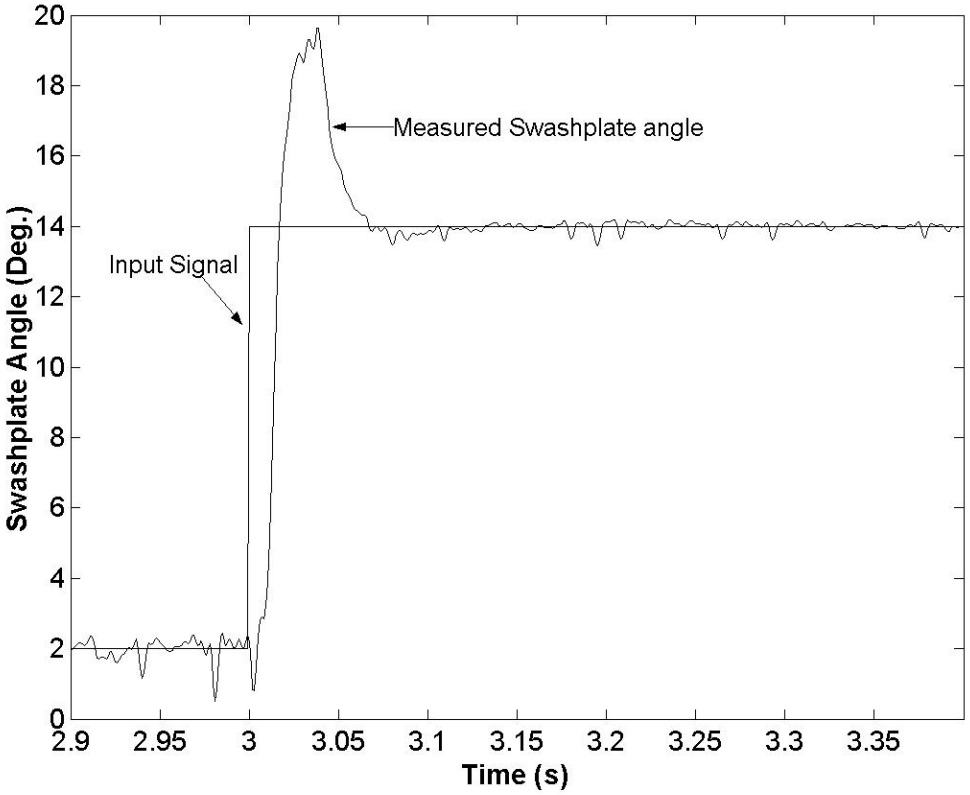

Figure 3.7 Measured dynamic response of the DC motor controlled pump

Since the rise time of the dynamic response was the main concern of the DC motor controlled pump, the rise times of the swashplate angle were measured at different pressure levels. Figure 3.8 shows the results of three tests and their average value. The rise time varied between 15 and 35 ms depending on pressure levels. It was observed that the rise time decreased with increasing pressure until the pressure reached 6.9 MPa and varied slightly around 16 ms when the pressure was higher than 6.9 MPa.

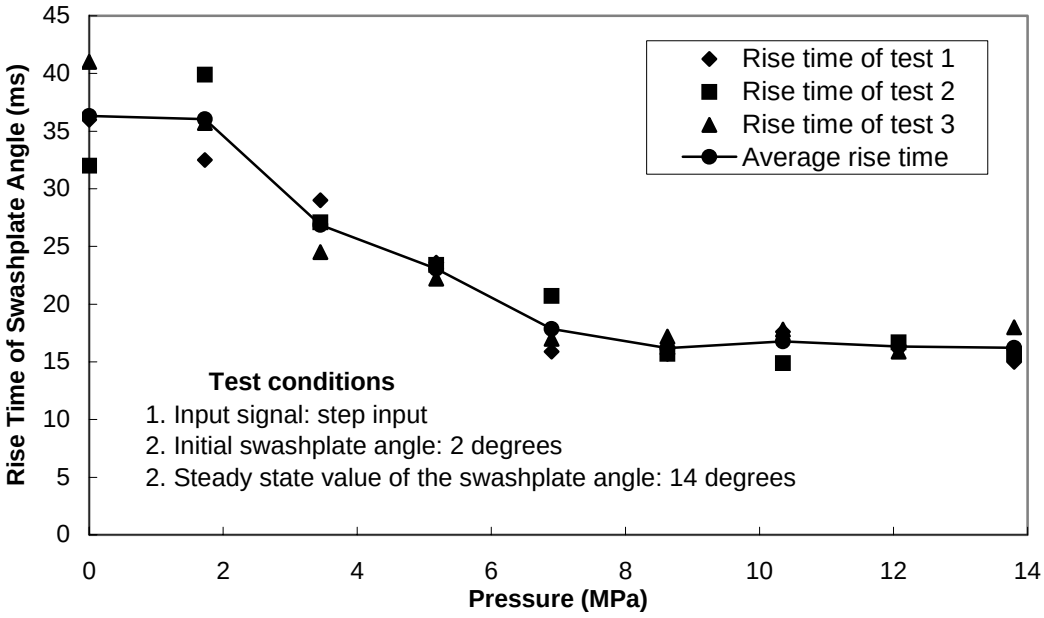

Figure 3.8 Rise time of pump swashplate angle with nonlinear PID controller

The test results shown in Figure 3.8 were measured only at one final swashplate angle (14 degrees). The reason for choosing 14 degrees as the final swashplate angle for all tests was that the swashplate could hit the hard stop for an swashplate angle larger than 14 degrees during the transient. If the swashplate hit the hard stop, the transient response would be affected. As will be seen in Chapters 4 and 5, the final swashplate angle chosen for these tests has the approximately same value for the tests conducted in those chapters. The rise times of the swashplate measured at other final angular positions (not listed here) showed a trend similar to the results shown in Figure 3.8; however, the values of the rise time varied slightly depending on the angular positions. The rise time for a negative step

input signal was slightly larger than that of a positive signal since the pressure effect acting on the swashplate was always in a direction of increasing swashplate angle.

All test results indicated that the DC motor controlled pump demonstrated a relatively fast dynamic response (15-35 ms). This rise time can be compared to the 10 ms rise time of typical relief valves [Yao, 1997], 30 – 60 ms of pressure actuated pumps [You, 1989] and 10 ms for the servo valve used in the bypass design [760 Series Servo valve, Moog Inc.].

Figure 3.9 shows the overshoot and undershoot of the swashplate angle during the transient. The undershoot of the response was small when compared with the overshoot. At some pressure levels, the undershoot was quite small and in some cases, zero. The overshoot varied between 30% and 50% and increased with increasing pressure. All results shown in Figure 3.9 were calculated from the same tests, which were used for calculating the rise time.

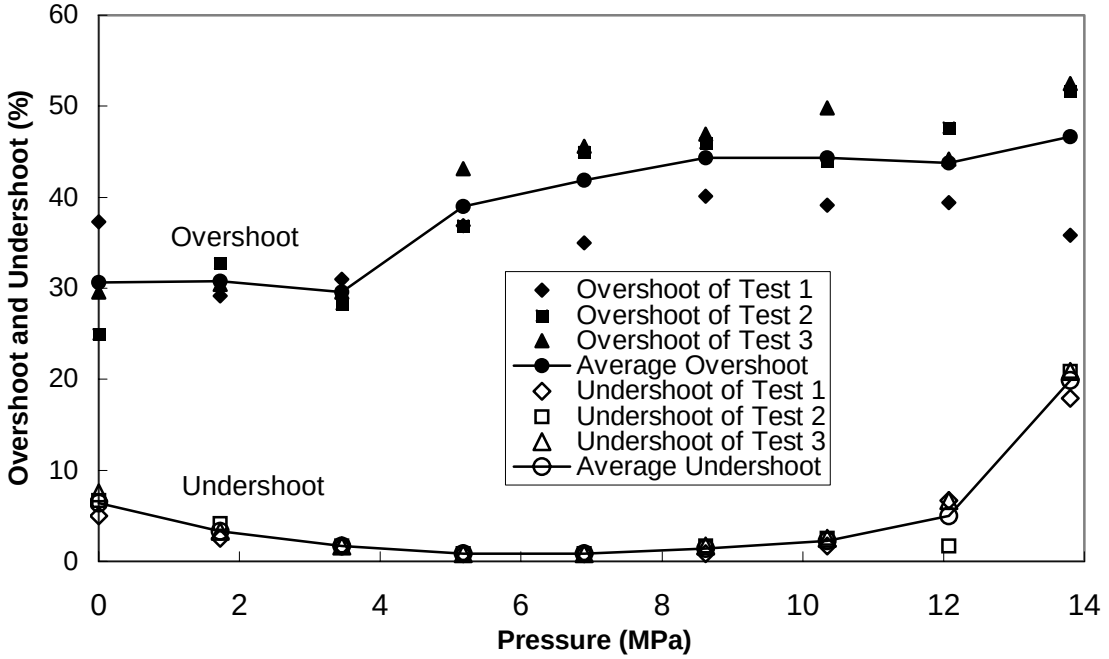

Figure 3.9 Overshoot and undershoot of pump swashplate angle

To summarize, the nonlinear DC motor controller could approach the steady state value in a stable manner at different pressure levels. By means of this controller, the pump exhibited a fast dynamic response with a rise time between 15 and 35 ms. However, the pump also produced a large overshoot (30% to 50%). This overshoot will contribute to an overshoot in the motor rotational speed response. This problem will be discussed in the next chapter in which reducing the motor rotational speed overshoot is the main concern.

Chapter 4

Controller Design of the Bypass Flow Control System

The design of the proposed bypass flow control system through a combination of simulation and experimental studies is discussed in this chapter. First, the configuration and operating principle of the bypass flow control system is presented. Some experimental considerations related to the bypass control valve are also discussed. Then, a preliminary controller is designed for the bypass control valve based on some experimental test results on the hydraulic motor system. The performance of the preliminary controller is analyzed and the structure of the controller modified and performance refined using simulation studies. Finally, the feasibility of improving the dynamic performance of a speed control system using the bypass flow control is examined using model simulation based on the complete system model (see Appendix D).

4.1 Configuration of the Complete Hydraulic System

The complete hydraulic system proposed for this study was previously shown in Figure 2.7. The main components of the system were a DC motor controlled variable displacement pump, a bypass valve (servo valve) and a hydraulic motor. The DC motor controlled pump was discussed in Chapter 3. This section will discuss the bypass control valve and the complete hydraulic system.

4.1.1 Bypass Flow Control Valve

As previously mentioned, the purpose for using a bypass control valve was to remove or minimize the overshoot associated with the overshoot of the pump swashplate and the compressibility effects of the fluid, as seen by the hydraulic motor, during transients. In order to achieve this target, the dynamic response of the bypass valve must be “faster” than that of the pump. Servo valves, however, are known to show superior

dynamic responses compared to other modulation devices and have transient responses comparable to the DC motor controlled pump. As mentioned in Section 3.3.2, the rise time of the DC motor controlled pump was between 15 and 35 ms depending on the pump pressure, and was less than 20 ms when the pressure was higher than 6.9 MPa. As will be discussed in Section 4.2, the rise time of the servo valve was around 10 ms when the pressure was higher than 6 MPa. Although the test conditions for the two systems were not the same, the test results did demonstrate that the dynamic response of the servo valve was faster than that of the DC motor controlled pump. Hence, this type of modulation device was chosen for this application.

4.1.2 Block Diagram of the Complete Hydraulic System

Figure 4.1 shows the block diagram of the complete speed control system. The input signal is the desired rotational speed of the hydraulic motor.

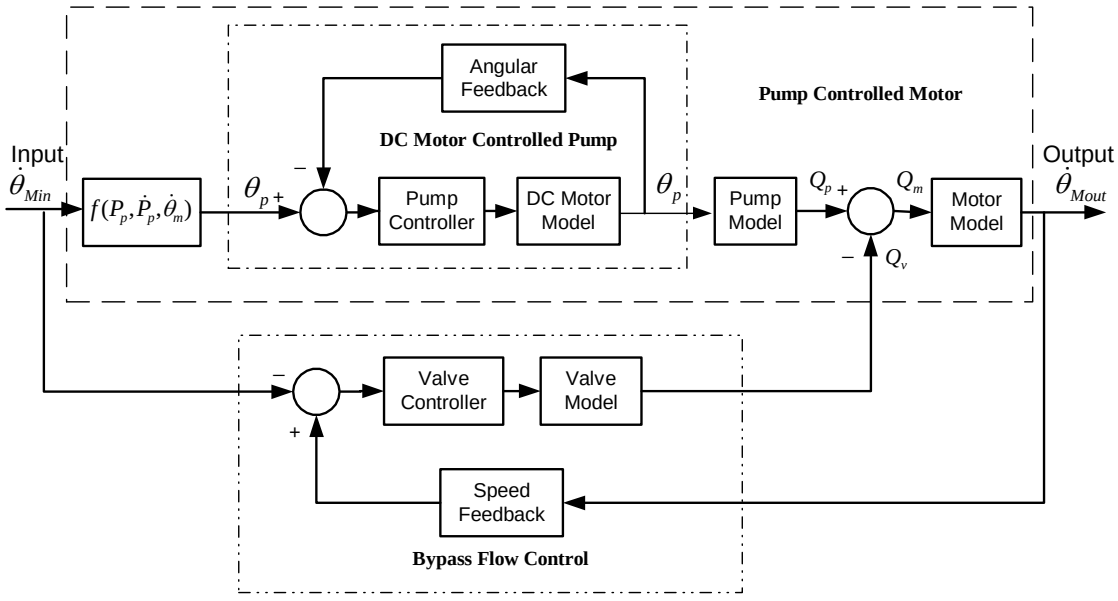

Figure 4.1 Block diagram of the complete hydraulic system

There are essentially three subsystems:

- DC motor controlled pump subsystem
- Pump controlled hydraulic motor subsystem

- Bypass flow control subsystem

Although all these subsystems have been discussed previously, it is useful to briefly discuss all three again but in terms of the overall system operation.

4.1.3 Principle of the Complete Hydraulic System

DC motor controlled pump subsystem

The pump subsystem is a closed loop system including a nonlinear PID controller, a power amplifier, a DC motor and a variable displacement pump. The feedback signal is the angular position of the pump swashplate, which is also the controlled variable. Changing the swashplate angle can vary the pump displacement. The purpose for controlling the swashplate angle is to control the flow rate of the pump.

Pump Controlled Hydraulic Motor Subsystem

This subsystem includes the DC motor controlled pump subsystem. The input signal is the desired rotational speed of the hydraulic motor ($\dot{\theta}_m$), and the output signal is the actual rotational speed of the hydraulic motor. The principle of the pump controlled hydraulic motor system is as follows: First, assuming ideal conditions, the rotational speed input signal is converted to a desired pump swashplate angle (θ_p) using the hydraulic system model (see Equation D.10). Then, this swashplate angle is fed into the DC motor controller to locate the swashplate to a desired angle. Finally the pump supplies the hydraulic motor with the required flow by which the hydraulic motor generates a rotational speed approximately proportional to the input rotational speed.

Bypass Flow Control Subsystem

This is a closed loop system. The controlled variable is the speed of the hydraulic motor ($\dot{\theta}_m$). The input signal is the same as that of the pump controlled hydraulic motor system. The rotational speed signal of the hydraulic motor is fed back to the input of the

valve controller. The bypass flow control is used to remove the excess flow from the pump if the motor rotational speed is larger than the desired rotational speed. This can occur under the condition when the motor exhibits a large overshoot during the transient response. In this case, the bypass flow control algorithm is designed to minimize the overshoot.

Principle of the Complete System

The operation of the complete system is as follows. First, the desired rotational speed of the hydraulic motor is converted to the pump swashplate angle (via Equation D.10). Then, the DC motor drives the pump swashplate to achieve this desired angle in the shortest time possible. Accordingly, the pump supplies the appropriate flow rate to drive the hydraulic motor. During the whole operation, the bypass flow control system monitors the rotational speed of the hydraulic motor and takes an appropriate control action when the motor rotational speed exceeds the desired rotational speed. Finally, because of the improved dynamic response of the DC motor controlled pump, the desired rotational speed of the hydraulic motor should be achieved with an improved dynamic response as well; the performance of the hydraulic motor would be further improved with a reduction in the overshoot due to the bypass valve.

The overall system is not a closed loop system since the motor rotational speed signal is not directly fed back to the main input of the system.

4.2 Experimental considerations: Bypass Control Valve

Before a controller for the bypass control valve could be developed, preliminary investigations revealed some peculiarities associated with the operation and configuration of the servo valve so chosen. This section will consider some of these characteristics as they play an important role in the final design of the controller. The process was one of experimentally evaluating the performance of the valve under variety of pressure

conditions and examining some preliminary controllers experimentally for the bypass system. Based on the results of these preliminary tests, a controller was then designed using an experimental approach and modified using model simulation.

To use the servo valve as a bypass flow control valve, some properties of the servo valve had to be investigated before designing the valve controller and experimental system. They were:

- The effect of the pressure drop across the bypass valve on its dynamic performance.
- How to install a servo valve as a bypass flow control valve.

These two questions arose due to the special properties of the bypass control configuration and servo valve structure. These questions are addressed in the following sections.

4.2.1 Pressure Effects on Servo Valve Performance

Servo valves are normally used in hydraulic circuits in which the supply pressure is constant and with the aid of feedback or pressure compensation, they can be used to control flow. As discussed in Appendix D.1, the pilot stage of the servo valve was a flapper valve. To make the flapper valve work properly, the fluid that came from the nozzles and acted on the flapper had to be maintained at a certain pressure level. Thus, the supply pressure from which the nozzle was fed, had to be maintained greater than a specified value. For Moog760 valve used in this study, the pressure drop across the valve is required to be greater than 6.9 MPa to get the best performance. However, in this study, the supply pressure of the valve was the same as the system pressure, and was not constant but varied with changes in loading conditions.

To test how the pressure drop across the valve affected the dynamic performance of the actual valve, (especially when the pressure drop was less than the specified value), an experimental test was designed to determine the transient response of the valve in terms of

flow rate under different pressure levels. The circuit is shown in Figure 4.2. The relief valve was used to adjust the pressure drop across the valve. A flow rate transducer was installed to measure the flow rate through the valve. The pump delivered the maximum flow rate (19 l/min).

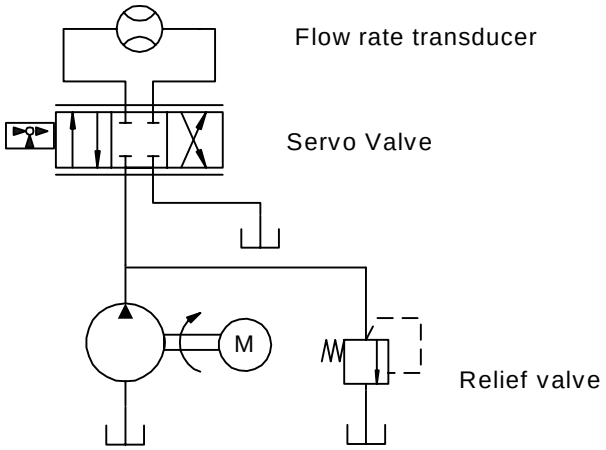

Figure 4.2 Hydraulic circuit for testing the servo valve performance

In the first instance, the bypass valve was closed and hence all the pump flow was over the relief valve at the set pressure. A simple PID controller was designed for the servo valve using Ziegler-Nichols rules. The controller was designed for a supply pressure of 6.9 MPa. This controller was not meant to be the final controller for the bypass control valve. It was only used for this particular test.

The procedure for measuring the flow rate of the valve during the transient was as follows:

1) A step input signal was applied to the servo valve and the flow rate measured.
2) The test supply pressure was increased by adjusting the relief valve from 0.69 MPa to 7.6 MPa in increments of 0.69 MPa.
3) The test was repeated with the temperature kept approximately constant (25±1.5°C).

The dynamic responses at different pressure levels were evaluated in terms of the

rise time and overshoot. The results, which are shown in Figure 4.3, indicated that the servo valve could not work properly if the pressure was under 2 MPa. In this case, the measured flow rate of the servo valve could not reach the desired value (15.1 l/min) because the flapper valve on the pilot stage of the servo valve could not function properly under low pressures. When the pressure was increased from 2 MPa to 3.45 MPa, there was a significant improvement in the dynamic performance. The valve could output the desired flow rate but with an overshoot. The rise time, however, decreased to about 20 ms as the pressure increased. This rise time was considered acceptable for the experimental feasibility study of the bypass flow control. Beyond 3.45 MPa, the rise time continued to decrease until the pressure reached 6.9 MPa but the amount of overshoot in flow increased slightly. Beyond 6.9 MPa, there was no appreciable change in the valve dynamic response. The tests were repeatable.

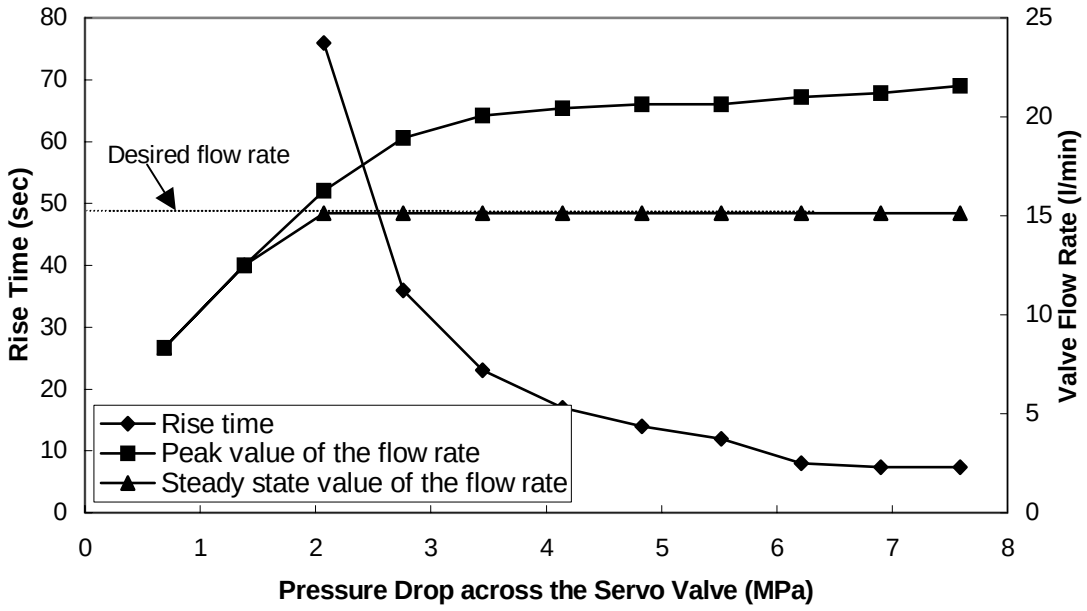

Figure 4.3 Pressure influence on the dynamic performance of the servo valve

Comparing the flow rate of the servo valve with the swashplate angle of the DC motor controlled pump, the servo valve demonstrated a smaller rise time at the same pressure level, except at pressures less than 3 MPa. Although the test conditions were not

the same for both systems, the comparison results showed that the servo valve had a faster dynamic response and should be able to accommodate the overshoot of the hydraulic motor.

As seen from Figure 4.3, the dynamic performance of the valve would be adversely affected if the pressure were low. To maintain an acceptable performance, a minimum pressure drop across the valve should be around 3.45 MPa. For the experimental system shown in Figure 2.7, it was possible to build up this pressure because of a combination of the friction in the hydraulic motor (which resulted in pressures of 1.5~2.5 MPa depending on the rotational speed), and the relief valve, RV2 (which could be used to adjust the motor backpressure and increase the system pressure to an acceptable level).

It should be noted that this pressure limitation is not a necessarily a constraint on the bypass flow control concept but is a constraint on the servo valve used in the study. As discussed in the next Section, a suitable two way valve was not available in the lab so the servo valve had to be used.

4.2.2 Installation of the Servo Valve

The installation of the bypass valve in a bypass flow control system is different from that in a normal flow control system. This configuration makes the design of the controller for the bypass flow control complex. In this section, how the installation of the bypass control valve affects the controller design is discussed.

Ideally, the proposed bypass flow control valve should be a two-way, closed centered device. From a practical point of view, a two-way high-speed valve was not available in the lab, so a four-way servo valve (described in Section 4.1.1) was used to serve this purpose. The four-way valve had four ports to connect to the hydraulic circuit; however, for the bypass flow control, only two ports were used. How to handle the other two ports of the servo valve was an issue that had to be carefully addressed.

Figure 4.4 shows 3 possible installations of the servo valve. In Figure 4.4(a), port

"T" and port "C2" are blocked. When the spool moves to the left valve position, pressure port "P" will be connected to port "C1". When the spool moves to the right, pressure port "P" will be blocked by port "C2". Theoretically, this configuration should be sufficient to simulate a two-way valve operation. However, the physical internal design of the valve makes this scenario impossible to implement. The flow from the pilot stage cannot make its way back to tank if the "T" port is blocked. Thus the valve cannot function properly.

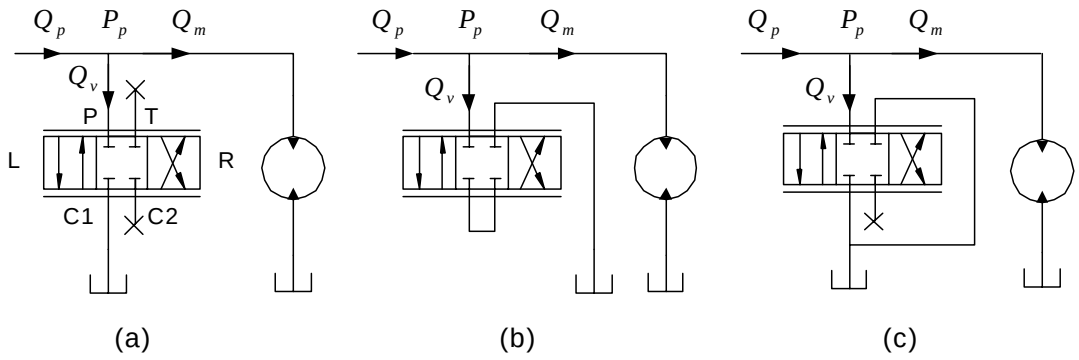

Figure 4.4 Installations of the servo valve

In Figure 4.4(b), pressure port "P' is always connected to the port "T", regardless if the spool moves to the left or right position. This configuration could create some difficulties when it comes to controller design. For a regular control system, different input signals generate distinctly different outputs. However, for the servo valve shown in Figure 4.4(b), a positive and negative input signal of the same value will produce the same output which could create problems in terms of controller design.

Consider Figure 4.4(c). The port "T" is connected to tank and port "C2" is blocked. In this configuration, if the spool is moved to the left position, then the fluid is bypassed to tank. Assuming that a positive signal will move the spool to its left position, then the bypassed flow rate will be proportional to the applied positive signal (pressure drop being assumed constant). For a negative signal, the valve spool moves to the right position (Figure 4.4(c)) and the flow is blocked for all negative signal inputs. The flow from the pilot stage can go back to the tank through the "T" port. This particular valve

configuration was feasible for bypass flow control.

Although it is unusual to use a servo valve in this mode, preliminary test results indicated that the high dynamic bandwidth of the servo valve in a four-way mode was not compromised with this particular arrangement.

4.3 Bypass Flow Control Design

The objective of this section is to present the design of a controller for the bypass flow control valve. The main steps for the controller design were as follows. First, a preliminary controller for the bypass control valve was designed in an experimental operating mode. Some difficulties were experienced with this controller and thus, an attempt was made to determine the cause of the problem based on the simulation of the bypass valve and motor models. Finally, the controller was modified using the simulation results and applied to the complete model of the system for "proof of concept". The following sections will present the process used to design the bypass valve controller.

4.3.1 Controller Design of the Bypass Control Valve (Experimental Approach)

The experimental system showing the motor with the bypass valve was previously shown in Figure 2.7; in this case, the flywheel was not attached to the motor. The system backpressure (and hence the upstream valve pressure) was set to 4 MPa by adjusting the relief valve installed after the hydraulic motor. At full stroke, the pump delivered the maximum flow rate of 19 l/m. Only one system pressure was considered (4 MPa) for the preliminary valve controller design. It was anticipated that the controller designed at this pressure level could provide a fast and stable dynamic response for most of the loading conditions expected. The reason for this assumption was that the servo valve demonstrated a comparatively fast dynamic response with a rise time less than 20 ms when the pressure was higher than 4 MPa (as shown in Figure 4.3). Hence, the controller designed at this pressure level should, at least, provide the same dynamic performance at high pressure

levels.

The design procedure for the bypass valve controller was quite similar to that for the design of the DC motor controller discussed in Section 3.2; thus, the experimental test and design procedures will not be repeated. The critical gain and oscillation period time were measured by increasing the proportional gain of the bypass valve controller until the hydraulic motor exhibited a limit cycle oscillation. The critical gain (K_{cr}) was determined to be 0.0021, and the oscillation period time (P_{cr}) to be 0.035 ms. Three controllers (P, PI and PID) were designed using Ziegler-Nichols rules to determine which controller demonstrated the best performance. The gains for these controllers are summarized in Table 4.1.

Table 4.1 Three bypass valve controllers designed using Ziegler-Nichols rules

Type of Controller	Proportional Gain K_p	Integral Gain K_i	Derivative Gain K_d
P	0.01 ($0.5\,K_{cr}$)		
PI	0.0095 ($0.45\,K_{cr}$)	0.33($0.54\,K_{cr}/P_{cr}$)	
PID	0.013 ($0.6\,K_{cr}$)	0.72 ($1.2\,K_{cr}/P_{cr}$)	0.00006 ($0.075\,K_{cr}\,P_{cr}$)

Three controllers were applied to the bypass control valve and experimental tests were conducted. The objective of the tests was to investigate the ability of the controller and bypass system to effectively remove or minimize the motor rotational speed overshoot. The test results showed that the bypass flow control valve was able to remove only a very small portion of the overshoot. (The test results are not shown here since the performance of all three controllers was considered to be unacceptable for bypass flow control.) It was believed that the poor performance of controllers was due to the bypass control valve since it could not respond to a negative input signal which the controllers did output. The valve controllers were analyzed in the next section with the model simulation. Since the controller performance was unacceptable, it was decided that a new controller had to be

considered and that the best approach would be to redesign this controller based on the model simulation of the servo valve, hydraulic motor and valve controller.

4.3.2 Analysis of the Bypass Flow Control (Simulation)

In a normal closed loop system, a controller must respond to a complete range of input signals, which includes both positive and negative values. However, this general rule cannot be applied to the bypass flow control since, as discussed in Section 4.2.2, the valve does not respond to a negative input signal. This property has a significant influence on the design of the bypass valve controller.

In order to analyze how the bypass flow control design was affected by this property, a simulation was developed based on models of the servo valve and hydraulic motor which are developed in Appendix D. The block diagram is shown in Figure 4.5.

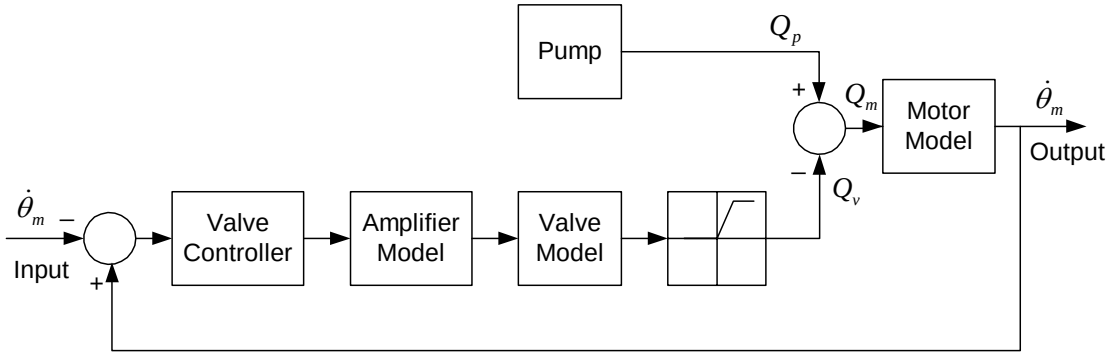

Figure 4.5 Block diagram of bypass flow control system

This block diagram is a part of the complete system block diagram shown in Figure 4.1. To design this closed bypass flow control system, the rotational speed output signal of the hydraulic motor was fed back to the input of the servo valve. The negative sign on the input desired rotational speed and the positive sign of the motor rotational speed was to accommodate the fact that a negative (subtraction) flow was required during the bypass mode. A signal conditioner block was designed to restrict the output of the valve to only positive values (ie, bypass flow was viewed by the system as negative flow). This block

was used to simulate the uniqueness of the bypass valve which could only response to a positive input signal.

The purpose of using the bypass control valve was to reduce the overshoot of the hydraulic motor rotational speed. To analyze the performance of the bypass flow control system, a simulation was conducted first by applying three valve controllers (listed in Table 4.1) to the model of the bypass control valve. The simulation conditions are as follows:

- The input signal was a desired constant rotational speed signal (100 rad/s).
- A sine wave with a magnitude of 10 rad/s and a bias signal of 2 rad/s were superimposed on the input signal to simulate an overshoot and undershoot condition.
- The system-simulated pressure was 4 MPa (same as the pressure in the experimental test).

By means of this input signal combination, the pump was assumed to supply a flow rate which was equivalent to a motor rotational speed of 100 rad/s with an overshoot of 12% and an undershoot of 8%. For the pump, this was a steady state response. However, from the viewpoint of the bypass control valve, it was considered to be a dynamic response because effective flow rate of the pump simulated overshoot and undershoot conditions.

The simulation results are shown in Figure 4.6. It was observed that the motor rotational speed for the system without using the bypass flow control exhibited an overshoot of 12% and an undershoot of 8%. When the bypass flow control was used, the overshoot was reduced for all controllers (between 5% to 7% overshoot) as illustrated. For the bypass control using a P controller, the overshoot was reduced about 50%. However, for the PI and PID controllers, the results for removing the overshoot were not as significant as that of the P controller by itself since the PI and PID controllers started to

take corrective actions after a time delay. Theoretically, for linear systems, the PI and PID controllers should have produced better results when compared with the P controller. A possible cause for this situation was that the integrator of the PI and PID controllers could not take the proper action in a bypass flow control system; this was an issue that had to be addressed before any controller could be reliably and effectively applied to the experimental system.

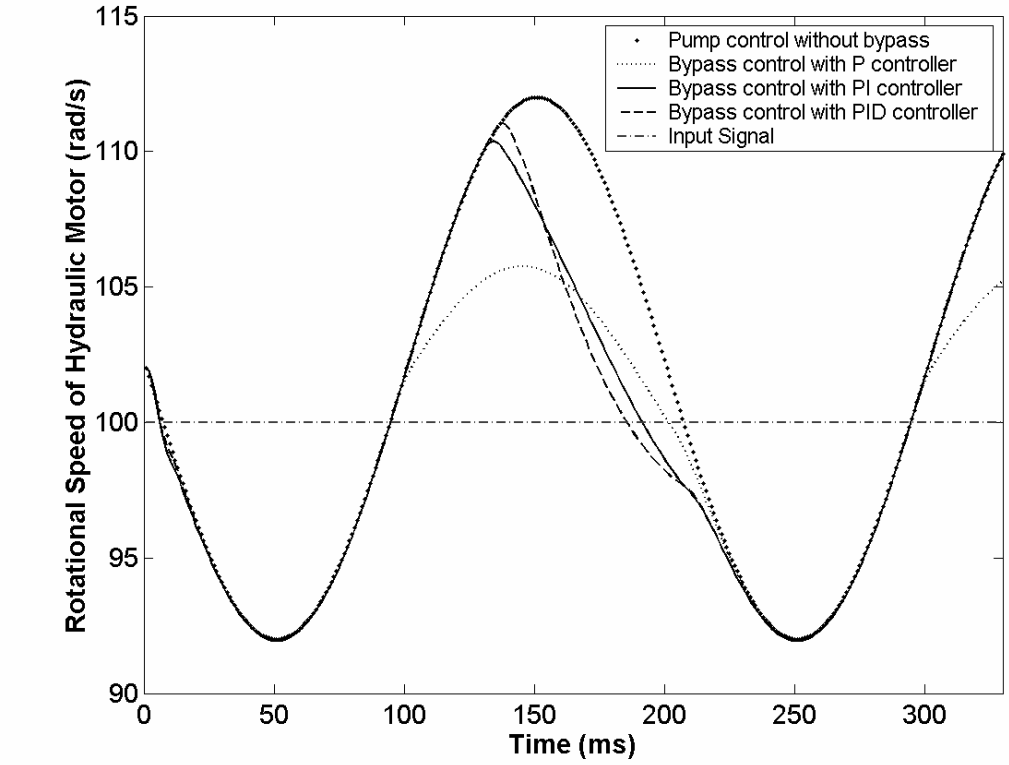

Figure 4.6 Valve controller performances

To investigate if the integration was indeed, the source of the problem, a PI controller was investigated (in fact, the PID controller had the same effect). The schematic of the PI controller is shown in Figure 4.7. The controller's output, C_{output}, is the sum of the proportional gain output, P_{output}, and integral gain output, I_{output}.

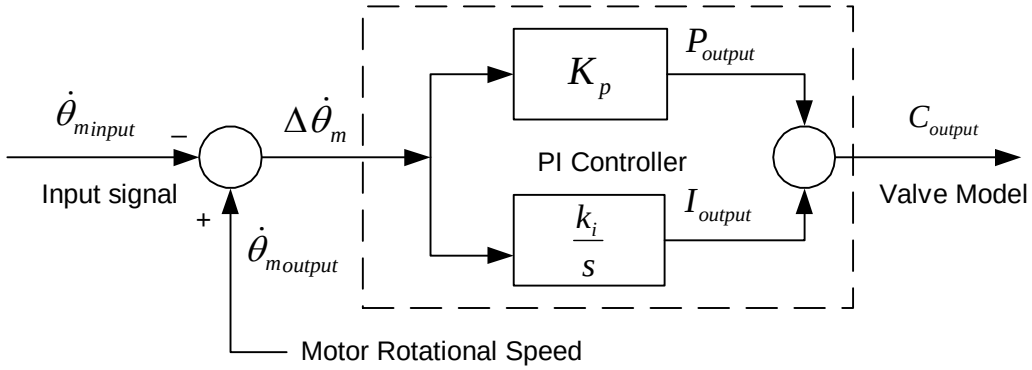

Figure 4.7 Schematic of the PI controller

The ideal operation of the bypass control valve required that the valve be completely closed when the motor demonstrated an undershoot and that the valve be partially open when the motor exhibited an overshoot. To understand how the integral portion of the controller reacts to this situation, consider Figure 4.8 in which the output values of the integrator, and proportional part of the controller are shown.

Figure 4.8(a) shows that the motor rotational speed demonstrated an overshoot at a time of 0.094 s. Theoretically, the bypass control valve should be opened to bypass the flow from the pump. However, the valve actually opened at 0.13 s (see Figure 4.8(a) and (d)). It appears that the valve controller took corrective action after a time delay of approximately 0.081 seconds. The cause for this situation was that the integrator accumulated a large negative value (I_{output}) during the time period when the motor rotational speed demonstrated an undershoot. Hence, when the motor rotational speed started to exhibit an overshoot at the time of 0.094 s, the controller output (C_{output}) was, in fact, a negative value, which was then recognized as a zero value by the bypass control valve, even though the proportional output (P_{output}) was positive at that time. The solution for this problem was to use a resetable integrator in the PI controller; this approach is now considered. For the valve controller, the controller should initiate control action only when the motor rotational speed is larger than the desired value.

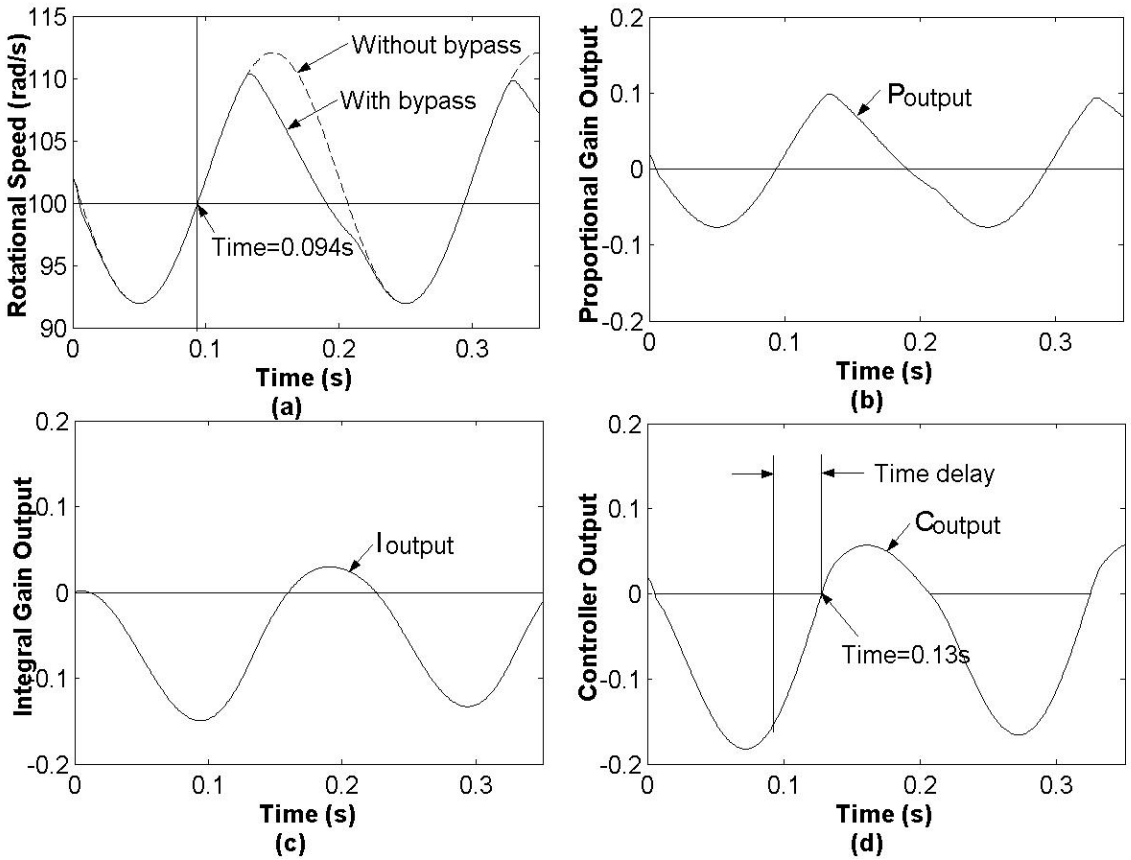

Figure 4.8 Rotational speed of the hydraulic motor and values of the PI controller gains (simulation)

To accomplish the bypass flow control function, the proper role of the integrator was:

- to accumulate a positive speed difference signal to reduce the motor rotational speed by opening the valve and hence, bypassing extra flow when the motor rotational speed was higher than the desired rotational speed and
- to output nothing when the motor rotational speed was equal to or less than the desired speed.

This was accomplished by designing a resetable integrator, illustrated in Figure 4.9. The controller now operates as follows. When the motor rotational speed is less than the desired rotational speed, the relational operation outputs a “true” signal. This signal

triggers the resetable integrator and resets the accumulated previous rotational speed difference signal to zero. The output of the PID controller is now zero or negative. The valve is closed and the motor keeps running at a rotational speed which matches the pump flow rate. If the pump cannot supply enough flow to drive the motor during the dynamic transient, the motor rotates at a relatively slower rotational speed and exhibits an undershoot. In this case, the bypass flow control system cannot contribute to a direct reduction in the undershoot of the motor. If the motor rotational speed is higher than the desired speed, the relational operation will output a “false” signal, which in turn will not trigger the resetable integrator. In this case, the PID controller works as a regular PID controller.

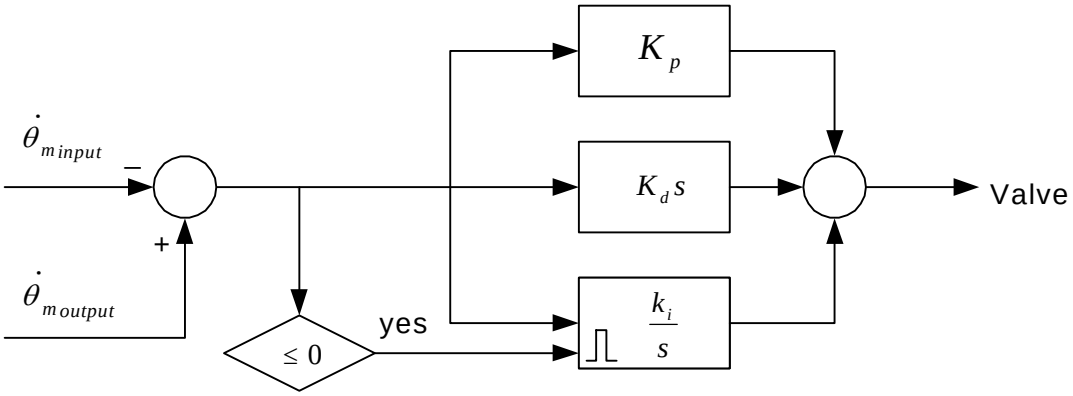

Figure 4.9 Schematic of a “resetable” PID controller

To test if the resetable integrator did indeed, improve performance, the simulation was reexamined with both the resetable PI and PID controllers and the results are shown in Figure 4.10 using the same simulation conditions as mentioned previously. The simulation results for the model without using the bypass are also shown in the same figure for comparison.

The result indicated that the improvement in reducing the overshoot was significant by using the resetable integrator strategy. When comparing the performances of two controllers, the resetable PID controller behaved marginally better than the resetable PI

controller. (In fact, the difference between the resetable PI and PID controllers was not significant.) Hence, the resetable PID controller was chosen as the final controller of the bypass control valve. As will be demonstrated in the next Chapter, the experimental test showed similar results.

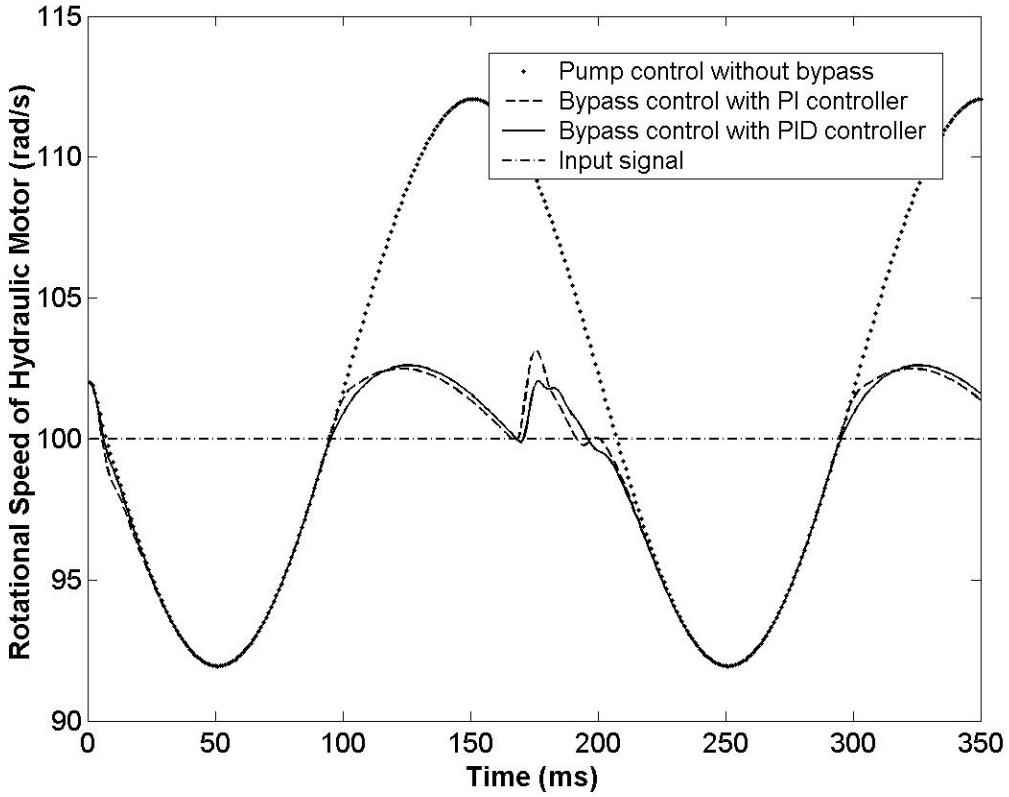

Figure 4.10 Comparison of resetable PI and PID controllers

4.4 Simulation "Proof of Concept": Bypass Flow Control

A complete speed control system model was developed by combining all component models and controllers together. Based on this system model, the bypass flow control concept, that is "proof of concept", was demonstrated using simulation results using the platform Matlab/ Simulink®. Proof of concept was established by applying the same input signal to the system models with and without bypass flow control and comparing the results.

It should be noted that the model of the DC motor and pump could not give an

accurate prediction for the system output during the whole load range due to nonlinear characteristics of the system. But, it could indeed give good predictions at some operating points if a few minor modifications were made to the model parameters. Hence, the model of the DC motor and pump was still used to test the overall "Proof of concept" on the whole system, but only used at operating points which were experimentally verified.

Figure 4.11 shows the dynamic responses of the system model with and without the bypass flow control for an input step signal. A step rotational speed signal (30 rad/s to 100 rad/s) was introduced at 0.2 s of the simulation. The backpressure of the hydraulic motor was set to 4 MPa. The rise times of the systems with and without the bypass flow control were the same (no visual difference). The overshoot of the pump-controlled system was reduced using the bypass flow control system. The time duration of overshoot region was shorter for the bypass control system compared with the pump-controlled system.

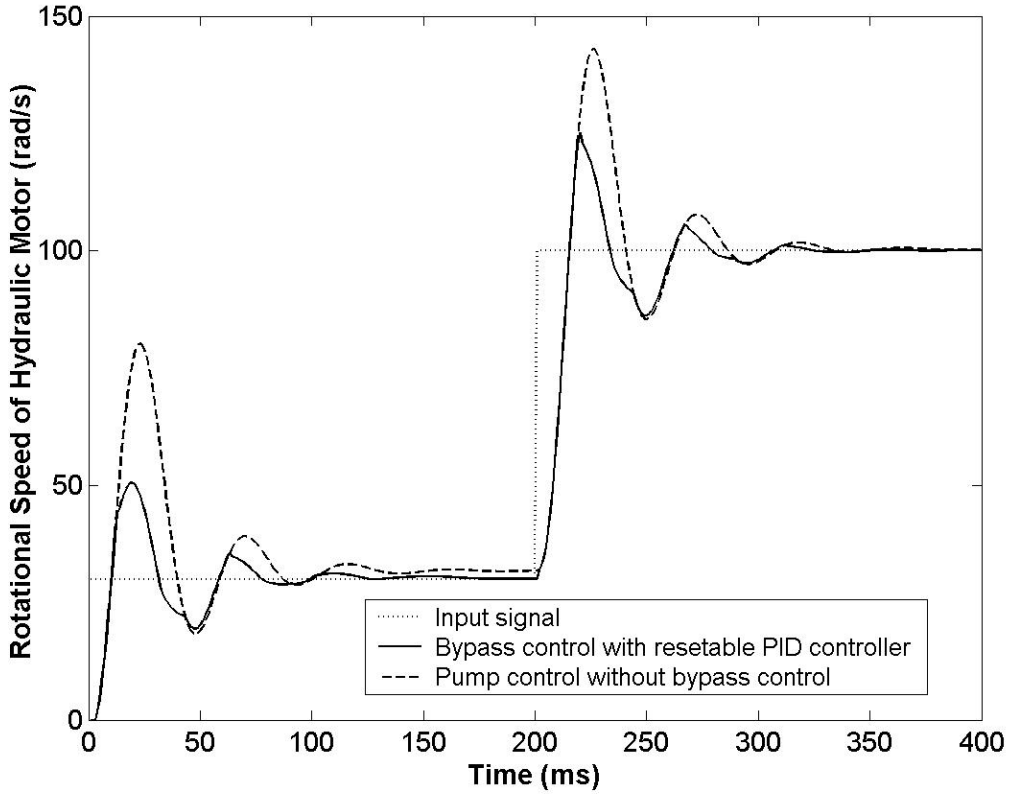

Figure 4.11 Dynamic response of the system model simulation

(Open loop for complete system)

In summary, this section has established “proof of concept” for the bypass flow control approach. The simulation results show that the proposed approach can improve the dynamic performance of the hydraulic motor by reducing the overshoot of the motor rotational speed.

Chapter 5

Experimental Verification of the Bypass Flow Control Concept

The controllers of the DC motor and bypass valve were designed and tested in previous chapters. Based on these controllers and the model of the complete hydraulic system, a simulation of the bypass flow control circuit was completed and used to establish the theoretical “proof of concept”; in addition, the model was used as an aid in the design of the bypass controller. This chapter will:

- Consider the pump-controlled hydraulic motor system with the bypass flow control,
- Examine the measurements of the dynamic responses of the system with and without the bypass flow control under different loading conditions and,
- Evaluate and discuss the test results according to the objective of this study.

5.1 General

5.1.1 Objective of the Test

As discussed in Chapter 1, the main objective of this study was to develop a hydraulic circuit with good dynamic performance and high relative efficiency. The hydraulic circuit designed for this purpose was presented in previous chapters. A high relative system efficiency was achieved using a pump control strategy in which the hydraulic motor was directly controlled by the pump. No pressure and flow losses (other than minor line and fitting losses) existed between the pump and hydraulic motor. This high system performance was realized in two ways: the first was to increase the dynamic response rate of the system by controlling the pump swashplate with a DC motor; the other

was to reduce the overshoot (a byproduct of the fast response) using the proposed bypass flow control strategy. The objective of experimental tests was to measure and evaluate the system performance using commonly known indicators such as the rise time and overshoot of the hydraulic motor rotational speed during the transient.

5.1.2 Experimental Setup

A schematic of the complete hydraulic system studied is shown in Figure 5.1. It is similar to the hydraulic system described in Figure 2.7. The operating principle of the system was previously described in Section 4.1.3. A relief valve (component 14 in Figure 5.1) was used to create a constant load to the hydraulic motor. An inertial load was generated with a flywheel attached to the shaft of the hydraulic motor. Many other loads could have been considered but the two examined here represent two extremes with most other loads falling somewhere in between.

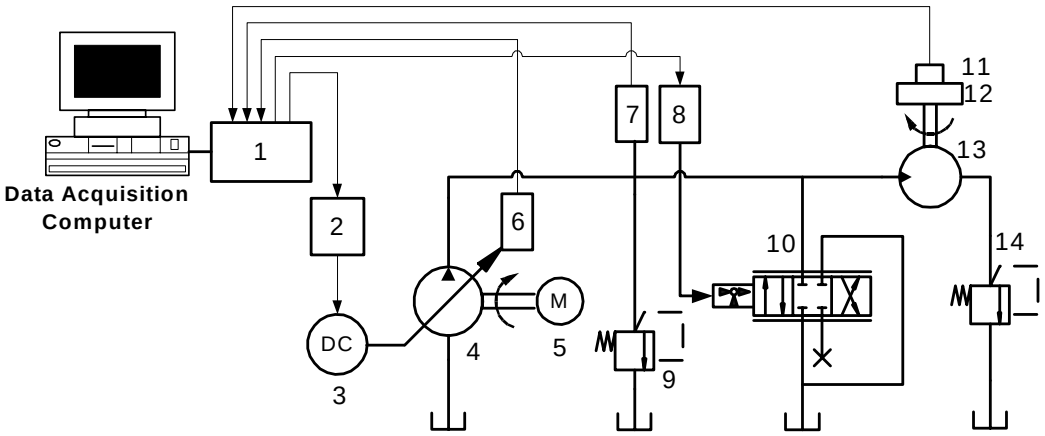

1. DAQ I/O box
2. DC motor amplifier
3. DC Motor
4. Pump
5. AC Motor
6. Angle transducer
7. Pressure transducer
8. Servo valve amplifier
9. Relief valve 1
10. Servo valve
11. Speed transducer
12. Fly wheel
13. Hydraulic motor
14. Relief valve 2

Figure 5.1 Schematic of the experimental setup

5.1.3 Test Conditions and Procedure

To make test results comparable, all experimental tests followed the same test

conditions. They were as follows:

- The temperature of the fluid was kept at 25±1.5°C during each test.
- The pressure of the relief valve 1 (component 9 in Figure 5.1) was set to 20.7 MPa (for safety purposes).
- The rotational speed input signal was a step function with an initial value of 40 rad/s and a final desired value of 100 rad/s. It was common for all tests. The step was initiated at 2 second to allow starting transients to die down.
- All tests were repeated three times to check the repeatability.
- All transducers were re-calibrated before each set of tests.

In order to evaluate the performance of the circuit, the rotational speed of the hydraulic motor was measured at different loading conditions by changing the pressure level and load type (fixed and inertial loads). A uniform measurement procedure was adopted to make test results comparable. The main steps were as follows:

1) A step input signal was applied to the DC motor controller (without using the bypass flow control), and the motor rotational speed measured.
2) Without changing test conditions, the same step input signal (desired value 100 rad/s) was applied to the DC motor controller and bypass valve controller (using the bypass flow control algorithm) simultaneously, and the motor rotational speed measured.
3) The backpressure on the hydraulic motor was increased by adjusting the load relief valve from 0 MPa to 12.8 MPa in increments of 1.73 MPa.

5.2 Experimental Test with a Fixed (Constant) Load

For a positive displacement pump, such as the axial piston pump, flow is generated, not pressure. The pump transfers the fluid at a controllable rate into the system which encounters some resistance to the fluid flow (due to a load or line losses etc.). The resistance from the piping, hoses, and fittings is quite small with proper component

selection. The largest part of the resistance to the fluid flow comes from the load itself. According to system external constraints, the load can be a constant (such as that due to gravity), resistive, capacitive, inertial, or some combination. Different kinds of loads have different characteristics and have different effects on the system performance. This first section will consider the performance of the bypass system under the conditions of a constant resistive load. An inertial load is considered in the next section.

The characteristic of the resistive or constant resistive (hereafter referred as just "constant") load is that the load reaction on the output device always opposes the motion of the hydraulic motor. In this test, a constant load was simply simulated by applying a backpressure to the outlet of the hydraulic motor using a relief valve. Because of the characteristics of a relief valve, the backpressure was not exactly constant but showed a pressure override of 3% at 5 GPM. This was considered to be an acceptable variation.

5.2.1 Experimental Test Results

According to the test procedure described in Section 5.1.3, the rotational speed of the hydraulic motor was measured at pressures varying from 0 MPa to 12 MPa. Figure 5.2 shows the dynamic responses of the hydraulic motor with a backpressure of 5.18 MPa.

It was observed that the rise time of the hydraulic motor rotational speed was about 34 ms. The rise time was the same for systems with and without bypass flow control since the valve was closed during this time period. The overshoot was reduced significantly when the bypass flow control system was used. The hydraulic motor rotational speed reached its approximate steady state condition after transients have died out. However, the motor rotational speed did experience an oscillation (defined in this thesis as a non-uniform flow, pressure or rotational speed ripple, hence forth referred to as simply "ripple") about its steady state value as illustrated in Figure 5.2. The presence of the ripple will be discussed in Section 5.2.3.

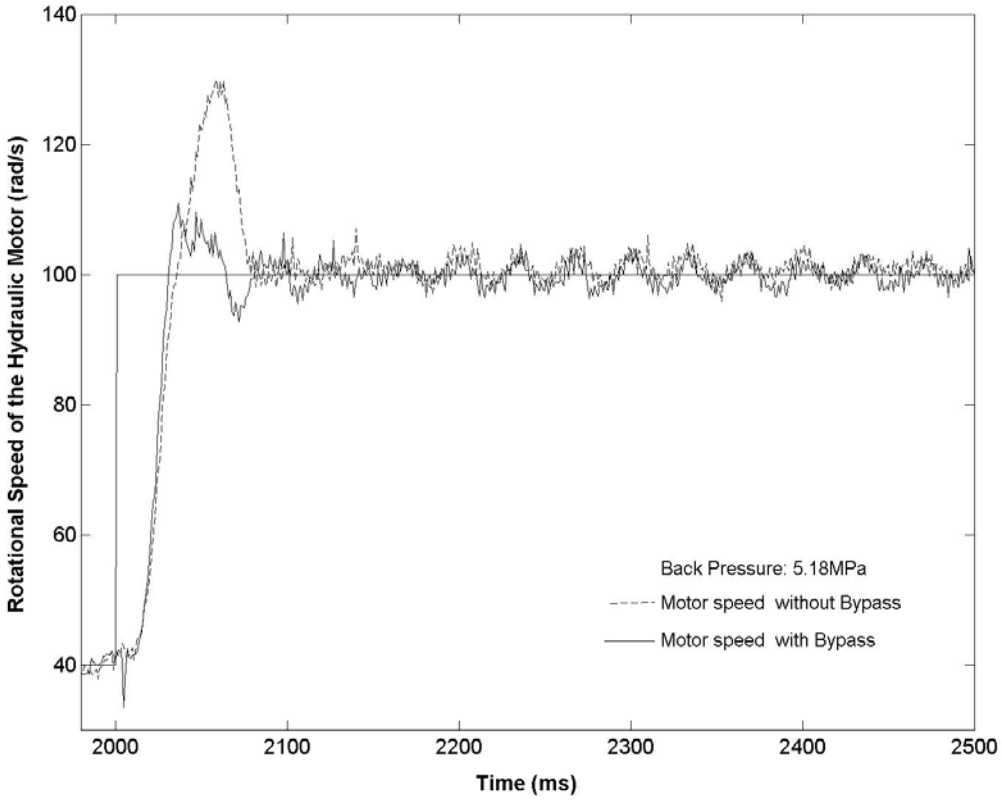

Figure 5.2 Dynamic responses of the hydraulic motor at a backpressure of 5.18 MPa

Figure 5.3 shows the dynamic performance of the hydraulic motor (in terms of its rotational speed) at four particular pressure levels. All measured rotational speed signals were filtered with a low pass filter. The cut-off frequency of the filter was 250 Hz. Figure 5.3 illustrates that the bypass flow control system was effective in reducing the overshoot at both low and high pressure loads. The dashed lines are the motor rotational speed of the system without the bypass control, and those curves with solid line represent those with bypass control. It is observed that the rise time is reduced and the overshoot increased with increasing backpressure. The bypass flow control was effective for all pressure levels.

For each test, the performance of the dynamic response was evaluated using indicators such as the steady state value, ripple magnitude (RMS), rise time and percent overshoot. The technical definitions of the specifications are given in Section 2.5. Their

values were calculated with a Matlab® program using the data measured during the transient or steady state.

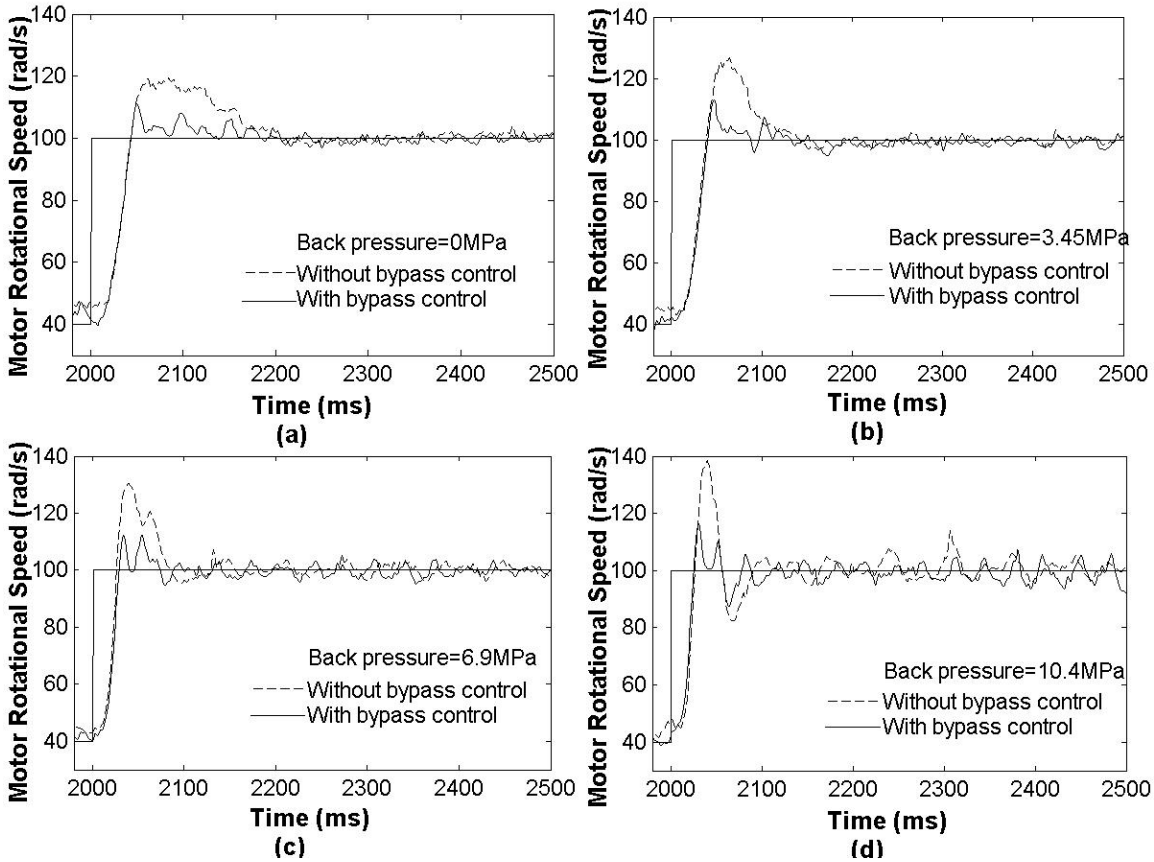

Figure 5.3 Dynamic responses of the hydraulic motor at 4 particular backpressures

Percent Overshoot

The primary purpose of using the bypass flow control was to remove the overshoot during the transient and hence, the percent overshoot of the hydraulic motor rotational speed was the main indicator in which the performance of the bypass flow control was assessed.

Figure 5.4 shows the percent overshoot of the motor rotational speed with and without the bypass flow control. Three test results and their average values are shown in the same figure. It was observed that the bypass flow control system could remove about half of the total overshoot.

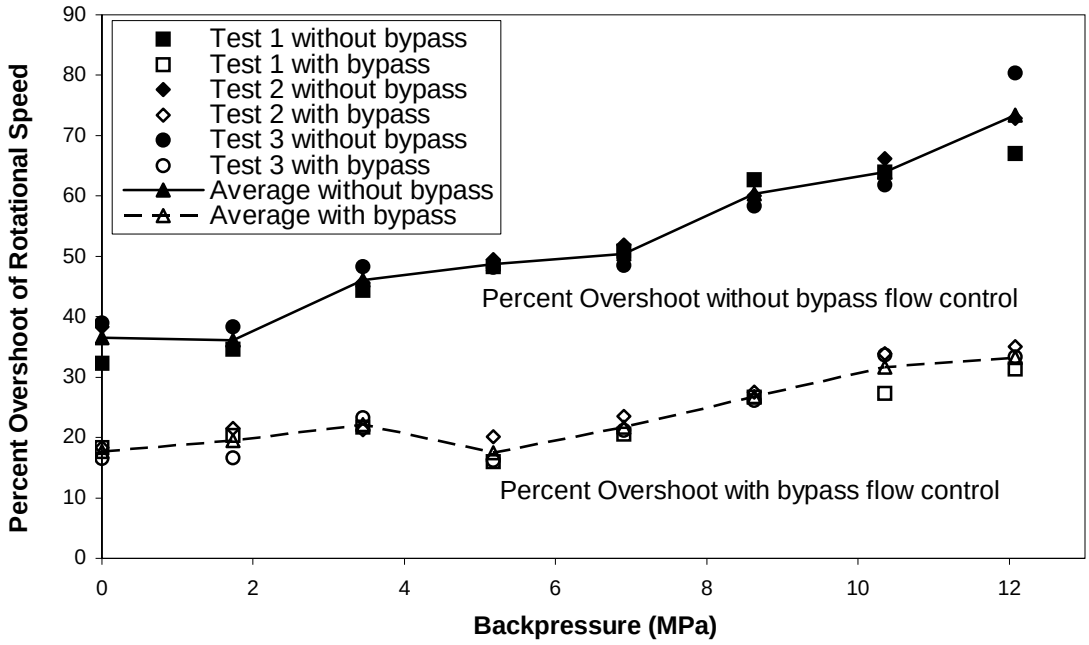

Figure 5.4 Comparison of overshoot between systems with/without bypass control

Rise Time

The main objective of this research was to improve the dynamic response of the pump controlled system. The rise time was a main indicator for evaluating the rate of the dynamic response. A smaller rise time represented a fast dynamic response. Figure 5.5 shows the rise time of the motor rotational speed with and without bypass flow control. The average value of the rise time with bypass control is shown in the dash thick line, and that without bypass control is shown in solid thick line. It was observed that the rise time was between 20 and 45 ms and decreased with increasing pressure.

As mentioned above, the rise time of the motor rotational speed changed with the pressure: large at low pressures and small at high pressures. This was a direct consequence of the nonlinear DC motor controller. The smaller DC motor controller gains at low pressures resulted in a slow (damped) response and large rise time, whereas the overshoot increased with increasing pressures due to the larger controller gains.

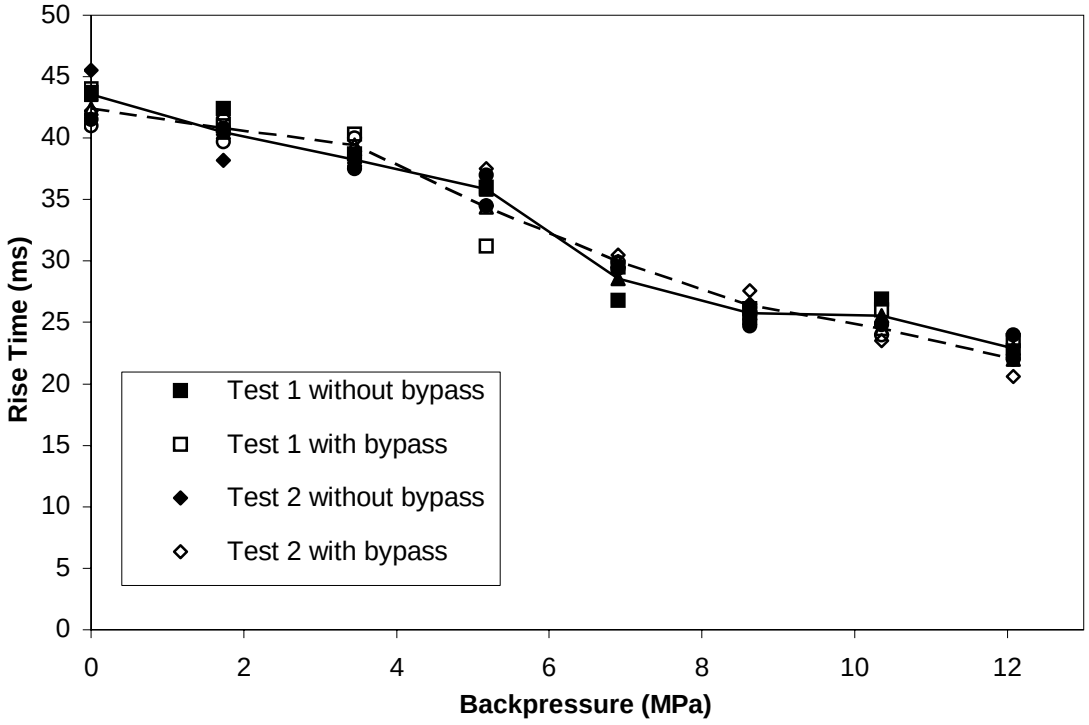

Figure 5.5 Rise time of the motor rotational speed

Ripple Magnitude

The dynamic responses of the hydraulic motor (shown in Figures 5.2 and 5.3) indicated that the motor rotational speed reached the steady state but was superimposed by "ripples". Figure 5.6 shows the relationship between the ripple RMS magnitude and pressure. It was observed that the ripple magnitude increased slightly with increasing pressure when the pressure was less than 5.2 MPa and increased significantly when the pressure was higher than 5.2 MPa. The RMS ripple magnitude of the test with bypass control was always about 20% higher than that without bypass control.

Steady State Value

The performance of the motor rotational speed was also evaluated with its steady state value. As shown in Figures 5.2 and 5.3, there were ripples superimposed on the measured steady state signal. Thus, an average value was used to represent the steady state value of the motor rotational speed.

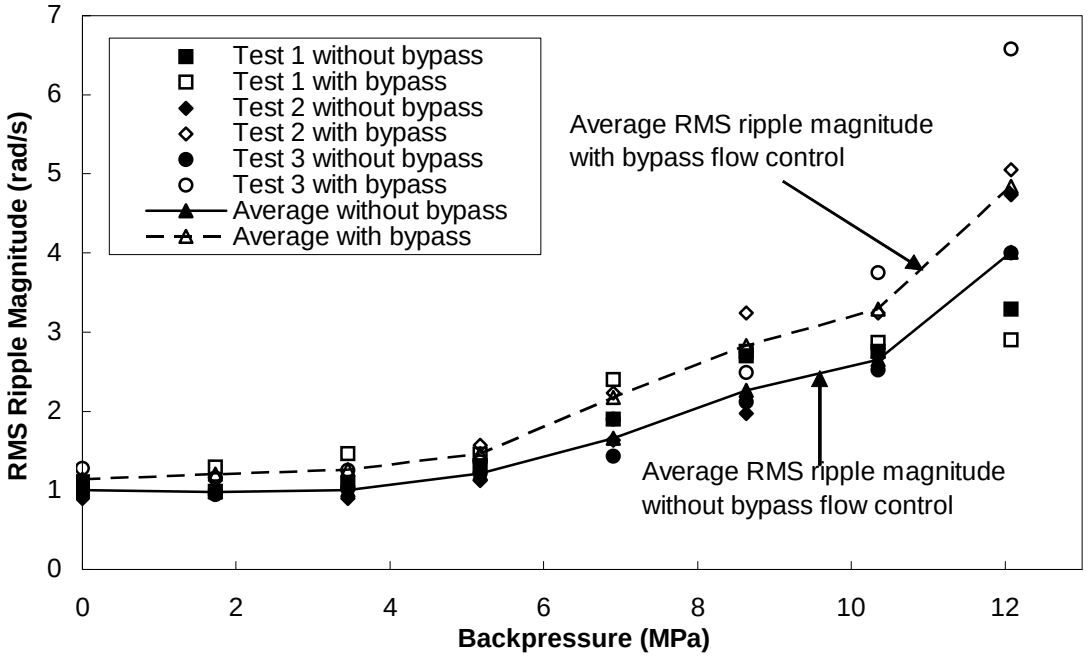

Figure 5.6 RMS Ripple magnitude of the motor rotational speed

Figure 5.7 shows the average steady state value of the motor rotational speed as a function of pressure. It was observed that the steady state values varied at 100±1 rad/s for tests with and without bypass control when the pressure was less than 6.9 MPa. When the pressure was higher than 6.9 MPa, the average steady state value increased with increasing pressure for tests without bypass control. For tests with bypass control, the average steady state value decreased slightly with increasing pressure and was always less than that without bypass control.

5.2.2 Relative Efficiency of the Bypass Flow Control System

As proposed in Section 1.4, the objective of this study was to improve the performance of an existing pump-controlled motor system without sacrificing its overall high relative efficiency. The test results discussed above showed that the performance of the pump controlled motor system was partly improved by using the bypass flow control system in which the overshoot was reduced by about 50%. However, the bypass control also had a negative effect on the relative system efficiency.

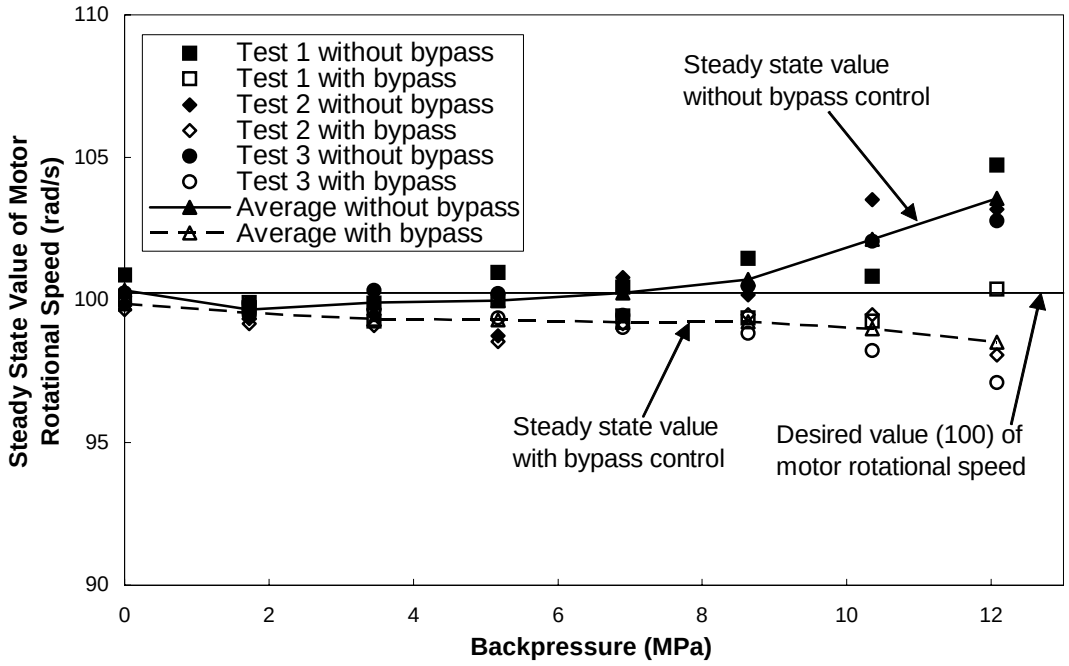

Figure 5.7 Steady state value of the motor rotational speed

To evaluate the influence of the bypass flow control on the relative system efficiency, a Matlab program was written to calculate the relative efficiency of the bypass flow control, which was defined in Section 2.5, as the ratio of the average motor input flow with bypass control over that without bypass control under the same operating condition and time period. This relative efficiency was with respect to the bypass flow control system. Leakage in the pump/motor was not included. Thus, the relative efficiency was not the overall system efficiency but just a local one and is for demonstrating the efficiency of the bypass flow control. To simplify the calculation, the average motor speed during the time period of calculation was used to replace the motor input flow (see Section 2.5).

The procedure to calculate the relative efficiency of the bypass flow control system is as follows:

1) The relative efficiency at each sampling point during a specific time period was calculated according to the definition described in Section 2.5.

2) The average relative efficiency was calculated by averaging the individual relative efficiencies calculated at all sampling points over the whole time period.

Figure 5.8 shows the relative efficiency of bypass flow control system in terms of this ratio.

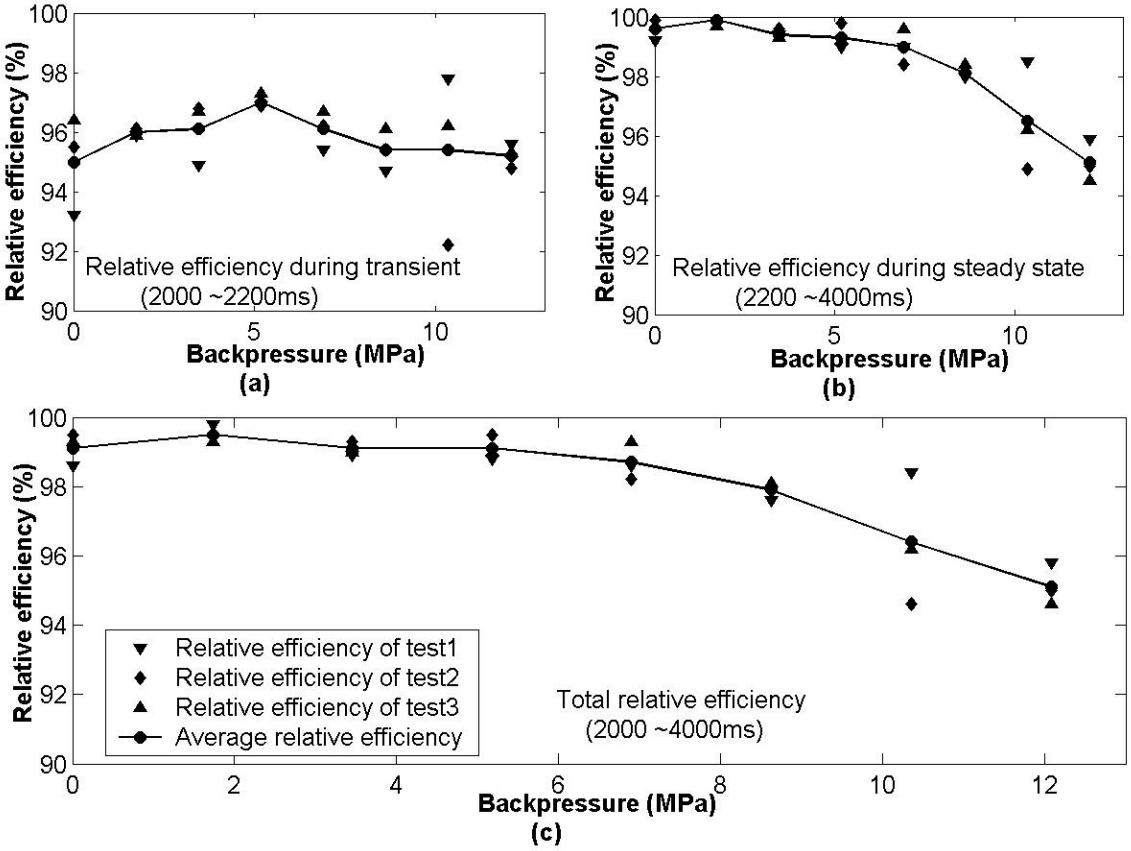

Figure 5.8 Relative efficiency of the bypass control system

Note: the step occurred at 2000 ms for all tests in this section.

The relative efficiency of the system with the bypass flow control was separately calculated during the transient and steady state (after transient) periods. The transient discussed in this case was considered as the time period started from the step point until the transient died out. Since the transient time changed with loading conditions, it was difficult to get a uniform transient time. On the other hand, the ripples also affected the

estimation of the transient time. Hence, a typical transient period of 200 ms was assumed for all tests, during which most transient had died out. Figure 5.8(a) shows the relative efficiency during the transient. It was observed that the relative efficiency of the bypass control during the transient was 96% with a scatter of about ±1%. Figure 5.8(b) shows the relative efficiency during the steady state, a time period of 1800 ms after the transient. This figure shows that the relative efficiency decreased slightly from about 100% to 99% when the backpressure increased from 0 MPa to 8.6 MPa and decreased quickly to 95% when the pressure increased to 12 MPa. Figure 5.8(c) shows the average relative efficiency during the whole time period (2000 ~ 4000 ms) including the transient and steady state. The trend of the combined average relative efficiency was quite similar to the trend of the steady state relative efficiency. The relative efficiency varied around 99% when the pressure was less than 6.9 MPa, and decreased with increasing pressure.

All results shown in Figure 5.8 indicated that the relative efficiency of the bypass flow control system was less than 100%. It varied between 99% and 95% depending on loading conditions. This meant the bypass valve was not fully closed during the steady state as expected. A small portion of the flow, which was approximately equal to 100% minus the relative efficiency, was bypassed through the valve. The reason for this was due, in part, to the motor rotational speed ripple which was fed back to the bypass valve controller through the rotational speed transducer. In essence, the bypass flow control system treated the rotational speed ripples as an overshoot. Because the valve was opened during the ripple overshoot, the effect was to bias the steady state value to something lower than that without bypass control.

5.2.3 Variations in the Rotational Speed Ripple: Discussion

Experimental results shown in the last section indicated that the rotational speed of the hydraulic motor approach steady state in less than 100 ms. However, superimposed on

the measured rotational speed signal was a periodic and non-uniform disturbance signal (ripple and noise) which did not diminish under steady state conditions. This section will discuss the source of the noise and ripple.

A typical motor rotational speed signal is shown in Figure 5.9 (a). The steady state value of the rotational speed (DC value) was 100 rad/s. It was observed that two kinds of signals were superposed on the DC signal. One was in the form of non-periodic noise, and the other one was a periodic, non-uniform ripple signal. The non-periodic noise signal, which occasionally appeared in random “spurts”, was mainly due to the amplifier of the DC motor (see the large spurts shown in Figure 5.9(a)). The DC motor amplifier used pulse width modulation methods to amplify the electrical signal. It controlled the current of the DC motor by varying the duty cycle of the output power under a fixed switching frequency (22 kHz). A noise signal with this frequency was transmitted from the amplifier to all electronic signals (such as rotational speed, swash plate angle and pressure transducers) through the electrical ground. Since the sampling frequency was only 1000 Hz, the noise signal was occasionally sampled by the data acquisition system and appeared randomly in the measured signals in the form of spurts. Many attempts were made to prevent the noise from appearing into the sampling system without compromising the information from the base signal but without success.

The most significant effect on the rotational speed was the non-uniform (magnitude wise) but periodic ripple. The ripple was, in fact, composed of several frequencies. To find out what the frequency spectrum of the non–uniform ripple was, an analytical method called the power spectral density (PSD) (see Appendix E) was used to process the noise signal. The noise signal used for the PSD analysis was not filtered. Figure 5.9(b) shows the PSD result of the motor signal (shown in Figure 5.9(a)).

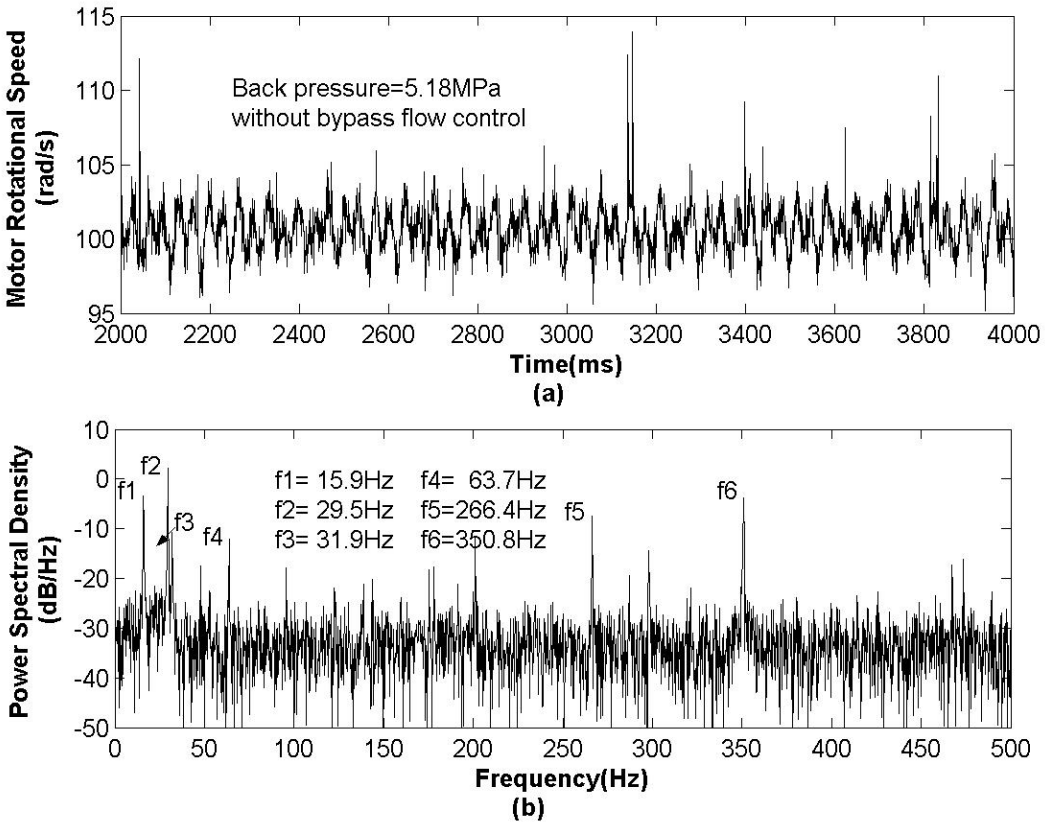

Figure 5.9 A typical motor rotational speed signal and its power spectral density

It was observed that the energy contained in the signal was mainly concentrated at 6 frequencies which could be directly correlated with physical conditions or component behavior. They were:

- f1=16 Hz, the rotational speed of the hydraulic motor,
- f2=30 Hz, the rotational speed of the pump and pump driver (AC motor),
- f3=32 Hz, the second harmonic of the hydraulic motor rotational speed,
- f4=64 Hz, the forth harmonic of the hydraulic motor rotational speed,
- f5=270 Hz, the rotational speed of pump pistons, equal to the product of the pump rotational speed and the number of pistons (9), and
- f6=352 Hz, the rotational speed of the rotational speed transducer commutators, equal to the product of the hydraulic motor rotational speed and commutator number (22).

As mentioned, these six frequencies were highly correlated to physical components in the system. The PSD result also showed some frequency components which had a smaller power. These frequencies corresponded to higher harmonics of the pump and motor rotational speed, and other characteristics of the system. They were, however, comparatively small in power than the six mentioned above.

The PSD as a function of pressure for the six main frequencies are shown in Figure 5.10. The actual frequency values were only approximately constant, and changed slightly with loading conditions. For example, the frequency of the pump rotation decreased from 29.8 Hz to 28.8 Hz when the pressure increased from 0 to 12.1 MPa. Test results for the system with the bypass flow control are also shown in the same figure for comparison.

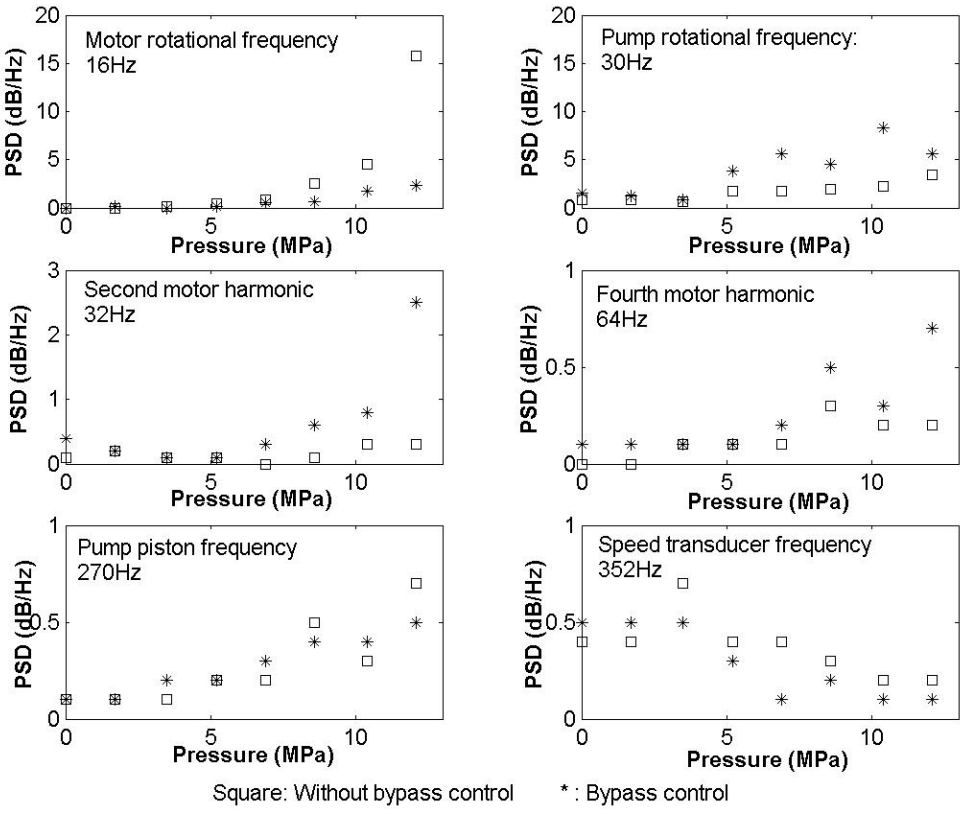

Figure 5.10 PSD magnitudes as the function of the pressure

The results from Figure 5.10 indicated that the PSD magnitudes increased with increasing pressure at most of the frequencies (except at the frequency of 352 Hz). This

pressure dependency was consistent in both the PSD magnitude and the ripple RMS magnitude results. The test results also showed the rotational speed ripple was mainly a consequence of the pump basic rotational frequency for the system with and without the bypass control. One such example can be observed in Figure 5.2, in which the underlying ripple frequencies (again, with and without bypass control) were both about 30 Hz, the frequency of the pump rotation.

Another observation that can be made from Figure 5.10 is that the PSD magnitudes for the system with bypass control are larger than those in the system without bypass control at most pressure levels.

An interesting situation occurs at pressures higher than 10 MPa. The ripples for the system without the bypass flow control were mainly a consequence of the motor rotational frequency (as opposed to the pump rotational frequency) - see the top left figure in Figure 5.10. The motor rotation frequency PSD magnitude increased significantly when the system operated at higher pressures. This result was consistent with the RMS ripple magnitude at pressures greater than 12 MPa (see Figure 5.6).

The dependency of the ripple base frequency on the rotational speed of the pump and at higher pressures, the motor, was not expected. Normally, one would expect the ripple to be dominated by the frequency associated with the nine pistons for both the pump and motor. This was not the case and does indicate that the PSD was picking up some disturbance introduced by some fault or wear in the pump and motor. Both units were off the shelf components and have been well used. As mentioned, these disturbances were highly dependent on the system load and hence pressure. This dependency on the pressure could be attributed, in part, to the nonlinear gains on the DC motor controller which would tend to amplify any perturbations in pressure due to the motor, for example. The point to be made here is that the presence of the ripple was a consequence of the pump and motor dynamics and was not introduced by the bypass control algorithm. The bypass controller

did, however, try to compensate for pump ripple as discussed above.

Compared to the pump and motor rotation, pump pistons and transducer commutators had comparably smaller effects on the ripple RMS value. At the frequencies of these components, there were no significant differences between the systems with and without bypass flow control.

5.3 Experimental Test with a Inertial and Constant Resistive Load

The controllers designed for the DC motor and bypass control valve were based on a constant resistive load. The results for a constant resistive load were consistent with that predicted by theory. This section will present the results of the DC motor controlled pump and bypass flow control system in the presence of an inertial load and a constant load. A flywheel was attached to the motor shaft to simulate the inertia load. The inertial load had a different characteristic from other load types due to its moment of inertia. Usually, a system with an inertial load will demonstrate a large overshoot and undershoot during the transient due to the presence of the inertia of both the fluid (due to the pump) and load.

Figure 5.11 shows the dynamic response of the hydraulic motor with an inertial load. A fixed backpressure was set to 3.45 MPa. It was observed that the system without using the bypass control exhibited a limit cycle oscillation. The system with bypass control did reach steady state but only with a long settling time and large undershoot. The test results measured at other pressures also exhibited a similar performance.

It was apparent that the limit cycle oscillation was not caused by using the bypass flow control since the system with the bypass control demonstrated a stable performance. It was believed that the limit cycle oscillation might be caused by the DC motor since the DC motor controller was heavily dependent on the load pressure. In the constant load, the DC motor did have an affect on the amplitude of the overshoot due to the controller gain's dependency on pressure. To see if this effect was present in the inertial load which showed extreme variations in pressure, a new DC motor controller was designed for the same

backpressure with the inertial load applied. The bypass flow control system was not included in the design and hence the control algorithm remained unchanged. A similar procedure, which was used to design the original DC motor controller, was followed.

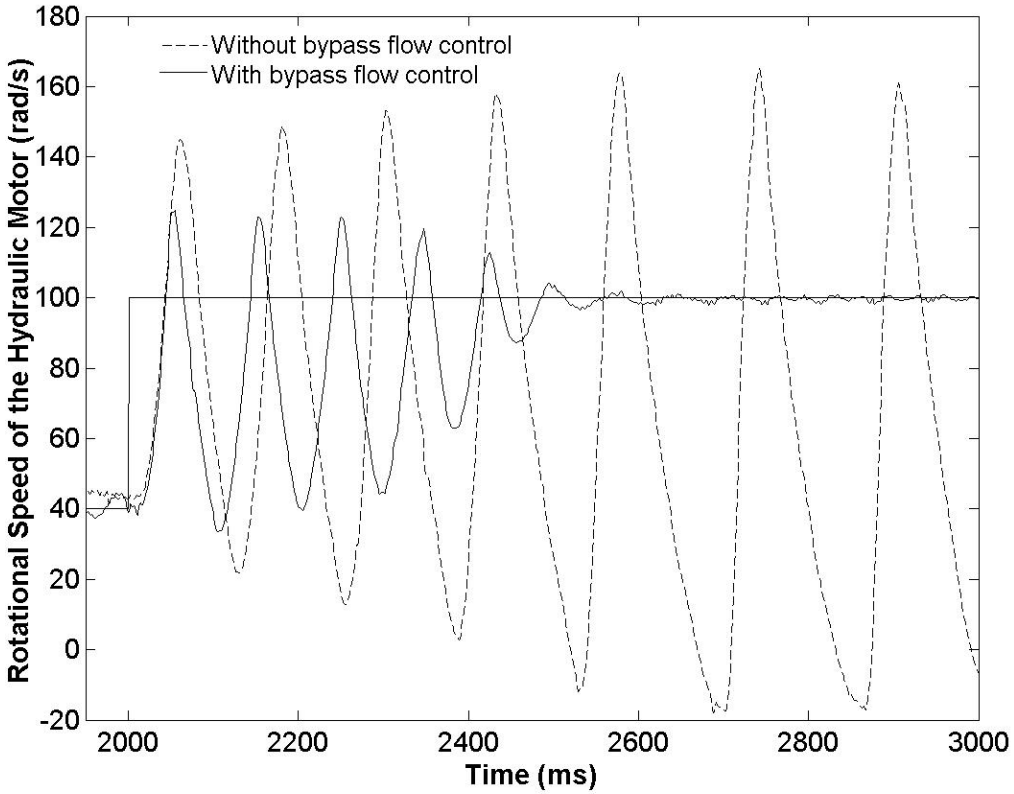

Figure 5.11 Dynamic response of the hydraulic motor with an inertial load

First, the proportional gain of the DC motor controller was increased until the hydraulic system exhibited a limit cycle oscillation (shown in Figure 5.12(a)).

It was observed that the pump swashplate angle experienced a limit cycle oscillation of 30 Hz. However, the hydraulic motor limit cycle frequency was at some value other than this. A PSD analysis indicated two dominant frequencies present in the motor rotational speed signal. The spread of frequencies about 30 Hz was quite narrow but showed a larger power in general. The second dominant frequency was at 11 Hz but showed a wide band and slightly smaller PSD magnitude.

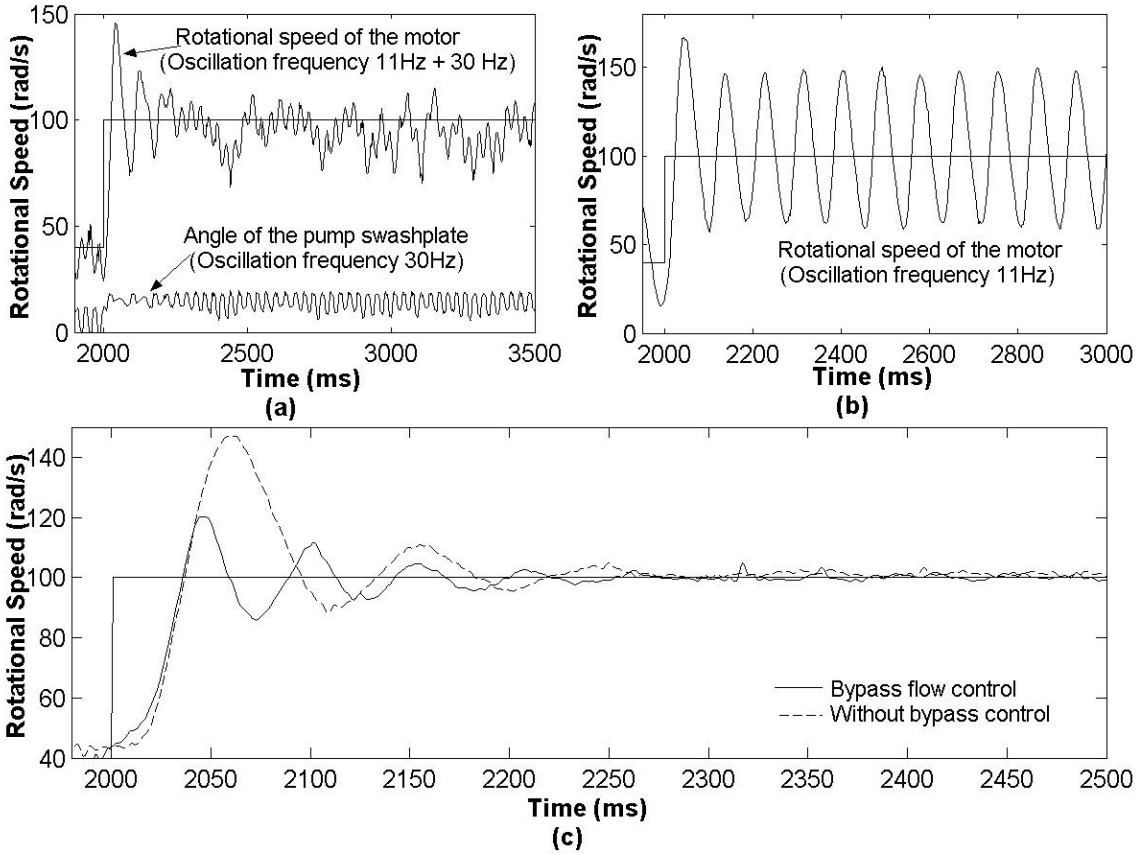

Figure 5.12 Redesign of the DC motor controller with the inertial load

As a first step, the 30 Hz was used as a basis for the design of the controller using Ziegler-Nichols tuning PID rules. However, the hydraulic motor exhibited a clear oscillation at the frequency of 11 Hz (shown in Figure 5.12(b)) when the controller was applied to the DC motor.

The final DC motor controller was thus designed based on a frequency of 11 Hz. Test results for the new designed controller are shown in Figure 5.12(c). It is observed that the new DC motor controller shows a better performance than the previous controller for the inertial load.

Using the same procedure as above two more controllers were designed at backpressures of 0 MPa and 6.9 MPa. Test results of these two controllers are shown in Figure 5.13.

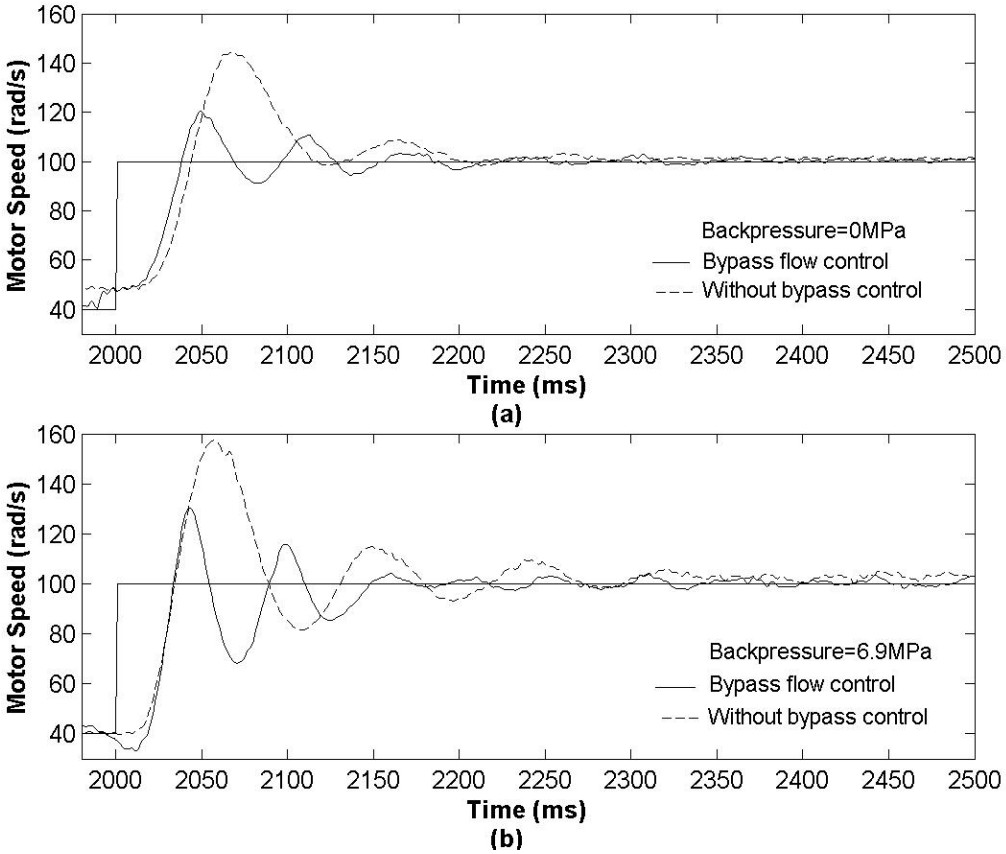

Figure 5.13 Dynamic responses of the motor with 2 redesigned controllers (Inertial load)

Based on test results shown in Figures 5.12 and 5.13, it was found that:

- The DC motor controller designed based on a constant resistive load could not work properly when an inertial load was applied.
- The DC motor controller was successfully redesigned for 3 pressure levels and good performance was achieved.
- The bypass valve controller was independent of loading conditions. It performed equally well with both types of loads studied here. What is significant is that the bypass control produced a stable response when the same system without the bypass exhibited a limited cycle. However, the overshoot was still large due to the inertia.

For the inertial load, a DC motor controller could be redesigned with an acceptable performance. At pressures higher than 12 MPa, the system performance was not acceptable and could not be improved by controller redesign. For pressures less than 12 MPa, a pressure dependent nonlinear controller could be designed for inertial loads.

In summary, the DC motor controller was dependent on both the system pressure, and load type. A nonlinear controller could be designed to adapt any load conditions.

5.4 Summary of the Experimental Tests

The concept of the bypass flow control was experimentally evaluated in the previous sections. Test results showed good performances of the DC motor controlled pump and bypass flow control system. The following presents a summary of the experimental tests.

Summary for the system without using the bypass flow control

1. The rise time of the hydraulic motor, which was directly controlled by the pump, was between 20 to 50 ms, depending on loading conditions.
2. The overshoot was more than 30% for a constant resistive load and inertia load.
3. The hydraulic motor rotational speed reached steady state in 100 ms for the constant load, and in about 250 ms for the inertial load.
4. A non-uniform ripple was superimposed on hydraulic motor's steady state rotational speed. The RMS magnitude of the ripple increased with increasing pressure.

Summary for the system using the bypass flow control system

1. The relative efficiency of the bypass flow control system varied from 99% to 95% depending on loading conditions. This meant that about 1% to 5% flow was bypassed through the bypass valve during the transient and steady state due to the overshoot and ripples. For a pump/motor that does not demonstrate

significant flow ripple of the magnitude experienced in this study, the relative efficiency would be the same as the pump/motor system without bypass.

2. The bypass flow control system effectively reduced the overshoot of the motor rotational speed by about 50%.
3. The rise time was not affected by using the bypass flow control.
4. The steady state error was slightly larger than the system without using the bypass flow control due to the inherent bias created by the ripples at most of the pressure levels.
5. The valve was not fully closed during the steady state as expected due to the presence of ripple. Hence, a very small portion of the flow was bypassed to the tank across the bypass valve. This would have an effect on reducing the efficiency but the reduction was considered to be small.

Chapter 6

Conclusions and Recommendations

6.1 General

The objective of this study was to develop a hydraulic circuit with good dynamic performance and high efficiency. This was, in part, realized by improving the dynamic performance of an energy efficient pump-controlled system. The pump-controlled system has a very high relative system efficiency due to the minimization of the power loss between the pump and actuator. To improve the dynamic performance of the pump, a DC motor was designed to directly control the pump swashplate. In order to facilitate the design of a DC motor controller with good performance, the pump and DC motor were mathematically modeled. Using this model, combined with some experimental results, a nonlinear PID controller was designed for the DC motor. The gains of the controller were designed to be a function of the pressure. By means of this nonlinear DC motor controller, the pump could operate in a relative stable manner without limit cycle oscillation at any pressure levels and at most swashplate angles (only swashplate angles between 3˚ and 14˚ were tested). Test results showed that the DC motor-controlled pump did indeed, demonstrate a fast dynamic response. The rise time of the pump swashplate angle was less than 40 ms over the whole range of pressures examined independent of the swashplate final angle. A fast dynamic response speed could be achieved with a rise time of less than 17 ms if the pump pressure increased to 6.9 MPa.

As the dynamic response speed of the pump was increased, the overshoot of the hydraulic motor's response also increased (between 35% and 70%). To reduce the overshoot, a bypass flow control system was designed to bypass part of the pump flow during the transient. Before designing the controller for the bypass valve, the complete

system model (including the bypass servo valve and hydraulic motor) was established. Since the bypass flow control system could not respond to a negative signal, a PID controller with a resetable integral gain was designed for the bypass valve based on the model simulation. “Proof of concept” of bypass flow control was established using a Matlab/Simulink® program. The simulation results showed that the bypass flow control could effectively reduce the overshoot of the motor rotational speed.

The dynamic performance of the pump controlled system and the concept of the bypass flow control were evaluated through a series of experimental tests. Two load types (constant resistive and inertial) were applied to the hydraulic motor. Test results showed that the experimental pump-controlled system indeed, demonstrated a very fast dynamic response. However, the DC motor controller designed for a constant load did not work in a stable fashion under inertial load conditions. The bypass control system was able to provide a stable response but the settling time was large. By redesigning the DC motor controller, the hydraulic motor could reach the steady state without any limit cycle oscillations. The bypass flow control system worked effectively for all controllers regardless of the loading conditions.

6.2 Conclusions

As the result of this study, the following conclusions are made.

1. It was concluded that the dynamic response of the pump was improved by using the DC motor control approach. The pump swashplate was directly controlled by a DC motor instead of using the more commonly used hydraulically actuated control approach. Because of the fast dynamic response of the DC motor, the DC motor controlled pump exhibited a rise time of 15 to 35 ms depending on the pump pressure.
2. The bypass flow control system was effective in removing the overshoot. Under different loading conditions, the bypass flow control could reduce the

overshoot of the hydraulic motor rotational speed by about 50%.

3. The relative efficiency of the circuit was almost the same as the pump-controlled system. It was affected slightly (in a negative sense) by using the bypass flow control. The bypass valve was not completely closed as expected during the steady state due to the rotational speed ripples. The relative efficiency of the circuit with the bypass flow control system was 1% to 5% lower for the particular pump-controlled system that was used in this study. If the pump/motor did not demonstrate the rotational speed ripples, the relative efficiency would be the same as the pump/motor system without bypass.

6.3 Recommendations

Some considerations that should be investigated in the future work are:

1. The bypass flow control system could effectively remove the overshoot, but not the undershoot. A "flow supplement" system might be considered as a means of providing the extra flow to the system when the motor exhibits an undershoot.
2. The rotational speed ripple was caused mainly by the rotation of the pump and motor. However, it was not clear how the pump and motor rotation affected the magnitude of the rotational speed ripple. More analysis and experimental tests needs to be done to solve this problem. The magnitude of the rotational speed ripples could be reduced with a new design approach.
3. The DC motor was not as stiff as its hydraulic counterpart. The load heavily affected its performance. Also, the DC motor controller was dependent on loading conditions. This problem could be solved by designing a DC motor controller that could adapt to different loading conditions. To do so, a wide range of loading conditions (such as the pressure, flow rate and load types)

should be investigated during the design.

4. The system stability may be improved by using system identification and pole-zero placement strategies.

References

1. Backe, W., 1991, “Electrohydraulic loadsensing”, *Proceedings of the International Off-Highway and Powerplant Congress and Expostion*, Sep 9-12, Milwaukee, USA.
2. Backe, W., 1993, “Recent Research Projects in Hydraulics”, *Proceedings of the Second JHPS International Symposium on Fluid Power*, September 6-9, Tokyo, Japan, pp.3-27
3. Backe, W. and Kogl, C., 1993, “Secondary controlled motors in speed and torque control”, *Proceedings of the Second JHPS International Symposium on Fluid Power*, September 6-9, Tokyo, Japan, pp.241-248.
4. Burgt, J., 1993, "A new approach to saving energy in cyclic loaded hydraulic systems: learning hydraulic systems", *Proceedings of the 3rd International Conference on Fluid Power Transmission and Control*, Hangzhou, China, pp.123-130.
5. Cundiff, J. S., 2002, "Fluid Power Circuits and Controls: Fundamentals and Applications", CRC Press, Roca Raton.
6. Habibi, S., 2001, "Lecture notes: Control System I", Department of Mechanical Engineering, University of Saskatchewan.
7. Käppi, K., 2000, "Modeling and Simulation Utilized in Research and Development of Mobile Hydraulics", *Proceedings of the 1st FPNI-PhD Symposium*, Hamburg, Germany, pp.353-361.
8. Kavanagh, G. P., 1987, "The Dynamic modeling of an Axial Piston Hydraulic Pump", M.Sc Thesis, Department of Mechanical Engineering, University of Saskatchewan.
9. Lantto, B., Krus, P. and Palmberg, J., 1991, “Interaction between loads in load-sensing systems”, *Proceedings of the 2nd Tampere International Conference on*

Fluid Power, March 19-21, Tampere, Finland.

10. Li, Z., Ge, Y. and Cheng, X., 1998, "Hydraulic Components and Systems" (in Chinese), China Mechanical Industry Press, pp2-3.
11. Liang, X., Virvalo, T. and Linjama, M., 1999, “The Influence of Control valves on the efficiency of a Hydraulic Crane”, *Proceedings of the 6th Scandinavian International Conference on Fluid Power*, May 26-28, Tampere, Finland, pp.381-394.
12. Liang, X. and Virvalo, T., 2001 (1), “What's wrong with energy utilization in hydraulic cranes”, *Proceedings of the 5th International Conference on Fluid Power Transmission and Control*, April 3-5, Hangzhou, China, pp.419-424
13. Liang, X. and Virvalo, T., 2001 (2), “Energy reutilization and balance analysis in a hydraulic crane”, *Proceedings of the 5th International Conference on Fluid Power Transmission and Control*, Hangzhou, China, pp.306-310.
14. Luomaranta, M., 1999, “A Stable electro-hydraulic load sensing system based on a microcontroller”, *Proceedings of the Sixth Scandinavian International Conference on Fluid Power*, May 26-28, Tampere, Finland, pp.419-432.
15. Mack, P., 1985, "Feasibility Study of the Use of a Microcomputer to Control the steady state Operating Characteristics of a Variable Displacement Hydraulic Pump”, Master’s Thesis, Department of Mechanical Engineering, University of Saskatchewan, University of Saskatchewan.
16. Malsen, R., Achten, P. and Vael, G. 2002, “Design of Dynamic and Efficient Hydraulic Systems around a Simple Hydraulic Grid”, *Proceedings of the SAE Off-Highway Congress*, March, Las Vegas, USA.
17. Mansouri, G., Misovec, K., Johnson, B., Babbitt, G. and Sturman, O., 2001, “Variable flow supply using switched-mode control of a fixed-displacement pump”, *Proceedings of the Seventh Scandinavian International Conference on Fluid Power*,

May 30-June, Linkoping, Sweden, pp.361-376.

18. Martin, M., 1992, "Load Simulator Using Hydraulics", Master's Thesis, Department of Mechanical Engineering, University of Saskatchewan, University of Saskatchewan.
19. Merritt, H., 1967, "Hydraulic Control Systems", John Wiley & Sons, Inc., New York, pp.152-157.
20. Nakano, K. and Tanaka, Y., 1988, "Energy-saving type electro-hydraulic servo system", *The Journal of Fluid Control*, v 18, n 3, p 35-51.
21. Post, W. and Druten, R., 2001, "The design of energy-efficient power transmissions: Learning hydraulic systems and zero-inertia power transmission", Bath Workshop on Power Transmission and Motion Control, Professional Engineering Publishing Ltd., London, pp.245-258.
22. Rahmfeld, R., 2000, "Development and Control of Energy Saving Hydraulic Servo Drives**",** *Proceedings of the 1st FPNI-PhD Symposium*, Hamburg, Germany, pp.167-180.
23. Rahmfeld, R. and Ivantysynova, M., 2001, "Displacement controlled linear actuator with differential cylinder –a way to save primary energy in mobile machines", *Proceedings of the 5th International Conference on Fluid Power Transmission and Control*, Hangzhou, China, pp.296-301.
24. Ramirez, R. W., 1985, "The FFT Fundamentals and Concepts", Prentice-Hall, Inc., New York.
25. Tanaka, Y., Nakano, K. and Yamamoto, N., 1989, "Energy–Saving Hydraulic Power Source Using Inverter-Motor Drive", *Proceedings of the First JHPS International Symposium on Fluid Power*, Tokyo, Japan.
26. Tikkanen, S., Herranen, M., Lammila, M. and Vilenius, M., 2001, "Performance of Dual Hydraulic Free Piston Engine", *Proceedings of the Seventh Scandinavian*

International Conference on Fluid Power, May 30-June 1, Linkoping, Sweden, pp.133-150.

27. Vael, G. E. M., Achten, P. A. J., 1998, “The Innas Fork Lift Truck -Working under constant pressure”, *Proceedings of the first International Fluid Power Conference*, Part 1, M Verlag Mainz, Aachen.
28. Vael, G. E. M., Achten, P. A. J., Fu, Z., 2000, “The Innas Hydraulic Transformer: The key to the hydrostatic Common Pressure Rail”, *SAE 2000 Transactions Journal of Commercial Vehicles*, Vol. 100, Section 2.
29. Wendel, G., 2000, “Regenerative Hydraulic Systems For Increased Efficiency”, *Proceedings of the 47th National Conference on Fluid Power*, April 4-6, Chicago, USA, pp.199-206.
30. Wendel, G., 2002, “Hydraulic System Configurations for Improved Efficiency”, *Proceedings of the 49th National Conference on Fluid Power*, March 19-21, Las Vegas, Nevada, USA, pp.567-573.
31. Wu, D., 2003, " Modeling and Experimental Evaluation of a Load-Sensing and Pressure Compensated Hydraulic System”, Ph.D Thesis, Department of Mechanical Engineering, University of Saskatchewan.
32. Yao, D., 1997, "Research on a Direct Pressure Sensing Relief Valve ", M.Sc Thesis, Department of Mechanical Engineering, University of Saskatchewan.
33. You, Z., 1989, "A Study on Interactions between Fluid Power Components", M.Sc Thesis, Department of Mechanical Engineering, University of Saskatchewan.
34. Ziegler, J. G. and N. B. Nichols, 1942, "Optimum Settings for Automatic Controllers", ASME Trans. 64 (1942), pp. 759-68.
35. “760 Series Servovalve”, Moog Inc., East Aurora, New York
36. “HT-High Torque, Direct Drive Series”, Emoteq Inc., Tulsa, Oklahoma

Appendix A

Calibration of the Measurement System

The measurement system shown in Figure A.1 consists of transducers, a data acquisition system (DAQ) and amplifiers. System variables such as swashplate angle, pressure and rotational speed are converted to voltage signals by the transducers and collected by the computer through the DAQ. Output control signals from the computer are amplified by the external amplifiers.

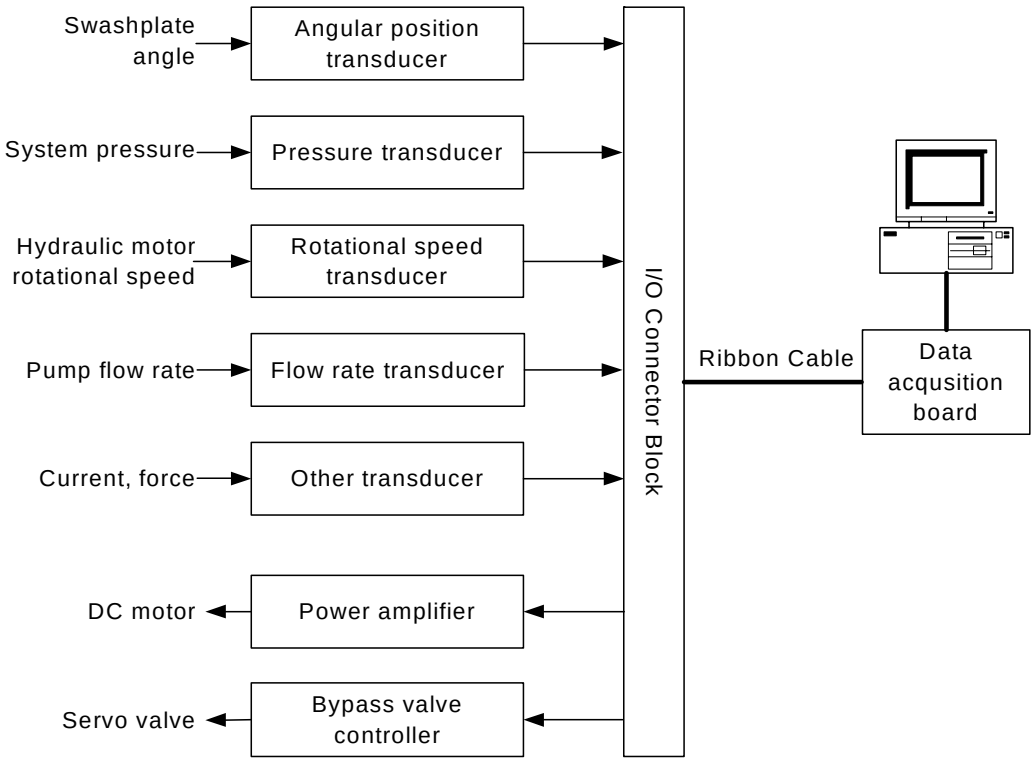

Figure A.1 Measurement system

As a first step, the calibration of all transducers was completed before taking any online measurements and control action to avoid measurements containing very large offset, gain and linearity errors. This section will discuss the calibration of all transducers and amplifiers used in the research.

A.1 Calibration of the Data Acquisition System

The DAQ includes a data acquisition board (NI PCI-6035E) and an I/O connector block. They are connected by a “ribbon cable”. The DAQ has 16 single-ended (eight differential) analog input channels and 2 single-ended analog output channels, and has a sampling frequency of 200 kHz. The resolution for the analog input (output) is 16 (12) bits.

The DAQ can measure and condition the input signals which are stationary but cannot compensate for time varying effects.

A.1.1 Calibration of analog input channels

In the calibration procedure, voltages are applied to the analog input and the input voltage from the DAQ via the computer recorded. Preliminary results indicated that a DC bias and a non-unity gain existed in the DAQ. The system gain was reset to achieve a unity gain as shown in Figure A.2. In this figure, as in subsequent ones, the “error” is defined as the difference between the measured output voltage (after adjustment) and a “best fit” line which constitutes the “calibration equation”.

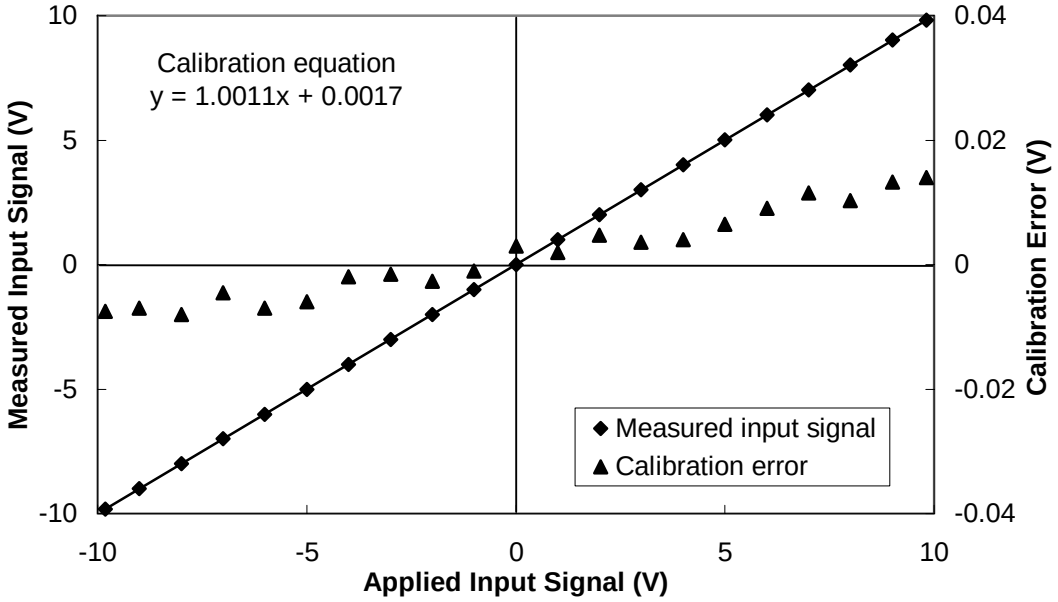

Figure A.2 Calibration of analog input

The scatter of measured data with respect to the calibration best fit line falls within a region of ±0.015 V (0.15% full scale). It was observed that after the adjustment to the DAQ, the calibration best fit line was the same for all channels. In addition, tests were repeatable with no visual difference.

A.1.2 Calibration of analog output channels

The calibration procedure of the DAQ analog output was as follows: Voltages were generated by the computer and directed through the DAQ to each analog output channel. The output voltages were measured at the terminal end of the connector block using a highly accurate multimeter (Fluke 37, 0.1% full scale).

Similar to the input, a bias and a non-unity gain were observed. The DAQ was adjusted and the calibration procedure repeated. The results are shown in Figure A.3 along with the error. It is noted that a maximum error of 0.008 V (0.08% full scale) was observed. The test was repeated for each channel and the same calibration equation occurred. The test was highly repeatable with no visual difference in the results.

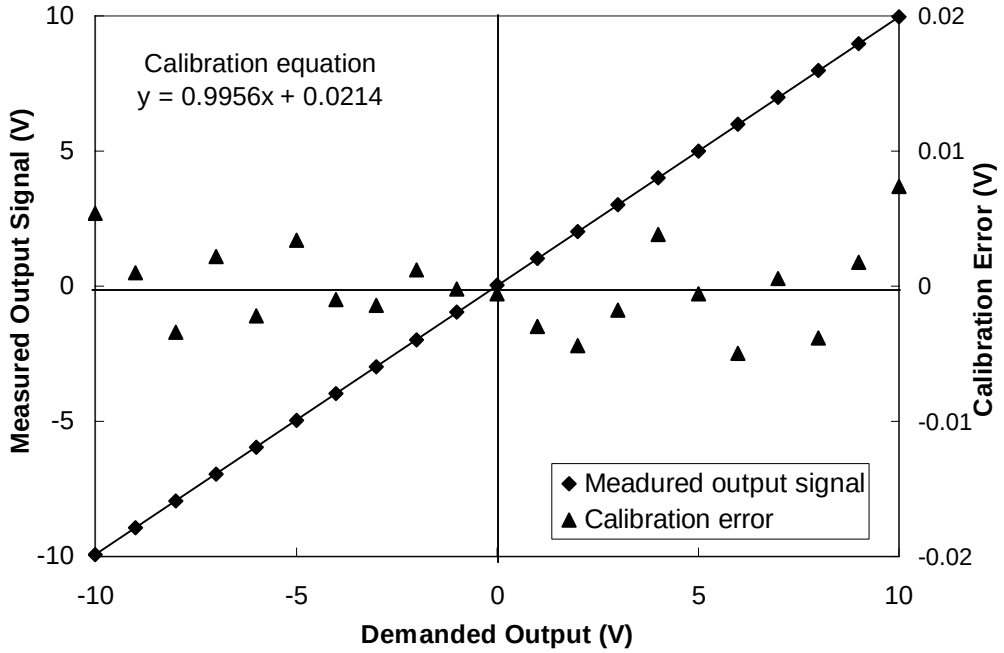

Figure A.3 Calibration of analog output

A.2 Calibration of the Angular Position Transducer

A Rotary Variable Inductance Transducer (RVIT, model R60D) was used to measure the angle of the swashplate. The RVIT incorporates a set of printed circuit coils and a conductive spoiler. During operation, the conductive spoiler rotates with the transducer shaft, altering the magnetic field generated by the printed circuit coils. The resulting imbalance is converted to a linear DC voltage output that is directly proportional to the angle of the rotor shaft. The output range of the RVIT is ±60º.

To calibrate the RVIT, the angle of the shaft must be precisely measured. This was done by converting the angular displacement to a linear displacement. A cylinder with a diameter of 19 mm was coupled to the rotor of the transducer. The conversion to linear displacement was achieved by connecting a thin wire wound on the cylinder to a linear variable differential transducer (LVDT). A plot of the output voltage from the RVIT vs the measurement source voltage is shown in Figure A.4. The error or deviation from a straight best fit line is also shown.

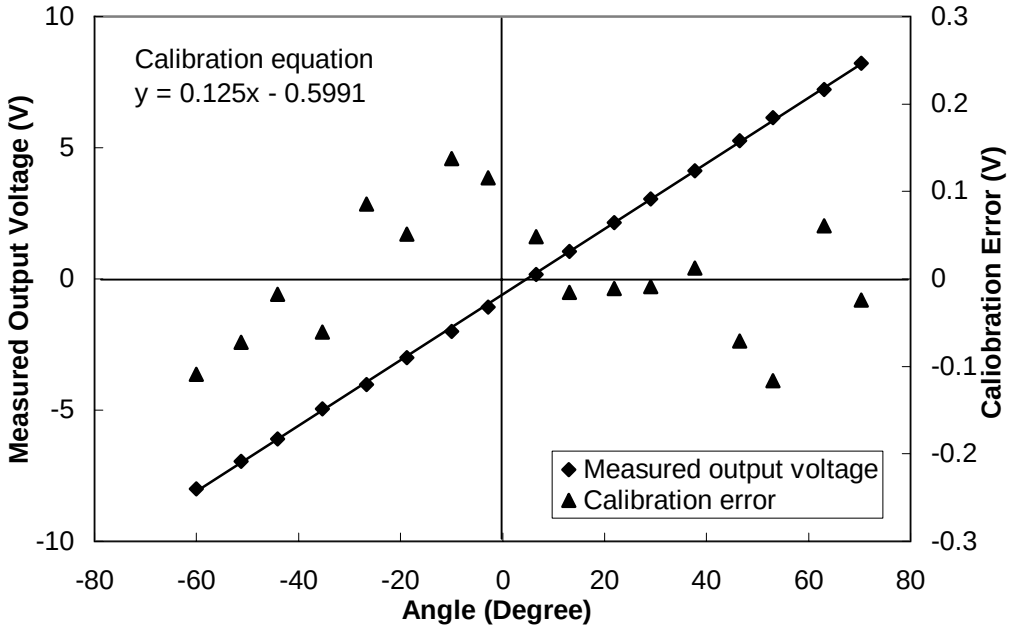

Figure A.4 Calibration of angular position transducer

Most of the error lies within a range of ±0.125 V which corresponds to an angle of ±1º. The actual angular displacement of the pump is 20º. It is observed that on an absolute scale, the range of 0~20º show a significant error variation. However, from 20~45º, the error variation is small (less than ±0.02 V), Thus the angular RVIT was adjusted in the 20~45º range to match the displacement of the swashplate 0~20º.

A.3 Calibration of the Pressure Transducer

The pressure transducer (Sensotec model Z/6415-01ZG), which was used to measure the pressure at the pump outlet, provides an output voltage directly proportional to the applied pressure. The pressure transducer senses the pressure through a silicon type pressure sensor diaphragm with strain resistors (a 4-arm active Wheatstone bridge) combined with a signal conditioning circuit. The excitation voltage was 10 V DC (regulated). The output signal range depends on the excitation voltage. The maximum output range is 0 V~5.5 V DC.

The pressure transducer was calibrated with a twin seal pressure test dead weight tester (Type 5525). Selected weights (representing system pressures) were applied to the test unit and the related transducer output voltages measured. The output voltage as a function of calibrated pressure is shown in Figure A.5. The calibration errors all fall in a range of ±0.05 V (0.5% full scale).

A.4 Calibration of the Tachometer

A tachometer (Kearfott CM09608007) is a small generator whose rotator is connected to the hydraulic motor shaft. The tachometer generates an output voltage which is proportional to the rotational speed. The rotational speed of the hydraulic motor was measured using a laser light source and the output voltage recorded by a multimeter.

The tachometer speed versus output voltage is shown in Figure A.6. The scatter of the error falls within a range of ±0.045 V (0.7% full scale). It is noted that the error

increases with the rotational speed.

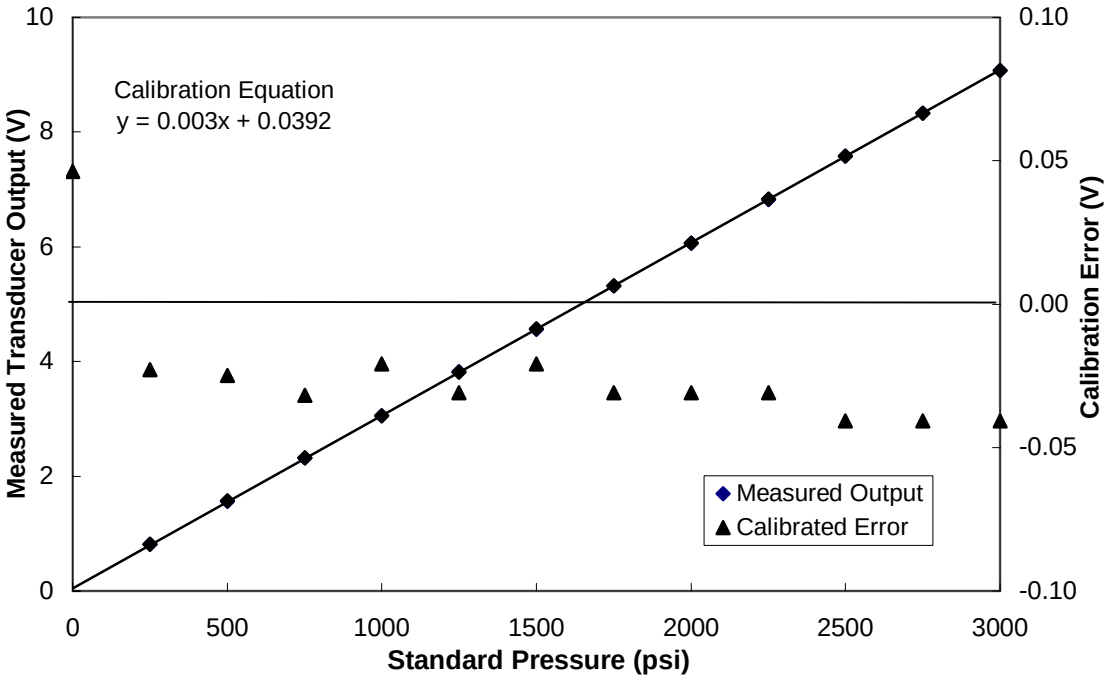

Figure A.5 Calibration of pressure transducer

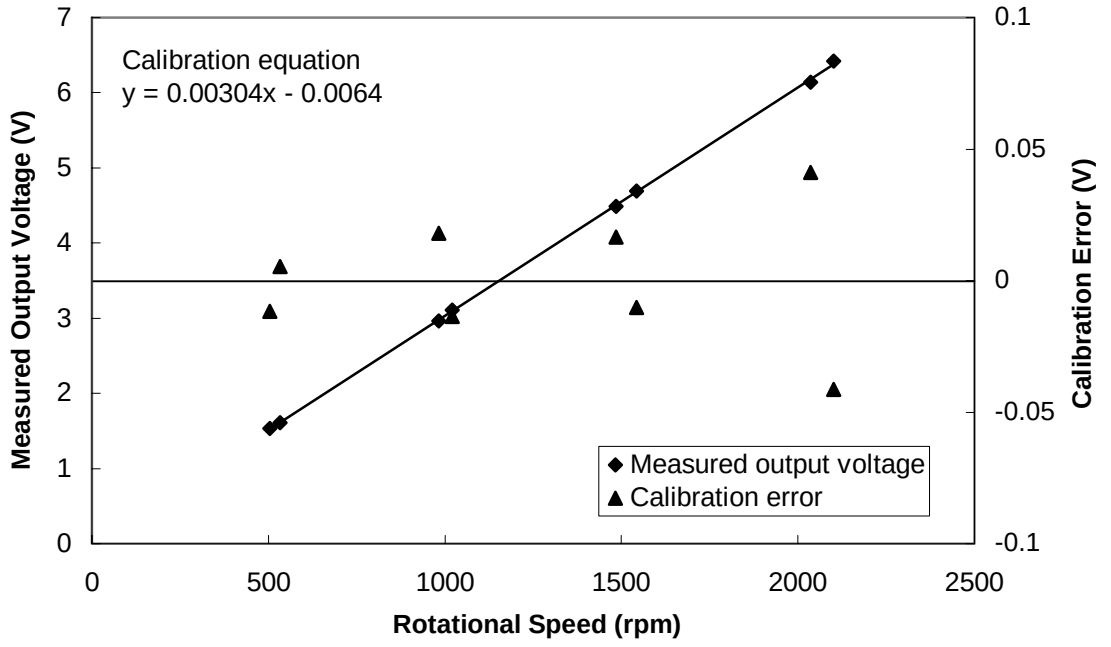

Figure A.6 Calibration of tachometer

A.5 Calibration of the Flow Meter

The flow meter measures the flow rate by measuring the force that is produced by the pressure drop across a drag element in the transducer. An output voltage proportional to the force is measured using a Wheatstone bridge built into the flow meter. The relationship between the flow rate and the measured output is a square root relationship (referring to the user manual of the flow meter) and is given by:

$$Q_i = \sqrt{\frac{V_i}{V_{fs}}} Q_{fs} \tag{A.1}$$

where Q_i and Q_{fs} are the instantaneous and full scale flow rate, V_i and V_{fs} are instantaneous and full scale voltage output.

To calibrate the flow meter (Ramapo model V-5-A0S5K6-E), an accurate flow source must be used. This was achieved using a position-controlled cylinder that can follow a triangular wave input. The flow rate is equal to the product of the piston area and the velocity. The velocity is the slope of the triangular wave. The flow from the cylinder passes through the flow transducer and the output voltage recorded. By changing the slope of the triangular waveform, the magnitude of the flow was changed. The output voltage from the transducer passes through the square root amplifier which gives an output voltage approximately proportional to the input flow. It is this output voltage that is plotted as a function of input flow and is shown in Figure A.7. The scatter of the error falls within a range of ±0.15 GPM (1.6% full scale).

A.6 Calibration of the Current Transducer

The current transducer (AM 503 current measurement system) was used to measure the current of the DC motor. The AM 503 current measurement system consists of an AM 503B Current Probe Amplifier, a current probe A6302 and a TM 502A Power Module. The bandwidth of the power module was 50 MHz. The maximum continuous current was 20 A.

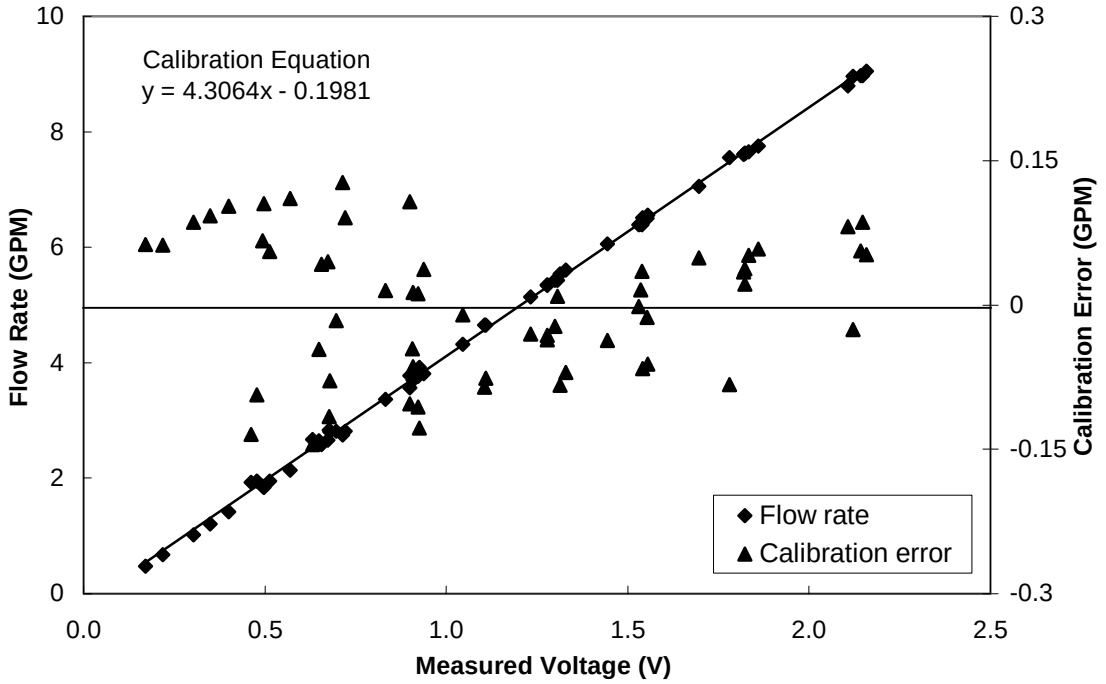

Figure A.7 Calibration of flow meter

A DC power supply, whose voltage range was 0~150 V DC, was used to vary the current of the DC motor which was blocked. The current was recorded by the current transducer and an ammeter (0.75% full scale accuracy) simultaneously. The calibration results are shown in Figure A.8. There are no visual differences between the three tests. The calibration error falls within a range of ±0.05 V (or 0.1% full scale).

A.7 Calibration of the DC Motor Torque Sensitivity

In order to model the DC motor and pump, the torques acting on the swashplate due to the friction and pressure effect are required. Since the space between the DC motor and pump was limited, it was difficult to measure the torque using a torque transducer. An indirect method was used in this study, which measured the torque by using a DC motor. The DC motor (EC 070205004) used here was a small regular brush DC motor and was different from the one used for the pump swashplate control (high torque brushless DC motor). This particular motor was used only for measuring parameters of

the pump model because of the motor's acceptable constant torque sensitivity and low noise level.

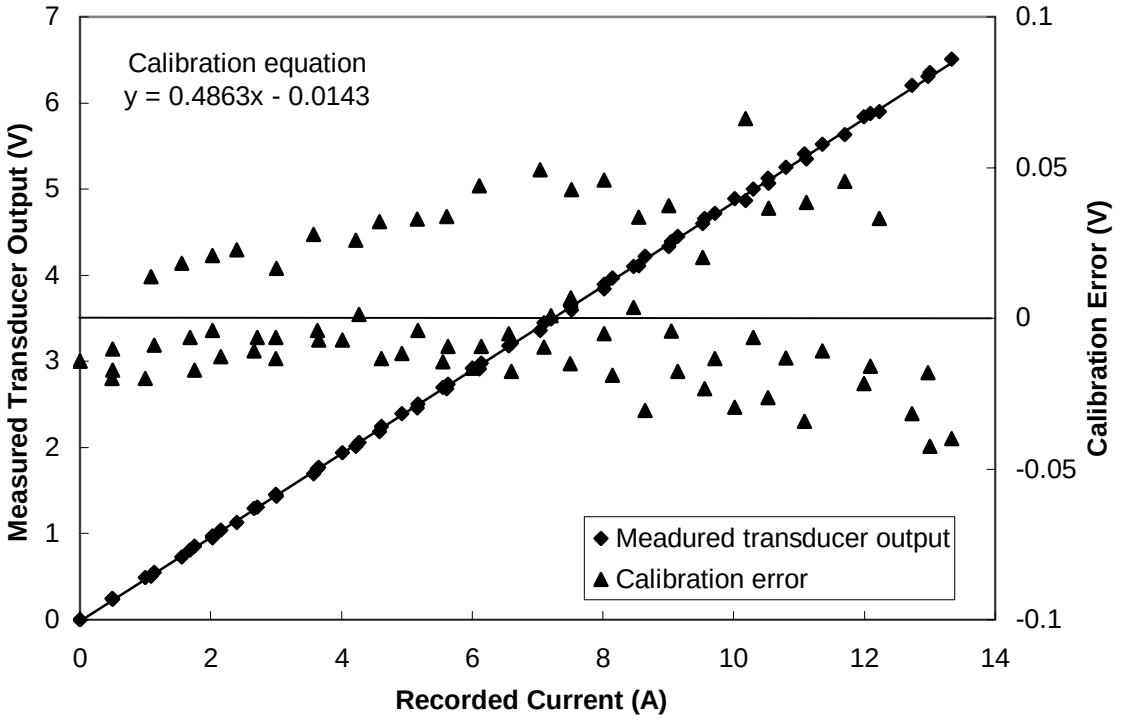

Figure A.8 Calibration of current transducer

The calibration procedure is as follows: A rod was attached to the shaft of the DC motor at rod's center point. The rod did not produce any extra torque to the DC motor shaft since it was self-balanced. The standard weight was added onto one end of the rod. The perpendicular distance from the acting point of the weight to the center of the shaft was measured and the torque was calculated. The current of the DC motor was recorded with a high accuracy multimeter when the torque acting on the motor shaft could lift the weight and keep the rod flat. The calibration results are shown in Figure A.9. The scatter of the current error lies within a range of ±0.15 A which corresponds to a torque error range of ±0.042 Nm. The torque sensitivity is 0.28 Nm/A.

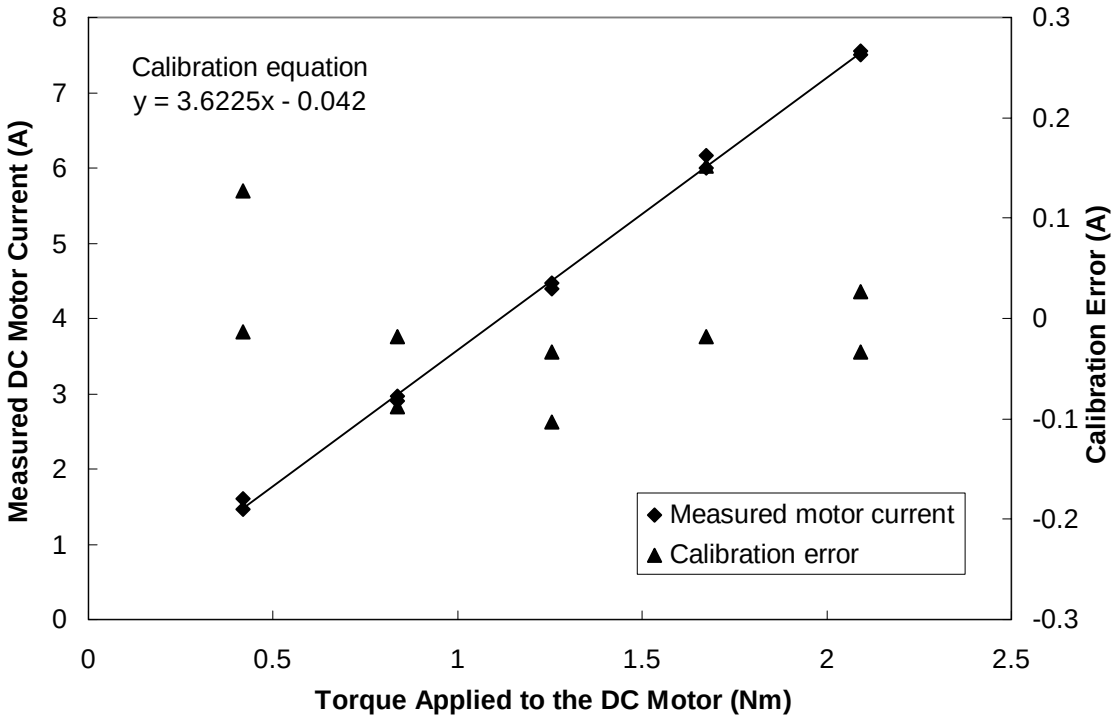

Figure A.9 Calibration of DC motor torque sensitivity

Appendix B

Mathematical Model of the DC Motor Controlled Pump

The purpose of modeling the DC motor and pump was not to develop accurate mathematical models for the DC motor and pump, but to develop basic models which demonstrated correct trends in order to assist in the design of the DC motor controller. In this appendix, the mathematical model of the DC motor and pump was developed. Then, model parameters that are not listed in product manuals were measured and identified through experimental tests. Finally, the steady state and dynamic response of the model of the DC motor and pump were obtained using a computer simulation (Matlab/Simulink®) of the dynamic equations and compared to responses obtained experimentally.

B.1 Mathematical Model of the DC Motor

For a variable displacement piston pump, the flow rate is determined by the angle of the swashplate. In this study, the swashplate angle was controlled using a DC motor. From the viewpoint of the pump control, the DC motor can be considered as a part of the pump. Hence, the model of the DC motor was also a part of the pump model.

A permanent magnet DC motor converts electrical energy into mechanical energy by the interaction of two magnetic fields. A permanent magnet assembly produces one field; an electrical current flowing in the motor windings produces the other field. These two fields produce a torque that tends to rotate the rotor. As the rotor turns, the current in the windings is commutated to produce a continuous torque output. For a brushless DC motor, the permanent magnet is on the rotor; the windings of the DC motor are on the stator.

The mathematic model of a DC motor can be derived using a schematic diagram of the motor circuit shown in Figure B.1. The DC motor is assumed to consist of an inertia,

J_d, with damping, B_d. The torque developed by the current in motor windings not only overcomes the friction in the DC motor and load torque, T_{dl}, on the motor shaft but also accelerates the rotor.

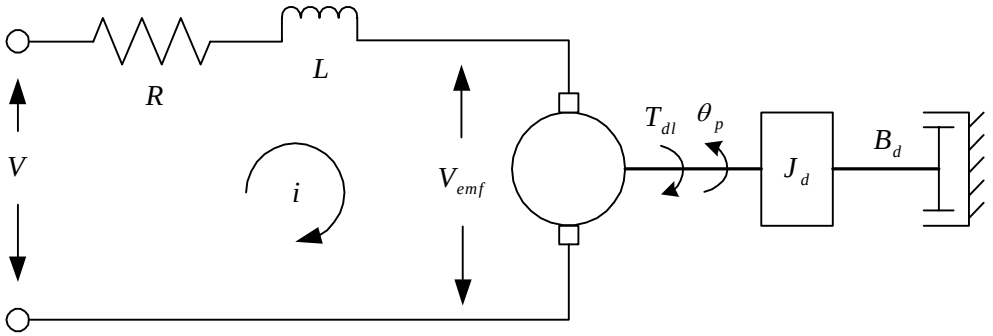

Figure B.1 Schematic Diagram of a DC motor [Habibi, 2001]

The electrical circuit of the motor can be simply described by

$$V = V_{emf} + Ri + L\frac{di}{dt} \tag{B.1}$$

$$V_{emf} = K_b\dot{\theta}_p \tag{B.2}$$

where V, V_{emf} = Input voltage and back EMF voltage (V),

i = Armature current (A),

R = Terminal resistance of the DC motor windings (Ohm),

L = Terminal inductance of the DC motor windings (Henry),

K_b = Back EMF constant of the DC motor (V·rad^{-1}s) and

θ_p = Angular position of the DC motor shaft and pump swashplate (rad).

The torque developed at the shaft of the motor is proportional to the armature current and given by

$$K_t i = J_d\ddot{\theta}_p + B_d\dot{\theta}_p + \text{sgn}(\dot{\theta}_p)(T_{ds} + T_{dc}) + T_{dl} \tag{B.3}$$

where K_t = Motor torque sensitivity (NmA^{-1}),

J_d = Moment of inertia of the motor rotator (Nm·rad^{-1}s^2),

B_d = Viscous damping coefficient (Nm·rad^{-1}s),

T_{ds} = Static friction torque (Nm),

T_{dc} = Coulomb friction torque (Nm) and

T_{dl} = Load torque acting on the DC motor shaft (Nm).

There are eight parameters in the DC motor model described by equations B.1 to B.3. The product manual for the DC motor gives most of the parameters (see Appendix C). These parameters can be used as a basis for later "fine tuning" the transient model. Some parameters related to the friction cannot be measured directly. The friction torque consists of three terms: static friction, coulomb friction, and viscous damping. Normally, the static friction and coulomb friction of the DC motor are negligible compared to that of the pump swashplate. This is evident by the effortless torque that is required to manually turn only the shaft of the DC motor.

Neglecting the static and coulomb friction and taking Laplace transforms of Equations B.1 to B.3 yields the model of the DC motor in the following transfer function form.

$$\theta_p(s) = \frac{K_t V(s) - (Ls + R)T_{dl}(s)}{s((Ls + R)(J_{dm}s + B_{dm}) + K_t K_b)} \tag{B.4}$$

The numerator of Equation B.4 includes two terms. One term is the input signal and the other one is the load, which can be considered as a "disturbance" input signal. If only the input signal is considered in the numerator, the no-load transfer function of the DC motor is

$$\frac{\theta_p(s)}{V(s)} = \frac{1/K_b}{s(T_e T_m s^2 + (T_m + T_e\gamma)s + \gamma + 1)} \tag{B.5}$$

where $T_m = J_d R / K_b K_t$ Motor mechanical time constant (sec),

$T_e = L / R$ Motor electrical time constant (sec) and

$\gamma = B_d R / K_e K_t$ Damping factor.

The terminal inductance, L, and resistance, R, are measured between any two

leads of the winding in either delta or wye configuration [HT-High Torque, Direct Drive Series]. The system mechanical time constant is the time required to reach 63.2% of motor steady state rotational speed after the application of a constant DC voltage through the communication electronics, ignoring friction, windage, and core losses.

Substituting the parameters for the DC motor and pump used in this study (listed in Appendix C) into Equation B.5 yields

$$\frac{\theta_p(s)}{V(s)} = \frac{48800}{s(s^2 + 146s + 111000)} \tag{B.6}$$

The natural frequency of the DC motor is 333 rad·s^{-1} or 53 Hz; and the damping coefficient is 0.22.

B.2 Mathematical Model of the Pump

One approach to modeling a dynamic system is to use linear or small signal analysis. The linear analysis method is based on the assumption that a linear transfer function can be used to describe the behavior of the plant over the complete operating range. On the other hand, the small signal analysis method assumes that the plant behavior is nonlinear but the model can be linearized over a small range near an operating point. Both methods are very powerful analytical tools but have limitations, especially for a highly nonlinear dynamic system such as the DC motor controlled pump. In this study, the pump was modeled using nonlinear large signal techniques which were represented by a series of differential equations. Although it was difficult to analyze the dynamic performance of a nonlinear model using conventional control theories (transfer function approaches), it was feasible to do this using a simulation program and a trail and error approach.

In 1987, Kavanagh [1987] developed a comprehensive model for a variable displacement axial piston pump which was used as the basis for modeling the pump in this study because the same pump type (model: Vickers PVB5) was used. Some modifications to the model were necessary due to different pump control modes. The pump model

consisted of two parts: the torque model and fluid flow model. The motion of the swashplate was described by the torque model; and the flow rate of the pump was described by the flow model.

B.2.1 Assumptions

Some general assumptions are made regarding the pump model. They are:

- Constant prime drive speed on the pump,
- Zero suction and drain pressure,
- Constant chamber volume (although, in reality, the volume does change with the rotation of the pump) and
- Constant fluid density and temperature.

B.2.2 Torque Model

The motion of the swashplate is dictated by the summation of torques acting on the swashplate and yoke assembly. Figure B.2 illustrates the components and forces that have an effect on the total torque. They are:

- The drive force applied by the DC motor,
- Pressure forces acting on the pistons,
- Inertia effects of pistons and swashplate yoke assembly,
- Forces applied by the shoe plate and
- Friction and viscous damping forces acting on the yoke.

The friction and pressure are the dominant components of the net torque. The yoke rotates within the pump case which is filled with hydraulic fluid. The viscous damping torque acts on the yoke in a direction opposite to the motion of the swashplate. This is a consequence of fluid motion between the yoke and pump case. The yoke also “rubs” the inside parts of the pump through the pintle and swashplate, causing a resisting stiction. However, if the pump is in operation, piston induced vibration inside the pump tends to

eliminate stiction and hence can be assumed to be negligible [Kavanagh, 1987]. However, the torque applied to the swashplate due to the pressure effect is significant. This torque is a function of both the pump pressure and swashplate angle.

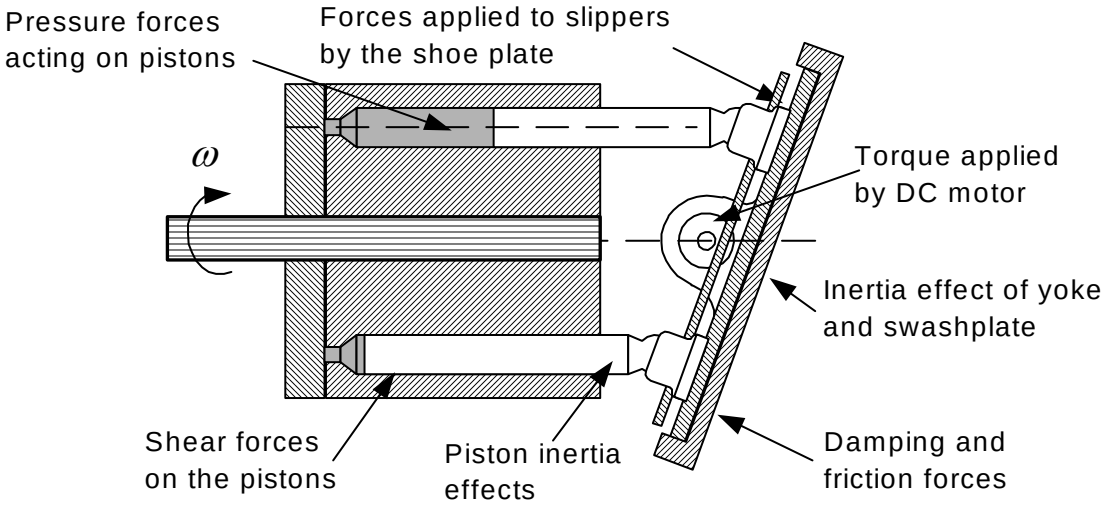

Figure B.2 Forces that give rise to torques acting on the swashplate and yoke assembly

In Kavanagh's study, the swashplate was controlled by a control piston and balanced by a return spring. However, in this study, certain components were not present in that the swashplate was actuated by a DC motor. Under these conditions, Kavanagh's model can be simplified to yield

$$J_p\ddot{\theta}_p = T_d - S_1 - S_2\theta_p - \text{sgn}(\dot{\theta}_p)T_{fc} - B_p\dot{\theta}_p + K_{p1}P_p - K_{p2}P_p\theta_p \qquad \text{(B.7)}$$

where J_p = Average moment of inertia of swashplate yoke assembly (Nm·rad^{-1}s^2),

T_d = Torque applied to the yoke by the DC motor (Nm),

T_{fc} = Torque produced by the coulomb friction force (Nm),

P_p = Pump pressure (Pa),

B_p = Damping coefficient of the swashplate yoke assembly (Nm·rad^{-1}s),

S_1 = Simplified pump model constant (Nm),

S_2 = Simplified pump model constant (Nm·rad^{-1}),

K_{p1} = Pressure torque constant ($Nm \cdot Pa^{-1}$) and

K_{p2} = Pressure torque constant ($Nm \cdot Pa^{-1} \cdot rad^{-1}$).

S_1, S_2, K_{p1} and K_{p2} are empirically obtained pump constants with the same meanings as in Kavanagh's model but in different symbols. Equation B.7 can be rearranged to provide a more physical interpretation of equation terms, that is:

$$J_p \ddot{\theta}_p = T_d + T_p + T_r - T_f \tag{B.8}$$

where T_f = Torque produced by friction forces (Nm),

T_p = Torque relating to the pressure effect (Nm) and

T_r = Torque relating to the rotation of the barrel (Nm).

The frictional torque includes coulomb friction, viscous damping friction and stiction. As mentioned, the stiction friction is assumed to be negligible. Hence the frictional torque can be represented by

$$T_f = \text{sgn}(\dot{\theta}_p) T_{fc} + B_p \dot{\theta}_p \tag{B.9}$$

The torque produced by the pressure effects is a nonlinear function. It can be written as

$$T_p = K_{p1} P_p - K_{p2} P_p \theta_p \tag{B.10}$$

This equation is nonlinear due to the presence of the product of pressure and angular displacement. When the pump is in operation, there is a torque applied to the swashplate by the piston slippers. This force is a result of the inertia of pistons and the shoe plate and is known to be a function of the swashplate angle. The torque related to the rotation of the barrel can be represented as

$$T_r = -S_1 - S_2 \theta_p \tag{B.11}$$

B.2.3 Flow Model of the Pump

The displacement of the pump is defined as follows:

$$D_p = N A_p R_p \tan\theta_p / \pi \tag{B.12}$$

where D_p = Displacement of the pump ($m^3 \cdot rad^{-1}$),

R_p = Radius of the piston pitch (m),

N = Number of pistons and

A_p = Area of the piston (m^2).

Assuming that the rotational speed of the prime mover is ω_p, the ideal flow rate of the pump is as follows:

$$Q_{pidea} = \omega_p D_p = \omega_p N A_p R_p \tan\theta_p / \pi \tag{B.13}$$

The actual flow rate of the pump is less than the ideal flow rate due to the fluid leakage and fluid compression. There are two types of leakage flows in the pump. One is the internal leakage flow between the suction port and the discharge port of the pump and the other is the external leakage from the high-pressure chamber to the case drain through the pump casing. From the continuity equation, the flow equation for the pump can be written as

$$Q_{pidea} - Q_{ip} - Q_{ep} - Q_p = \frac{V_p}{\beta_e}\frac{dP_p}{dt} \tag{B.14}$$

where Q_p = Output flow of the pump ($m^3 s^{-1}$),

Q_{ip} = Internal leakage flow of the pump ($m^3 s^{-1}$),

Q_{ep} = External leakage flow of the pump ($m^3 s^{-1}$) and

V_p = Volume of the pump forward chamber (m^3).

Since the suction pressure is assumed to be zero, the leakage flow of the pump (including the internal leakage and the external leakage flow) can be approximated by

$$Q_{lp} = Q_{ip} + Q_{ep} = C_{tp} P_p \tag{B.15}$$

where C_{tp} = Total leakage flow coefficient ($m^3 s^{-1} \cdot Pa^{-1}$).

Substituting Equations B.13 and B.15 into Equation B.14, yields

$$\omega_p N A_p R_p \tan\theta_p / \pi - C_{tp} P_p - Q_p = \frac{V_p}{\beta_e}\frac{dP_p}{dt} \tag{B.16}$$

Equation B.16 is thus the flow model of the pump.

B.3 Preliminary Controller Design for the purpose of Measurement

B.3.1 Controller Design Problem

The model of the DC motor which is represented by Equation B.4 indicates that the DC motor is a type one system with a pole at the origin. The steady state error for this kind of system is infinite. A closed loop system with an angular position feedback must be designed to achieve the desired angular control. Since the pump swashplate was the main load of the DC motor, the performance of the pump directly affected the controller design for the DC motor. Although equations of the pump model were derived in Section B.2, the model was not really completed because some parameters of the model were still unknown. These parameters were: coulomb friction torque, T_{fc}, viscous damping ratio, B_p, simplified pump model constant (S_1, and S_2) and pressure torque constant (K_{p1} and K_{p2}). All these parameters could not be measured directly if the pump was not in operation. In order to measure the viscous damping ratio, for example, the torque acting on the swashplate had to be measured under different rotational speeds.

This posed a problem. On one hand, a controller for the DC motor could not be designed without knowledge of the pump dynamics. On the other hand, in order to measure or identify the pump parameters, a controller had to be used for the DC motor; otherwise the pump could not be operated in a stable mode in order to measure these unknown parameters.

In the absence of pump motor parameter values, an analytical approach to the design of the controller did not seem to be practical. However, it was possible to design a simple controller for the DC motor based on experimental tests, such as using Ziegler-Nichols turning PID rules. This controller would make it possible to measure unknown parameter

values by operating the DC motor and pump in a reasonably stable manner.

The purpose of the controller design in this appendix was to facilitate the measurement and identification of unknown parameters of the pump model. It was not the controller to be used in subsequent studies. Therefore, the actual system performance was not an issue. The next section will discuss the controller design based on the experimental approach.

B.3.2 Preliminary Controller Design for DC Motor

A PID controller was chosen to control the DC motor. It was described in Section 2.5. The transfer function form of the PID is rewritten here.

$$G_c(s) = K_p + \frac{K_i}{s} + K_d s \tag{B.17}$$

From the analysis of the model and preliminary tests, the second method of Ziegler-Nichols turning PID rules can be used to design a controller for the DC motor. Ziegler-Nichols tuning PID rules are based on experimental tests. The rules use an experimental approach to design a controller. The advantage of this method is that the model of the plant is not required for the design of the controller. However, the controller designed at a specific operating condition using this method may not work well at other operating conditions, if the plant performance is heavily dependent on the load.

Although the experimental approach was not the ideal controller design method for the DC motor controlled pump system, a simple controller designed using this method was sufficient to control the pump to facilitate the measurement of unknown parameter values.

Preliminary test results indicated that the pump exhibited sustained oscillations at low pressure when only proportional gain was involved; further the dynamic response decreased with increasing pressure if the gains stayed the same. Designing the controller using Ziegler-Nichols rules at high pressures resulted in an unstable condition at low pressures. Thus, the controller was designed at low pressures and the reduced dynamic

performance accepted as the pressure increased. Although the performance of the system was poor at high pressures, the pump performance was acceptable. The dynamic performance was not as important as the steady state performance at this stage since only the steady state values of the experimental test results were used to identify pump parameters.

The block diagram of the DC motor control is shown in Figure B.3.

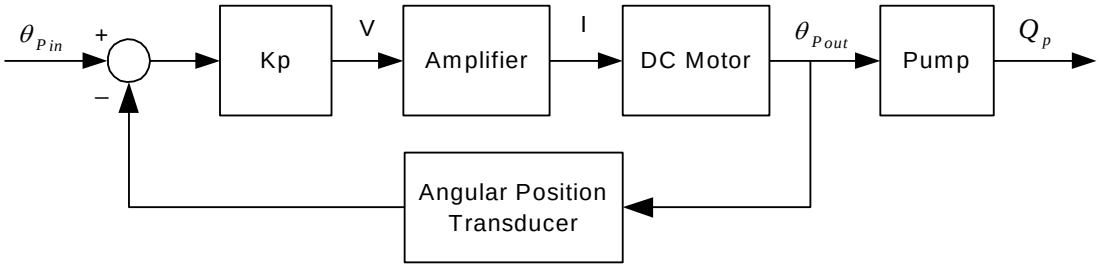

Figure B.3 Block diagram of the DC motor control

The procedure for tuning the controller was as follows:

1) The closed loop system was constructed and the pump pressure was set to zero by fully opening the main relief valve;
2) A square input signal was applied to the DC motor;
3) The proportional gain, K_p, was increased from 0 until the swashplate of the pump exhibited sustained oscillation;
4) The critical gain and period time (from the limit cycle) was recorded at the same time;
5) Gains of the PID controller were calculated using Equations 2.7 ~ 2.9; and
6) The test was repeated several times.

The final PID controller was tested at different pump pressures (from 0 to 13.8 MPa). Typical results are shown in Figure B.4. It was observed that the pump swashplate had a fast dynamic response at low pressure levels. The rise time of the pump swashplate increased and the overshoot decreased with increasing pump pressure. The results also

showed that the controller exhibited an acceptable steady state performance which was really important. The angle of the swashplate approached the steady state with an error of ±0.2° after the transients die out. This performance was considered to be sufficient for the measurement and identification of unknown pump parameters.

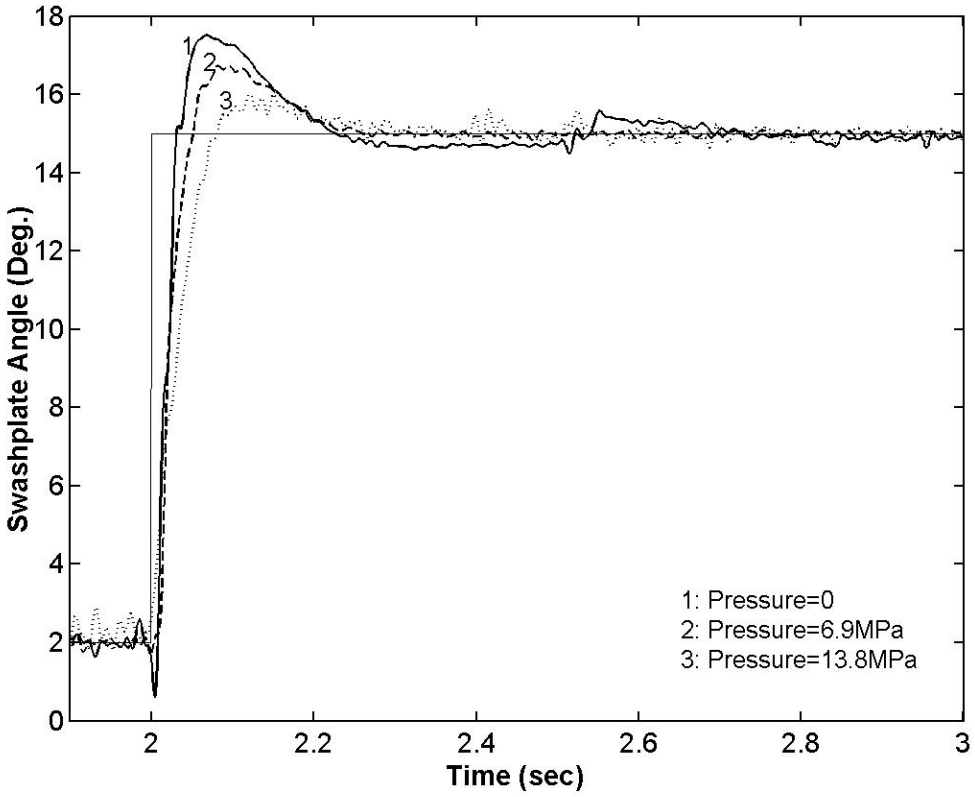

Figure B.4 Step Responses of the PID Controller

B.4 Parameter Identification

The model of the pump was described by equations B.7 and B.16. Some parameters of the model could be directly measured or calculated, while other parameters had to be estimated through experimental tests. As mentioned in Section B.3.1, these parameters were:

- Coulomb friction torque, T_{fc},
- Viscous damping ratio, B_p,

- Simplified pump model constant S_1 and S_2, and
- Pressure torque constant K_{p1} and K_{p2}.

The details describing these parameters can be found in Section B.2. To complete the model of the DC motor and pump, it was necessary to identify the values of these parameters. By means of the controller designed in the last section, the following sections introduce some of the testing strategies that were used to identify parameters which could not be directly measured.

B.4.1 Frictional Torque

The frictional torques (reference to Equation B.7) act on the swashplate yoke assembly in a direction opposite to the motion of the swashplate. However, other torques acting on the swashplate yoke assembly act in the same direction, regardless of the rotational direction of the swashplate. In order to measure the frictional force, a test was designed such that

- The forward and backward angular velocities of the swashplate were the same and had a constant value, and
- The load pressure was the same for the same angular position during the forward and backward rotation of the swashplate.

Under these conditions, as will be shown, the effects of the pressure and swashplate rotation could be canceled out from the model equation with only frictional torque terms remaining.

This can be explained as follows. At constant velocity, the acceleration of the swashplate is zero in any rotating direction. At any angle, θ_p, consider measurements of torque in the forward and backward directions individually. If:

- the measured pressure is P_p,
- the measured driving torques are T_{d1} and T_{d2}, and

- the rotation speed of the swashplate is positive in the forward direction,

then Equation B.7 in two directions can be written as

$$T_{d1} - T_{fc} - B_p\dot{\theta}_p - S_1 - S_2\theta_p + K_{p1}P_p - K_{p2}P_p\theta_p = 0 \qquad \text{(B.18)}$$

$$T_{d2} + T_{fc} + B_p\dot{\theta}_p - S_1 - S_2\theta_p + K_{p1}P_p - K_{p2}P_p\theta_p = 0 \qquad \text{(B.19)}$$

It is assumed that the terms S_1, $S_2\theta_p$, $K_{p1}P_p$ and $K_{p2}P_p\theta_p$ in Equation B.7 have the same values at the same angle θ_p in both the forward and backward directions.

Subtracting Equation B.19 by B.18 and rearranging yields

$$T_f = T_{fc} + B_p\dot{\theta}_p = (T_{d1} - T_{d2})/2 \qquad \text{(B.20)}$$

This can be further explained using Figure B.5, which illustrates one of a series of test results. A positive ramp signal was applied to the DC motor amplifier which forced the swashplate to move in a positive direction (from 0˚ to 20˚) at a constant rotational speed. This ramp signal was changed to a negative value after the swashplate reached an angle of 20˚. During the test, the pressure of the pump was set to zero by fully opening the relief valve installed near the pump outlet. The pressure curve showed that the pressure of the pump was, in fact, not zero (about 0.35 MPa) but increased slightly with increasing swashplate angle. The pressure drop across the relief valve was attributed to internal valve losses. This did not affect the measurement of frictional torques since the pressure was identical during both the forward and backward rotations of the swashplate, the exception being the transient conditions near the zero angular position.

The driving torque applied by the DC motor was obtained indirectly by measuring the current of the DC motor windings. The calibration of the relationship between the current and torque of the DC motor is presented in Appendix A.7. The pressure and torque were also recorded and are shown in Figure B.5.

The measured torques changed dramatically near the 0° and 20° angular positions due to transients. The data used for the calculation were therefore only taken from the

regions shown in Figure B.5. Average values from both regions were used to calculate the frictional torque for this specific rotational speed.

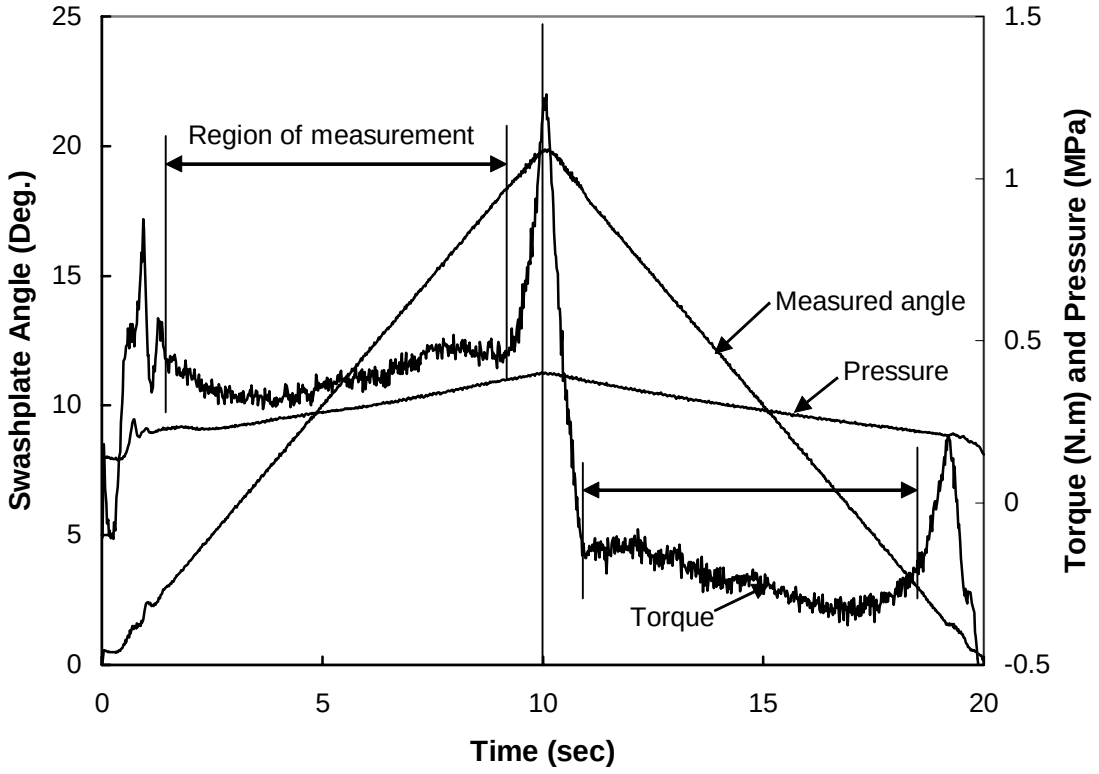

Figure B.5 Frictional torque measurement design

The complete procedure to identify the frictional torque was as follows:

1) A ramp signal was applied to the DC motor.
2) Fluid temperature was recorded and the tests conducted when a preset temperature had been reached.
3) The torque applied to the pump swashplate by the DC motor was measured.
4) The frictional torque was calculated using Equation B.20.
5) The test was repeated with different rotational speeds which were achieved by changing the slope of the ramp signal.

Typical results are shown in Figure B.6. The curve of measured frictional torque shows that

$$T_{fc} = 0.36 \ \text{Nm}$$

$$B_p = 0.28 \ \text{Nm·rad}^{-1}\text{s}$$

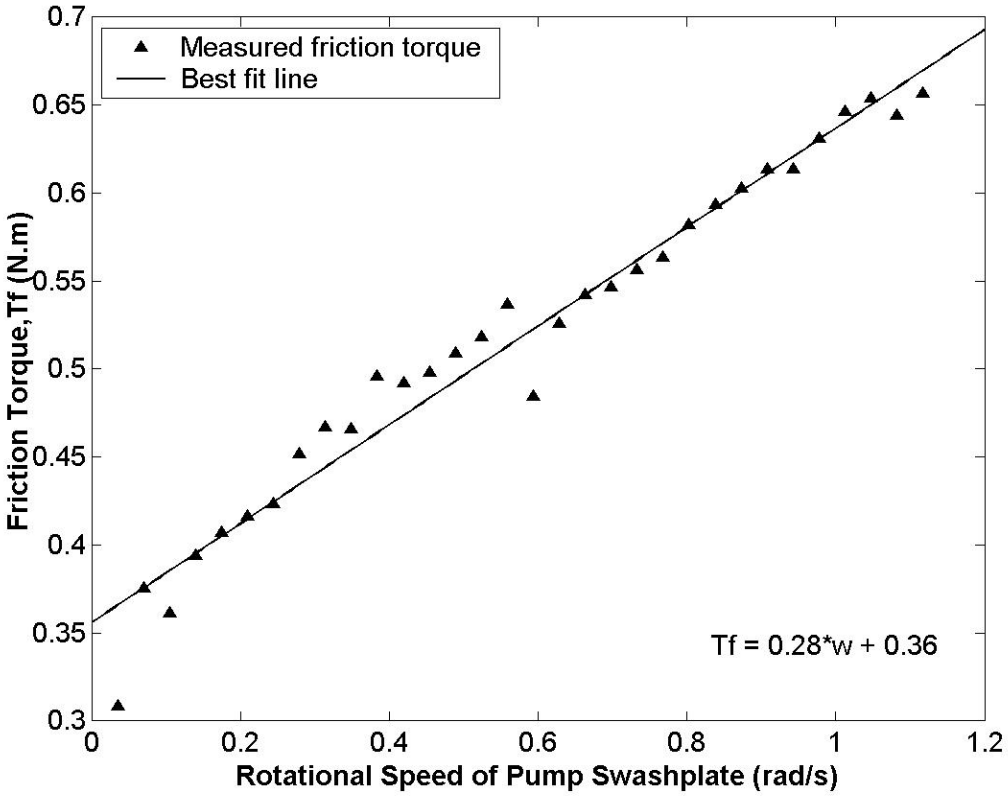

Figure B.6 Frictional torque of the swashplate

B.4.2 Measuring Torque Related to Pressure and Rotation

As discussed in Section B.2.2, the torque generated by pressure effects and pump rotation is a function of both the pressure and swashplate angle (see Equation B.10). As will be shown, a special test was used to estimate the parameters related to this pressure effect and pump rotation.

Equation B.8 can be rearranged as:

$$T_{pr} = -(T_d - T_f) + J_p \ddot{\theta}_p \tag{B.21}$$

where $T_{pr} = T_p + T_r$ Torque relating to the pressure effect and pump rotation (Nm)

On the right side of the equation, the torque outputted by the DC motor (T_d) can be indirectly measured (via motor current), and the frictional torque can be measured and calculated using Equation B.9. If $\dot{\theta}_p$ is kept constant, then $\ddot{\theta}_p$, the acceleration of the swashplate, is zero.

In order to generate a constant rotational speed, an input ramp signal, which is shown in Figure B.7, was applied to the DC motor control system. The swashplate was initially located at 1° to avoid disturbances from the swashplate stop. The output swashplate angle is also shown, and it was observed that the swashplate follows the input signal almost exactly, except at 20° where the swashplate hits the stop. The rotational speed of the swashplate was observed to be constant, and hence the acceleration was zero. The pressure increased slightly when the flow rate increased from zero to its maximum value (θ_p =20°). In this study, the load pressure (manually set by the relief valve) was changed in increments of 0.69 MPa.

It should be noted that the measured torque (T_d) shown in Figure B.7 was the torque applied on the swashplate by the DC motor. From the viewpoint of the swashplate, the positive torque acted on the swashplate in a direction of increasing swashplate angle. On the other hand, the negative torque acted on the swashplate in a direction of decreasing swashplate angle.

The procedure to identify the parameters related to the pressure effect was:

1) A ramp signal was applied to the DC motor with a slope of 1°/s which resulted in a positive rotational speed (increasing swashplate angle).
2) The torque applied to the swashplate by the DC motor was measured.
3) The frictional torque was eliminated from the measured torque by calculating $T_d - T_f$.

4) The test was repeated by changing the pressure from 0 to 7.6 MPa.

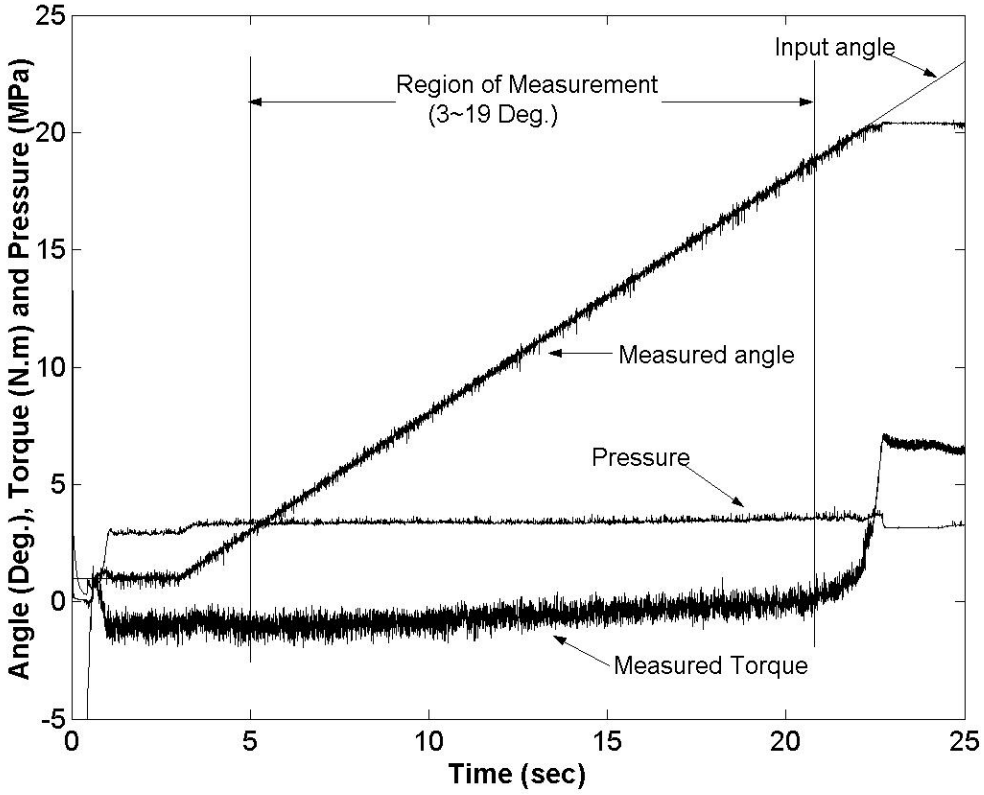

Figure B.7 Measurement of the torque related to pressure and rotation

Typical results for this procedure are shown in Figure B.8. Since the frictional torque was eliminated from the test results, the torque shown in Figure B.8 is a consequence of the DC motor driving and frictional torque, $T_d - T_f$.

It was observed that the torque ($T_d - T_f$) increased (in a negative sense) with increasing pressure. On the other hand if the pressure was kept approximately constant, the torque decreased with increasing angle. The curves also indicated that the relationships between the torque, pressure and angle were somewhat nonlinear, which was consistent with the trends predicted by Equation B.7.

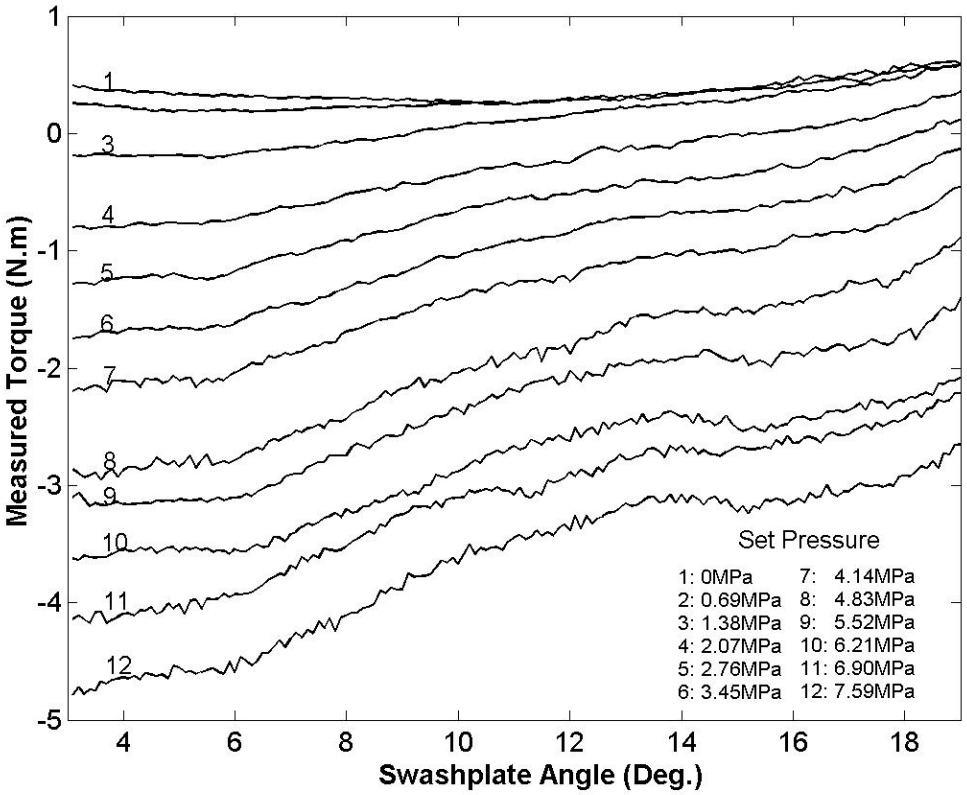

Figure B.8 Measured Torque as a function of swashplate angle

There are 12 curves shown in Figure B.8, which represent the relationship between the torque and swashplate angle for a prescribed pressure. These curves could be represented in a different manner by using the angle as the family parameters and the pressure as the independent variable. A Matlab® program was developed to complete this conversion. The 12 torque-angle curves were converted to 17 torque-pressure curves which represented the angles from 3° to 19°. Some torque-pressure curves are shown in Figure B.9. Using the same Matlab program, every curve was fitted to a best-fit line. To accommodate visualization of the graph, only two extreme best-fit lines representing angles of 3° and 19°, are shown in the same figure.

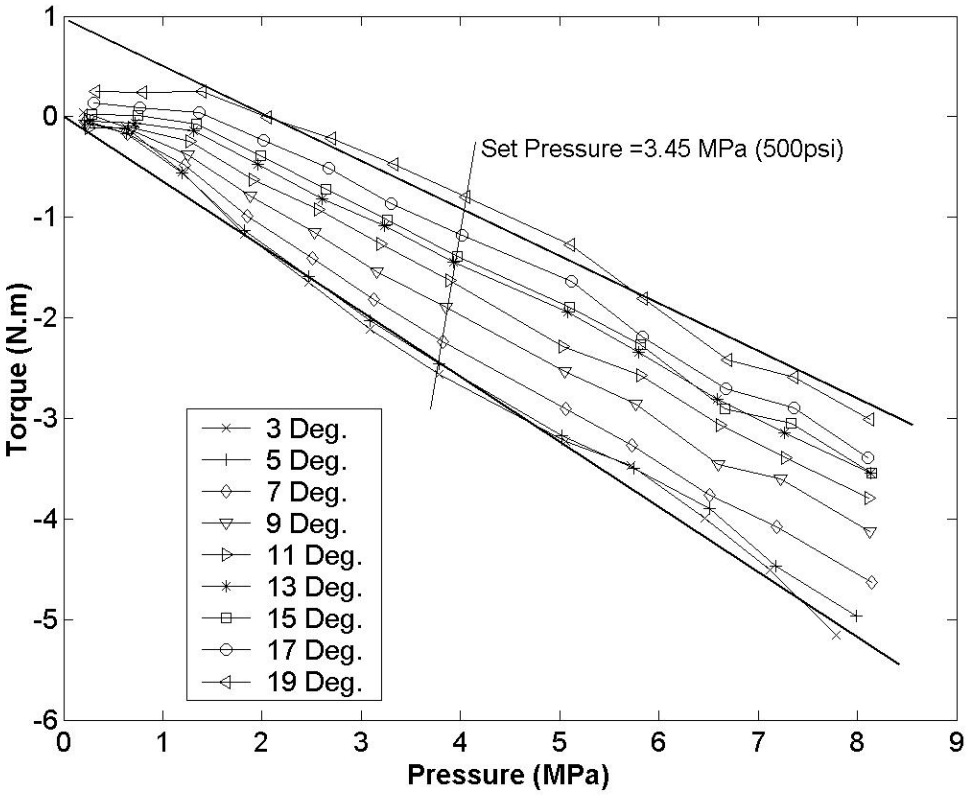

Figure B.9 Torque related to the pressure effect and pump rotation

It can be observed that the symbols, which represented torques at different pressure levels, were not lined up in a straight line when the pressure was less than 1 MPa. This was due to the nonlinearity of the friction characteristic. Frictional torques became the dominant torques acting on the swashplate when the pressure was low. Further, the accuracy of the measurement was also affected by the small amount of the measured torque which was around zero for small pressures. It was also observed that the measured pressure was not a constant at the specific pressure level which was manually set and fixed. One line indicating the trend of the pressure is shown in Figure B.9. The pressure increased slightly with an increase in the swashplate angle, except at a few points. The reason for this was that the pressure drop across the relief valve increased with increasing flow rate which was approximately proportional to the angle.

Based on these best-fit lines, a single equation was derived to describe the relationships between the torque $T_d - T_f$ (Nm), pressure (Pa) and angle (rad) using the Matlab program. The relationship can be approximated by

$$T_d - T_f = 0.0963 + 2.36\theta_p - 7.46\times10^{-7} P_p + 8.3\times10^{-7} P_p\theta_p \quad \text{(B.22)}$$

Arranging Equations B.10, B.20 and B.21, yields:

$$-(-S_1 - S_2\theta_p + K_{p1}P_p - K_{p2}P_p\theta_p) = 0.096 + 2.36\theta_p - 7.46\times10^{-7} P_p + 8.3\times10^{-7} P_p\theta_p \quad \text{(B.23)}$$

The parameters of Equation B.2 are listed in Table B.1. Parameters K_{p1} and K_{p2} are close to Kavanagh's parameters [1987]. In Kavanagh's study, values of these two parameters were 7.25×10^{-7} Nm·Pa^{-1} and 6.25×10^{-7} Nm·Pa^{-1} (different symbols were used in his study). Values of parameters S_1 and S_2 were not comparable because of the absence of the return spring. Due to the nonlinearity of the friction characteristic, it must be noted that these parameters are not accurate at small pump pressures.

Table B.1 Model parameters related to pressure and rotational effects

S_1 (Nm)	S_2 (Nm·rad^{-1})	K_{p1} (Nm·Pa^{-1})	K_{p2} (Nm·Pa^{-1}·rad^{-1})
0.096	2.36	7.46×10^{-7}	8.3×10^{-7}

According to Equation B.10 and the parameters listed in Table B.1, the torque produced by the pressure effect is as follows:

$$T_p = (7.46\times10^{-7} - 8.3\times10^{-7}\theta_p)P_p \quad \text{(B.24)}$$

The value of the torque T_p was always positive since the swashplate angle (θ_p) was also positive over a range of 0 ~ 0.349 rad. Hence, the torque T_p always acts on the swashplate in a direction of increasing swashplate angle.

The torque produced by the rotation of pump barrel is:

$$T_r = -0.096 - 2.36\theta_p \tag{B.25}$$

Different from the torque produced by the pressure effect, the value of the torque due to the pump rotation was negative. It acted on the swashplate in a direction of increasing swashplate angle.

Appendix C

System Parameters

The following table is a list of all the constants, coefficients and determined parameters of the servo valve, hydraulic motor, DC motor and hydraulic pump used in this study (see Table 2.1).

Components	Symbol	Parameter Definition	Value	Unit
Servo Valve	K_a	Servo valve amplifier gain	9.82	mAV^{-1}
	K_q	Linear flow gain of the servo valve	0.028	$m^3s^{-1}A$
	ξ	Fundamental damping ratio	1.2	
	ω_n	Hydro-mechanical natural frequency	220	$rad{\cdot}s^{-1}$
Hydraulic Motor	D_m	Volumetric displacement of the motor	2.38×10^{-6}	$m^3{\cdot}rad^{-1}$
	J_m	Inertia of the motor and the load	0.0016	$Nm{\cdot}rad^{-1}s^2$
	C_{tm}	Motor leakage coefficient	2.0×10^{-13}	$m^3s^{-1}Pa^{-1}$
	B_m	Motor damping ratio	0.044	$Nm{\cdot}rad^{-1}s$
	T_{fm}	Motor coulomb friction torque	2.14	Nm
	V_m	Volume of the motor and pipe	2.4×10^{-4}	m^3
DC Motor	R	Terminal resistance	4.83	Ohm
	L	Terminal inductance	0.0332	H
	K_t	Torque sensitivity	2.27	$Nm{\cdot}A^{-1}$
	K_b	Back EMF constant	2.27	$V{\cdot}rad^{-1}s$
	J_d	Moment of inertia of the motor rotor	1.4×10^{-3}	$Nm{\cdot}rad^{-1}s^2$
	B_d	Viscous damping coefficient	1.43×10^{-3}	$Nm{\cdot}rad^{-1}s$
	T_e	Electrical time constant	6.87×10^{-3}	sec
	T_m	Mechanical time constant	1.3×10^{-3}	sec

Components	Symbol	Parameter Definition	Value	Unit
Hydraulic Pump	ω	Pump rotational speed	183.3	$rad \cdot s^{-1}$
	N	Number of pistons	9	
	A_p	Piston area	83.5×10^{-6}	M^2
	B_p	Viscous damping ratio of the swashplate	0.28	$Nm \cdot rad^{-1}s$
	R_p	Piston pitch radius	0.0224	m
	D_p	Maximum pump displacement	1.95×10^{-6}	m^3rad^{-1}
	β_e	Bulk modulus of the fluid	1.45×10^{9}	Pa
	C_{tp}	Total pump leakage flow coefficient	4.3×10^{-13}	$m^3s^{-1}Pa$
	V_p	Volume of pump (high pressure side)	3×10^{-5}	M^3
	J_P	Average swashplate yoke inertia	1.06×10^{-3}	$Nm \cdot rad^{-1}s^2$
	S_1	Simplified pump model constant	0.096	Nm
	S_2	Simplified pump model constant	2.36	$Nm \cdot rad^{-1}$
	K_{pr1}	Pressure torque constant	7.46×10^{-7}	$Nm \cdot Pa^{-1}$
	K_{pr2}	Pressure torque constant	8.3×10^{-7}	$Nm \cdot Pa^{-1}rad^{-1}$
	T_{fc}	Coulomb friction torque of the pump	0.36	Nm

Appendix D

Mathematical Model of the Hydraulic System

To have a good understanding of the bypass flow control concept, it was necessary to model and simulate the bypass valve and to integrate component models into an overall model of the complete hydraulic system. The objective of modeling was to provide a means by which the bypass valve controller could be analyzed and modified off line before implementing it on a physical system. This appendix will develop the mathematical model of the hydraulic system. First, mathematical models of the bypass control valve and hydraulic motor are presented. Then the model of the complete hydraulic system (using the models for the DC motor and pump developed in Appendix B) is presented.

D.1 Modeling the Bypass Control Valve

The servo valve used in this study was a Moog760, two-stage valve consisting of a polarized electrical torque motor and two stages of hydraulic power amplifier. The structure of the valve is shown in Figure D.1. The pilot stage was a symmetrical, double-nozzle and flapper system driven by a double air gap, dry electrical torque motor. Mechanical feedback of the spool position was provided by a feedback wire (a cantilever spring). The output stage was a closed center, four-way, sliding spool.

The operation principle of the servo valve has been described in the product manual [760 Series Servovalve, Moog Inc., p1] as follows: “An electrical command signal (flow rate set point in this case) is applied to the torque motor coils and creates a magnetic force which acts on the ends of the pilot stage armature. This causes a deflection of armature/flapper assembly within the flexure tube. Deflection of the flapper restricts fluid flow through one nozzle which is carried through to one spool end, displacing the spool. Movement of the spool opens the supply pressure port (P) to one control port while

simultaneously opening the tank port (T) to the other control port. The spool motion also applies a force to the cantilever spring, creating a restoring torque on the armature/flapper assembly. Once the restoring torque becomes equal to the torque from the magnetic forces, the armature/flapper assembly moves back to the neutral position, and the spool is held open in a state of equilibrium until the command signal changes to a new level".

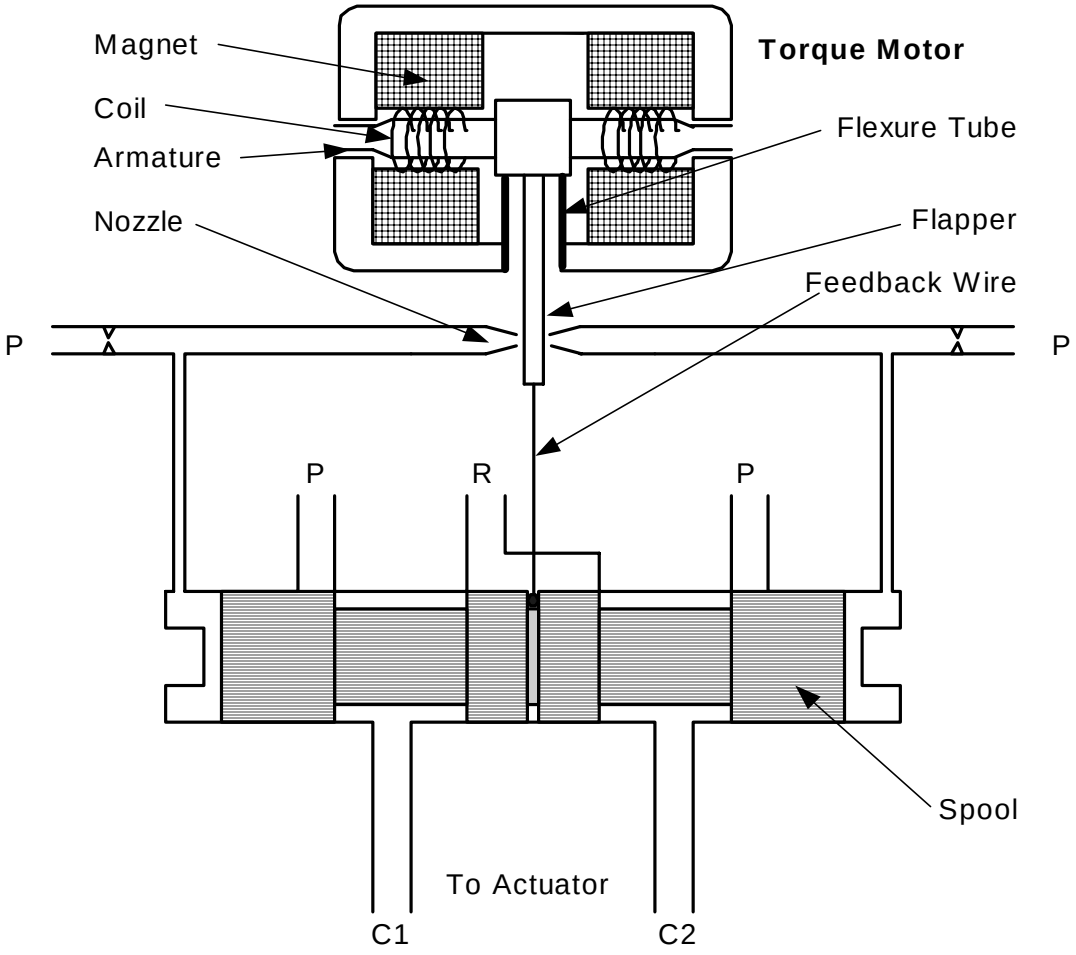

Figure D.1 Schematic diagram of a servo valve

In summary, the spool position is proportional to the input current; and the flow to the load is proportional to the spool position if the pressure drop across the valve is constant. Hence, the output (flow rate) of the servo valve is proportional to the input signal (current).

Compared with the steady state performance, the dynamic response of the servo valve is more complicated. Servo valves are complex devices and have many nonlinear characteristics which are significant in their operation. These nonlinearities include: electrical hysteresis of the torque motor, change in torque-motor output with displacement, change in orifice discharge coefficient with pressure ratio, sliding friction on spool, the basic orifice flow pressure relationship, and others [Merritt, 1967].

However, it is possible to derive a meaningful model for the servo valve if only an approximate performance is required. A similar study has been done by Martin [1992] in which a model for a Moog773 servo valve was developed and then simplified by (a) neglecting factors which had minimal effects on the performance of the system and (b) by linearizing the model. Martin found that there are two important model equations for the servo valve. One is the electrical model of the torque motor that relates the current through the coils of the torque motor to the voltage across the coils. The other equation is the hydraulic model that relates the flow rate through the valve to the current in the coils.

The electrical model is similar to the model of the DC motor described in Section B.1. It is

$$V_c = V_b + R_c i_c + L_c \frac{di_c}{dt} \tag{D.1}$$

where V_c = Voltage across the coil of the torque motor (V),

V_b = Back EMF voltage by the motion of the armature (V),

R_c = Resistance of the coil (Ohm),

L_c = Inductance of the coil (H) and

i_c = Current through the coil (A).

The electrical time constant, which is the ratio of the inductance to the resistance of the coils, varies significantly from 20 ms to 49 ms for different kinds of servo valves

[Martin, 1992]. To improve the response of the servo valve, a servo amplifier (N121-132A) was used as a simple controller. The controller measured the current in the torque motor coils and then used a feedback control loop to control this current. This design extended the corner frequency of the torque motor to a value exceeding 200 Hz. Compared with the bandwidth of the rest of the valve components, the electronic portion of the valve could be considered as a pure gain, K_a. Thus, Equation D.1 can be simplified as

$$V_c = K_a i_c \tag{D.2}$$

where K_a = Gain of the servo valve amplifier (VA^{-1}).

The relationship between the coil current and the flow rate through the valve can be described by the following simplified transfer function [Martin, 1992].

$$\frac{Q_v(s)}{i_c(s)} = \frac{K_q \omega_n^{\,2}}{s^2 + 2\xi\omega_n + \omega_n^{\,2}} \tag{D.3}$$

where Q_v = Flow rate through the valve (m^3s^{-1}),

K_q = Linear flow gain of the valve ($m^3s^{-1}A$),

ω_n = Hydro-mechanical natural frequency of the valve ($rad \cdot s^{-1}$) and

ξ = Fundamental damping ratio of the valve.

With reference to Martin's model, the natural frequency of the valve was 220 $rad \cdot s^{-1}$ and the damping ratio was 1.2. Since the valve used in his study (Moog773) was quite similar to that used in this study (Moog760), the values of damping ratio and natural frequency were adopted in this simulation study. Other parameters of the model are listed in Appendix C.

D.2 Modeling the Hydraulic Motor

The hydraulic motor, in this case, a Sauer Danfoss 15 Series, was a fixed

displacement axial piston motor with a displacement of 15 cc/Rev. The motor is illustrated in Figure D.2. The motor had a stationary swashplate which was used to move the piston forward and backwards. Only two pistons are drawn to simplify the illustration. The leakages and friction losses were lumped at these pistons.

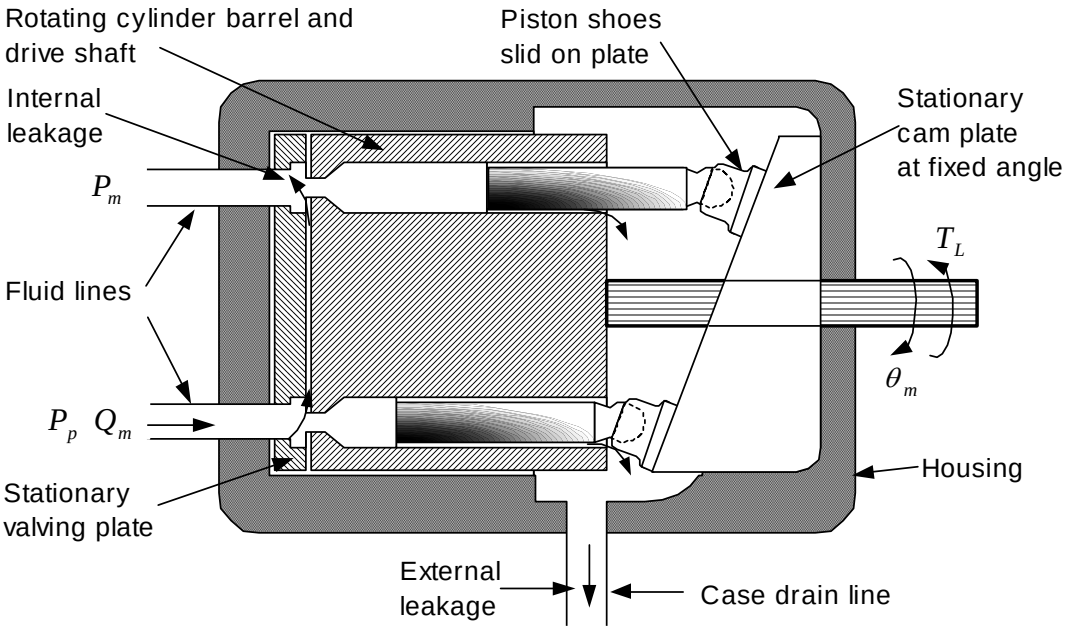

Figure D.2 Schematic diagram of a fixed displacement axial piston motor [Merritt, 1967]

The mathematic model of the hydraulic motor was quite similar to that of the pump. It was described by two equations: the first was the continuity equation that described flow through the motor, and the second, the torque equation that related the fluid pressure to the output motor torque.

According to the continuity equation, the flow equation is described as

$$Q_m - C_{im}(P_p - P_m) - C_{em}P_p - D_m \frac{d\theta_m}{dt} = \frac{V_m}{\beta_e}\frac{dP_p}{dt} \qquad \text{(D.4)}$$

where C_{im} = Internal leakage coefficient of the hydraulic motor ($m^3s^{-1}Pa$),

C_{em} = External leakage coefficient of the hydraulic motor ($m^3s^{-1}Pa$),

D_m = Volumetric displacement of the hydraulic motor ($m^3 \cdot rad^{-1}$),

θ_m = Angular position of the hydraulic motor shaft (rad),

V_m = Forward chamber volume of the hydraulic motor (m^3),

Q_m = Input flow rate of the hydraulic motor (m^3s^{-1}) and

P_m = Outlet pressure of the hydraulic motor (Pa).

The flow rate across the hydraulic motor is affected by leakage and fluid compression. The leakage term in Equation D.4 is proportional to the pressure drop across the leakage path. Leakage in the hydraulic motor is also known to be the function of motor rotational speed [Merritt, 1967] but for this model and for the initial controller design, the simplified model of leakage in Equation D.4 was used. For the feasibility study, the effects of the lines between the pump and motor are considered negligible. Compressibility effects due to the volume of fluid in the connecting lines are simply lumped into the volume of motor piston chambers.

Using Newton's second law, the torque equation of the motor is [Merritt, 1967]:

$$(P_p - P_m)D_m = J_m \frac{d^2\theta_m}{dt^2} + B_m \frac{d\theta_m}{dt} + \text{sgn}(\dot{\theta}_m)T_{fm} + T_L \qquad \text{(D.5)}$$

where J_m = Total inertia of the hydraulic motor and load ($Nm \cdot rad^{-1}s^2$),

B_m = Total viscous damping coefficient ($Nm \cdot rad^{-1}s$),

T_{fm} = Coulomb friction torque of the hydraulic motor (Nm) and

T_L = Load applied on the hydraulic motor shaft (Nm).

The friction of the hydraulic motor was indirectly measured through experimental tests by measuring the pressure drop across the hydraulic motor at different operating

conditions. To do so, the outlet of the motor was connected to the tank so that the outlet pressure was essentially zero. The inlet of the motor was connected to the outlet of pump with a short pipe to minimize the pressure drop along the transmission line. The backpressure of the system was adjusted by a relief valve and recorded by a pressure transducer located at the motor inlet.

The procedure used is summarized as follows:

1) The pump pressure (or system pressure) via the RV and flow rate (full stroke) were set to the maximum.
2) The needle valve (between the pump and motor) was closed so that no flow to the motor could occur.
3) The needle valve was opened slowly until the motor started running. The maximum pressure recorded at the motor inlet at this moment was the static friction torque of the motor.
4) The needle valve was opened in a slow but continuous fashion, which resulted in a corresponding increase in the motor flow rate, until the valve was fully opened (maximum pump flow).
5) The needle valve was slowly closed in a continuous fashion resulting in a decrease in the motor flow rate until the motor came to a full stop.
6) Steps 1) to 5) were repeated several times.

Measured pressure drop as a function of motor rotational speed are shown in Figure D.3. Hysteresis in the friction characteristics can be observed.

As shown in Equation D.5, the motor torque equals the product of the pressure drop and motor displacement. Hence for a fixed displacement motor, the frictional torque is related to the pressure drop across the motor. Figure D.3 indicates that the static friction pressure is about 1.37 MPa, coulomb friction pressure about 0.9 MPa and the “pressure” viscous damping coefficient (the slope of the line) about 18700 $Pa \cdot rad^{-1}s$. Using the

conversion $T = P_p D_m$, the static friction is 3.28 Nm. The coulomb friction and viscous coefficients are:

$$T_{fm} = 2.14 \text{ Nm}$$

$$B_m = 0.044 \text{ Nm·rad}^{-1}\text{s}$$

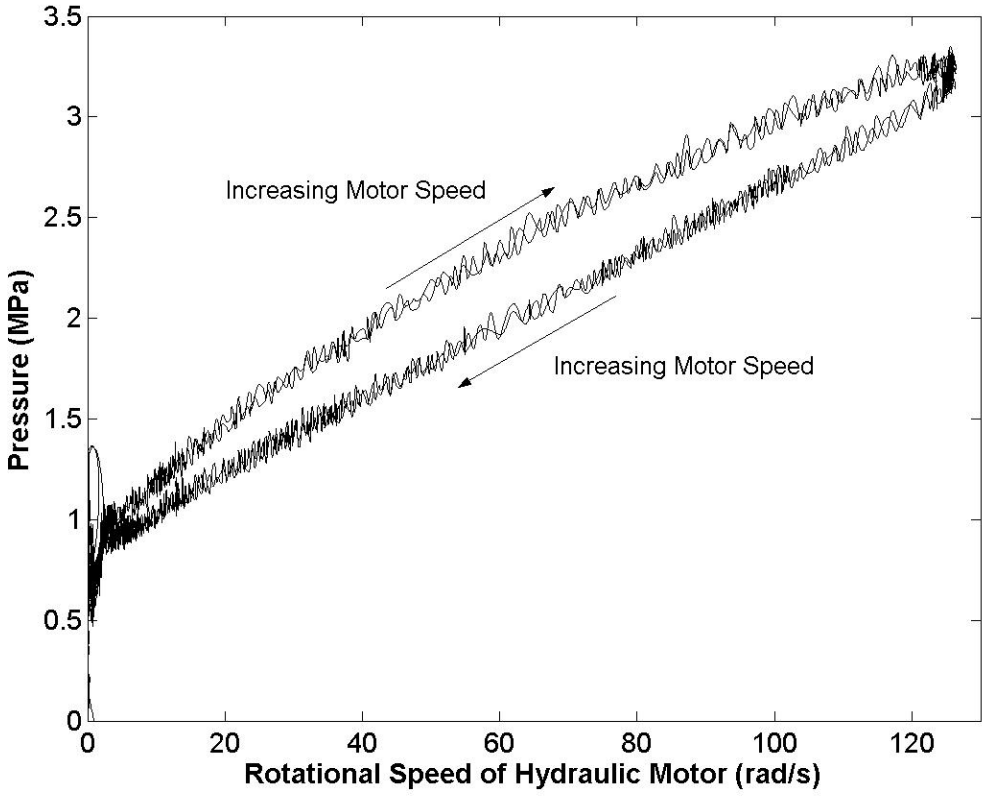

Figure D.3 Friction torque (via pressure measurement) of the hydraulic motor

Depending on the application, the load of the motor can appear in different forms. To simplify the study and model, only an inertial load was considered in this part of the study. The load inertia was lumped into the motor inertia (the load of the motor, T_L, disappears from the motor model). To further simplify the model, the internal and external leakages of the motor were combined into one term which was solely dependent on the inlet pressure. Although this assumption is true only when the outlet pressure of the motor

is zero, the influence of this simplification on the dynamic performance of the model is known to be relatively insignificant [Merritt, 1967].

Using the aforementioned assumptions and simplifications, Equation D.4 and D.5 become:

$$Q_m - C_{tm}P_p - D_m\frac{d\theta_m}{dt} = \frac{V_m}{\beta_e}\frac{dP_p}{dt} \tag{D.6}$$

$$(P_p - P_m)D_m = J_m\frac{d^2\theta_m}{dt^2} + B_m\frac{d\theta_m}{dt} + \text{sgn}(\dot{\theta}_m)T_{fm} \tag{D.7}$$

where C_{tm} =Total leakage coefficient of the motor ($m^3s^{-1}Pa$).

In Equations D.6 and D.7, there are seven parameters. The frictional torque, T_{fm}, and the viscous damping ratio, B_m, have been identified through experimental tests. The displacement, D_m, and the bulk modulus, β_e (approximately), can be found in product manuals of the motor and hydraulic fluid. The inertia of the motor, J_m, was mathematically calculated by dissembling the motor. Values of the parameter C_{tm} and V_m for the same motor were established in Wu's research [Wu, 2003]. The values of all parameters are listed in Appendix C.

D.3 Modeling the System

The complete hydraulic circuit is shown in Figure D.4. There are two, two-stage relief valves. The main relief valve, RV1, worked as the safety valve. It was not necessary to model the RV1 because it was always closed when the system was in the normal operating state. The relief valve, RV2, worked as a constant "resistive" load. It was used to adjust the backpressure on the hydraulic motor. By neglecting the dynamics of the relief valve, it was modeled simply as a constant backpressure on the motor. This was a

reasonable assumption since the dynamic response of the relief valve would only play a role as the valve just started to open. In this case, the relief valve was partially opened and in a steady state condition when the motor was operating.

As mentioned, all transmission line losses were neglected, and hence the pump pressure was considered equal to the motor pressure and servo valve pressure. For the configuration shown in Figure D.4, the flow from the pump to the motor and valve (when opened) is

$$Q_p = Q_m + Q_v \tag{D.8}$$

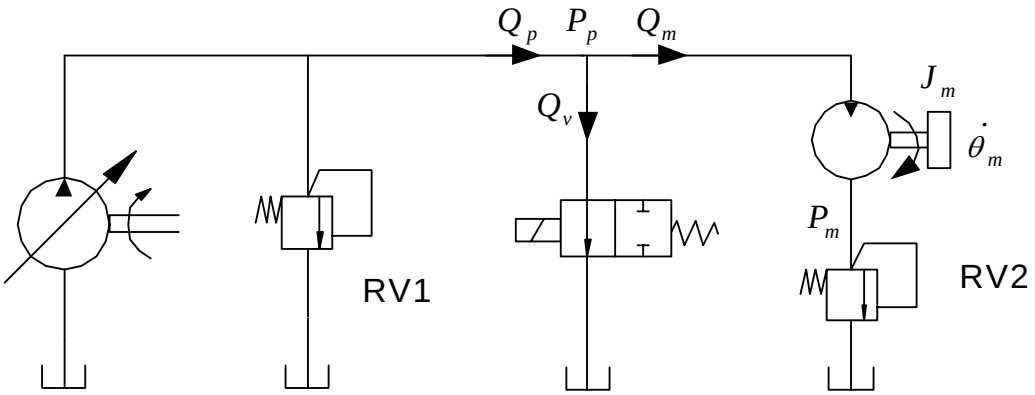

Figure D.4 Schematic diagram of the hydraulic circuit

This equation is essentially the link between models of the pump, load and valve. The complete system model is established by combining all component models in the circuit together. It should be noted that under steady state operating conditions, the flow rate of the valve, Q_v, is zero since it is assumed that the valve only opens during flow overshoot conditions. Substituting Equations B.16 and D.6 into Equation D.8, yields

$$K_p \tan\theta_p = C_t P_p + \frac{V}{\beta_e}\frac{dP_p}{dt} + D_m \frac{d\theta_m}{dt} \tag{D.9}$$

where $K_p = \omega_p N A_p R_p / \pi$ = Pump flow rate coefficient,

$C_t = C_{tp} + C_{tm}$ = Total leakage coefficient of the pump and motor and

$V = V_p + V_m$ = Total fluid volume of the pump, pipe and motor.

Equation (D.9) can be simplified to the following form.

$$\theta_p = f(P_p, \dot{P}_p, \dot{\theta}_m) \tag{D.10}$$

This equation shows the relationship between the swashplate angle and rotational speed of the hydraulic motor. To get the desired motor rotational speed ($\dot{\theta}_m$) at the pressure P_p, the pump swaspplate must be located at the angle of θ_p.

Appendix E

Calculation of the Power Spectral Density

It is difficult to identify the frequency components by studying the original signal in time domain. However, the time domain signal can be converted to the frequency domain by taking the discrete Fourier transform (DFT) using the fast Fourier transform. The DFT is a useful tool for processing the digital signal. A common use of the DFT is to find the frequency components of a periodic time domain signal buried in noise.

For a data sequence $x(n)$, the common form of the DFT is defined as follows [Ramirez, 1985]:

$$X(k) = \sum_{n=0}^{N-1} x(n) e^{-2\pi jkn/N} \tag{E.1}$$

where $0 \le k \le N-1$. N is the number of data samples being considered.

The DFT can be easily calculated using following Matlab function:

$$X = fft(x, n) \tag{E.2}$$

where n is the number of FFT points, and X is the DFT of x(n) computed with the FFT algorithm

The spectral estimation is used to describe the distribution (over frequency) of the power contained in a signal based on a finite set of data. One way for estimating the power spectrum of a data sequence is to find out the DFT of samples of a data series and take the magnitude of the result squared. The power spectral density (PSD) is commonly used to measure the energy at various frequencies. The PSD of a length-L signal $x(n)$ is defined as

$$\hat{P}_{xx}[f_k] = \frac{|X[f_k]|^2}{f_s L} \tag{E.3}$$

where f_s =Sampling frequency (Hz),

L =Length of the data sequence,

$\hat{P}_{xx}[f_k]$ = PSD at frequency f_k with a unit of db/Hz,

$f_k = kf_s / N \qquad (k = 0,1,...,N-1)$

A Matlab® program for calculating the PSD is listed below.

```
x=n1000;                    % Input signal
Fs=1000;                    % Sampling frequency
N=4096;                     % Number of FFT points
Y = fft(x, N);              % N-point FFT
P = Y.*conj (Y)/(N*Fs);     % Calculating the PSD
Pyy=10*log10 (P);           % Calculating decibels
f = 1000*(0:(N/2-1))/N;     % Frequency range
plot (f, Pyy (1:N/2))       % Plot the PSD magnitude vs frequency
xlabel ('Frequency(Hz)');   % X-axis title
ylabel ('Power Spectral Density (dB/Hz)');          % Y-axis title
```